Econometric Theory, **0**, 2026, 1–65.
doi:10.1017/S0266466626100607

ON THE RELATION BETWEEN DISCRETE- AND CONTINUOUS-TIME AFFINE OPTION PRICING MODELS

Maciej Augustyniak
University of Montreal

Alexandru Badescu
University of Calgary

Jean-François Bégin
Simon Fraser University

Sarath Kumar Jayaraman
University of Calgary

This article studies the weak convergence of discrete-time generalized autoregressive conditional heteroskedasticity (GARCH) and stochastic volatility (SV) option pricing models that allow for fat tails, multi-component volatilities, and non-monotonic pricing kernels. We introduce a general affine framework that enables the simultaneous derivation of new diffusion limits for Gaussian and inverse Gaussian GARCH models based on distributional invariant parametric convergence rates. When restricted to one-component specifications, our limits yield non-degenerate bivariate diffusions, generalizing the existing results in the affine GARCH literature. By using alternative parametric convergence rates, we further provide a comprehensive classification of all possible limits for two classes of affine and non-affine discrete-time SV models. Specifically, we show that the canonical affine classes of models popularized in discrete and continuous time are not analogous to one another. Our theoretical results are supported by a series of numerical experiments that investigate the impact of parametric scaling assumptions and model features on the convergence of European option prices. Overall, we find that the new limiting diffusions produce option prices that are closest to their discrete-time counterparts sampled at daily frequency.

1. INTRODUCTION

The development of adequate stochastic volatility (SV) models for the valuation and risk management of financial derivatives has played a crucial role in the

We are grateful to the Editor, Liangjun Su, the former Editor, Eric Renault, and three anonymous referees for their extensive comments, which substantially improved the article. We also acknowledge the helpful comments from the seminar participants at the Technical University of Munich, the University of Calgary, and the Quantact Actuarial and Financial Mathematics Laboratory, as well as the participants at the SSC 2024, Samos 2024, CAIMS 2024, SSC 2025, and QFFE 2025 conferences. Address correspondence to Alexandru Badescu, University of Calgary, Canada, e-mail: abadescu@ucalgary.ca

© The Author(s), 2026. Published by Cambridge University Press. This is an Open Access article, distributed under the terms of the Creative Commons Attribution licence (https://creativecommons.org/licenses/by/4.0), which permits unrestricted re-use, distribution and reproduction, provided the original article is properly cited.

Downloaded from https://www.cambridge.org/core. UNIVERSIDAD AUTONOMA METROPOLITANA, on 14 Nov 2026 at 21:01:13, subject to the Cambridge Core terms of use, available at https://www.cambridge.org/core/terms. https://doi.org/10.1017/S0266466626100607

financial economics literature. Generally, any no-arbitrage valuation framework comprises two fundamental elements: a model for the underlying asset dynamics under the physical measure and a martingale measure (i.e., pricing kernel) that prescribes how to fairly price contingent claims. The dynamics of the underlying asset may be modeled in either discrete or continuous time, with the choice largely driven by well-known trade-offs. For instance, while discrete-time models lack the analytical tractability provided by continuous-time models, they are often preferred for numerical implementations, especially in the context of estimation and forecasting. Within each class, models can be categorized into affine and non-affine frameworks based on the structure of the joint characteristic function (cf) of the underlying asset and the model factors. This classification gives rise to another trade-off between model flexibility and computational tractability. Despite their restrictive assumptions, affine processes are widely favored in extensive pricing and hedging studies due to their implementation ease.

Although there is an ample body of literature studying the impact of underlying asset model features (e.g., fat tails or jumps, multiple factors, and leverage effects) and the shape of the pricing kernel (e.g., monotonic and non-monotonic) for pricing and hedging financial derivatives with affine and non-affine dynamics in both discrete and continuous time, most studies explore these settings separately.[1] Specifically, their theoretical properties and empirical performance have been typically investigated for a given time-frame specification—either discrete or continuous—without a thorough reconciliation of the results obtained across these settings. While most research relating discrete-time option pricing models to their diffusion counterparts has focused on non-affine settings, this relationship has been in comparison seldom explored for affine models. Moreover, the few existing results within the affine domain are not consistent with the findings from the non-affine literature. This is not only because affine and non-affine generalized autoregressive conditional heteroskedasticity (GARCH) models imply structurally different variance dynamics, but also because, as we show in this article, the parametric convergence rate assumptions adopted in the affine literature are inconsistent with those that underlie most non-affine weak limit results. This helps explain why the affine literature has obtained qualitatively different limits, such as degenerate diffusions in which returns and variance are driven by the same Brownian motion instead of two stochastically correlated ones. Consequently, many questions have yet to be answered, and our article seeks to address these by

[1] See, for example, Bakshi, Cao, and Chen (1997), Bates (2000), Andersen, Benzoni, and Lund (2002), Chernov et al. (2003), Eraker (2004), Broadie, Chernov, and Johannes (2007), Cheng and Scaillet (2007), Christoffersen, Heston, and Jacobs (2009), Andersen, Fusari, and Todorov (2015), Bardgett, Gourier, and Leippold (2019), Aït-Sahalia, Karaman, and Mancini (2020), Bates (2022), and Heston, Jacobs, and Kim (2024b) for continuous-time models, and Christoffersen, Heston, and Jacobs (2006), Christoffersen et al. (2008), Feunou and Tédongap (2012), Christoffersen, Heston, and Jacobs (2013), Ornthanalai (2014), Majewski, Bormetti, and Corsi (2015), Badescu, Cui, and Ortega (2017), Babaoğlu et al. (2018), Bégin, Dorion, and Gauthier (2020), Bormetti et al. (2020), Chorro and Fanirisoa Zazaravaka (2022), Augustyniak, Badescu, and Bégin (2023), and Heston, Jacobs, and Kim (2024a) for discrete-time GARCH and SV models.

Downloaded from https://www.cambridge.org/core. UNIVERSIDAD AUTONOMA METROPOLITANA, on 14 Nov 2026 at 21:01:13, subject to the Cambridge Core terms of use, available at https://www.cambridge.org/core/terms. https://doi.org/10.1017/S0266466626100607

presenting novel weak convergence results for general classes of affine GARCH and SV option pricing models that allow for fat tails, multi-component volatilities, and non-monotonic pricing kernels.

Establishing the weak diffusion limits of these discrete-time models is useful in an option pricing context for at least three reasons. First, in addition to gaining a better understanding of the model dynamics and pricing kernel characteristics, it allows us to identify which discrete- and continuous-time option pricing frameworks should be viewed as close counterparts. This is particularly important in the affine setting, where the existing literature has related the GARCH class of models to Heston-type SV models, while our results show that this analogy is not the most appropriate one from an option pricing perspective. In particular, we show that affine GARCH option pricing models converge to non-standard SV diffusions rather than to Heston-type limits. Second, the derivation of weak limits allows us to identify the parametric scaling assumptions that preserve the conditional moment structure of the discrete-time model as the time step goes to zero. From a practical standpoint, the limiting diffusions obtained under the scaling assumptions we advocate deliver option prices that are the closest to those of the underlying discrete-time models at daily frequency, providing support for our choice of assumptions. Third, in some cases, the weak limits can provide a tractable continuous-time proxy that can be used for option pricing and hedging when the discrete-time model itself does not admit closed-form expressions. In that sense, the weak limits indicate which continuous-time approximation is the most appropriate in practice and how it should be implemented.

1.1. Literature Review and Motivation

Following the theoretical framework developed in Stroock and Varadhan (1979) and Ethier and Kurtz (1986) on the convergence of discrete-time Markovian processes, Nelson (1990) derives weak limits for two GARCH processes, that is, the GARCH-in-mean model of Engle and Bollerslev (1986) and the Exponential ARCH model of Nelson (1991). In both cases, the limits correspond to non-degenerate bivariate diffusions for the returns and variance processes driven by (independent) Brownian motions. The results of Nelson (1990) rely on specific convergence rate assumptions made on the underlying model parameters, which determine how these parameters scale as the time step between observations approaches zero. Interestingly, using alternative convergence rates yields different weak limits for GARCH models. For example, for the standard GARCH(1,1) model of Bollerslev (1986), Corradi (2000) obtains a diffusion limit with deterministic variance by changing only the speed of convergence for the ARCH parameter, while retaining the other assumptions used by Nelson (1990). Although both limits are technically valid, they have rather different impacts on modeling and pricing financial assets, so choosing one over the other requires a mathematical or an economic justification. In this context, Kim and Meddahi (2017) argue that Nelson's

Downloaded from https://www.cambridge.org/core. UNIVERSIDAD AUTONOMA METROPOLITANA, on 14 Nov 2026 at 21:01:13, subject to the Cambridge Core terms of use, available at https://www.cambridge.org/core/terms. https://doi.org/10.1017/S0266466626100607

(1990) convergence rates maintain some of the empirical properties of the daily aggregated returns when the time between high-frequency observations vanishes. Moreover, Alexander and Lazar (2021) prove that the *unique* convergence rates of the model parameters implied by the temporal aggregation property of the weak GARCH model of Drost and Nijman (1993) are consistent with Nelson's (1990) assumptions.

The results of Nelson (1990) have been generalized to various other non-affine GARCH and SV models, and the limits rely on similar convergence rates. Most notable contributions in the GARCH class include extensions with respect to the volatility dynamics (e.g., Duan, 1997; Arvanitis, 2004; Fornari and Mele, 2006), the conditional distribution of the return innovation (e.g., Fornari and Mele, 1997; Duan, Ritchken, and Sun, 2006), and multivariate extensions (e.g., Hafner, Laurent, and Violante, 2017). Outside of the standard GARCH class, Buccheri et al. (2021) investigate the diffusion limits of score-driven volatility models, while Ding (2020, 2023) derive the weak limits of two classes of hybrid GARCH-SV processes.

With the exception of Duan et al. (2006), these studies analyze exclusively the weak limits under the physical probability measure, and consequently, the majority of their empirical applications focus on the interplay between discrete- and continuous-time models from a statistical inference perspective.[2] However, the convergence of derivative prices also requires the weak convergence of the underlying asset price process under a risk-neutral measure, or equivalently, the joint convergence of the underlying asset price and Radon–Nikodym process under the physical measure. Duan (1996) is the first study to establish a link between martingale measures used for GARCH and diffusion processes. Specifically, he shows that the locally risk-neutral valuation relationship (LRNVR) introduced by Duan (1995) is consistent with the minimal martingale measure (MMM) associated with the continuous-time limit of the underlying GARCH process under the physical measure.[3] Further applications on the weak convergence of prices of other types of derivatives computed based on the LRNVR principle have been considered by Duan and Pliska (2004), who evaluated spread options

[2]Interchanging GARCH and diffusions for statistical inference purposes has been a well-debated topic in the literature. On the one hand, GARCH models are robust to different types of misspecification, thus providing a very useful tool for filtering, estimating, and forecasting in the context of SV models (see, e.g., Nelson, 1990, 1992; Nelson and Foster, 1994, 1995; Fleming and Kirby, 2003). On the other hand, Wang (2002) shows that GARCH models and their diffusion limits are not asymptotically equivalent with respect to Le Cam's deficiency distance, as both models exhibit different mechanisms of noise propagation in the conditional variance. Although this may have a significant impact on the asymptotic behavior of the maximum likelihood estimates of the two processes' parameters, it should not affect the convergence of derivative prices, which is the main objective of our article (see Duan, Wang, and Zou, 2009).

[3]The weak convergence of option prices and locally risk-minimizing trading strategies computed based on the MMM have been investigated by Prigent (1999), Lesne, Prigent, and Scaillet (2000), and Prigent and Scaillet (2002). However, in GARCH settings, since the MMM is a signed measure leading to option prices that are not guaranteed to be arbitrage-free, valuation is typically performed using other risk-neutral measure candidates.

Downloaded from https://www.cambridge.org/core. UNIVERSIDAD AUTONOMA METROPOLITANA, on 14 Nov 2026 at 21:01:13, subject to the Cambridge Core terms of use, available at https://www.cambridge.org/core/terms. https://doi.org/10.1017/S0266466626100607

with co-integrated GARCH models, and by Stentoft (2011), who priced American options under Duan's (1995) model. Since the LRNVR is only compatible with the conditional Gaussian assumption imposed on asset returns, the weak convergence of non-Gaussian GARCH option pricing models has been considered under other martingale measures, such as the mean-correcting martingale measure, the conditional Esscher transform, and Gaussian distortions. For example, Badescu, Elliott, and Ortega (2015) show that, similarly to the LRNVR, the conditional Esscher transform aligns with the MMM for non-Gaussian settings.[4] The results under various pricing kernels have been unified by Badescu et al. (2017), who investigate the weak limits of a general asymmetric non-Gaussian GARCH option pricing model risk-neutralized with a variance-dependent pricing kernel that features time-varying risk preference parameters.

While all of the above studies explore the weak convergence within non-affine frameworks, two important contributions linking discrete- and continuous-time affine models have been provided in the literature. Heston and Nandi (2000) introduce the first affine Gaussian GARCH option pricing model, which allows for closed-form solutions for European option prices, and derive the weak limits under both the physical and risk-neutral measures—the latter using Duan's (1995) LRNVR. However, unlike in the non-affine cases, both of these limits correspond to two-dimensional degenerate diffusion processes. More specifically, they resemble a special case of Heston's (1993) model where returns and volatility are driven by the same Brownian motion. To incorporate conditional skewness, Christoffersen et al. (2006) extend the affine framework to inverse Gaussian innovations and provide its weak limit as a bivariate SV model driven by the same pure-jump inverse Gaussian model. The discrepancies with the non-affine GARCH limits can be attributed to the use of different parametric convergence rates. In particular, both papers assume convergence rates that are not consistent with those used in Nelson (1990) and do not recover the initial GARCH model at daily frequency.[5] Since both affine GARCH specifications, together with their multi-component and SV extensions, are among the most popular option pricing models in discrete time, their relationships with continuous-time counterparts are of great interest and need to be further explored. This motivates the main goal of this article: to provide a general framework for the weak convergence of Markovian affine discrete-time models which allows us to construct novel diffusion limits for different classes of affine GARCH and SV models.

[4]They further prove that the GARCH diffusion limit based on the mean-correcting martingale measure can be recovered by applying Girsanov's theorem to the GARCH limit under the physical measure for a specific choice of the market price of variance risk preference parameter, which depends on the skewness and kurtosis of the GARCH innovations.

[5]See Badescu, Cui, and Ortega (2019) for a discussion and an alternative set of assumptions leading to the same limiting diffusion of Heston and Nandi (2000).

Downloaded from https://www.cambridge.org/core. UNIVERSIDAD AUTONOMA METROPOLITANA, on 14 Nov 2026 at 21:01:13, subject to the Cambridge Core terms of use, available at https://www.cambridge.org/core/terms. https://doi.org/10.1017/S0266466626100607

1.2. Our Main Contributions

Our article makes two important contributions to the literature. First, we introduce a general affine GARCH volatility component framework, which encompasses both Gaussian and inverse Gaussian option pricing models and allows us to simultaneously compute their weak limits under the physical and risk-neutral measures, the latter being constructed based on an exponential linear pricing kernel. The convergence rates that we assume for the underlying model parameters are invariant to the distributional assumption and align with those proposed by Nelson (1990) and Duan (1997). Under the physical measure, we show that the weak limits of both the Gaussian and inverse Gaussian GARCH component models correspond to a three-dimensional affine SV model, with the short- and long-run variance components driven by the same two independent Brownian motions, one of which also drives the return process. Moreover, these diffusion limits coincide if and only if certain relationships between the two model parameters hold. The risk-neutral convergence is carried out by incorporating an additional assumption on the convergence rate of the variance risk-preference parameter in the pricing kernel. We show that the resulting limit can be recovered directly by applying Girsanov's theorem to the physical limit for particular choices of the market prices of risk associated with the Brownian motions governing the variance component dynamics. The proofs of our results rely on a general approach that only requires the knowledge of the one-step conditional cumulant generating function (cgf) of the underlying process. This indicates that our methodology could be applied to other classes of discrete-time affine Markovian processes, especially in scenarios where identifying the risk-neutral dynamics is challenging or not feasible. Additionally, we derive the cf of these risk-neutral limits, as this is the main ingredient for the valuation of European-style options in semi-closed form.

Our second contribution centers on exploring how varying assumptions about the convergence rates of underlying model parameters impact the diffusion limit. We show that, when restricted to a single component, the diffusion limit that we derive for the affine Gaussian GARCH model generalizes the one established in Heston and Nandi (2000). Specifically, our limit is a two-dimensional non-degenerate affine diffusion driven by two stochastically correlated Brownian motions, in contrast to Heston and Nandi's (2000) degenerate diffusion limit driven by perfectly (negatively) correlated Brownian motions. The disparity between these two limits can be explained by the fact that the literature on affine GARCH models has employed convergence rate assumptions that do not align with those proposed by Nelson (1990) and Duan (1997). To our knowledge, our article is the first that brings this disparity to light. Motivated by this finding, and aiming to better understand the link between discrete- and continuous-time option pricing models, we also provide a comprehensive classification of potential limits for two distinct classes of discrete-time SV models. The first model is affine and has been recently proposed by Heston et al. (2024a) as a generalization of the Heston and Nandi (2000) model to allow for SV. The second model is non-affine and extends upon the non-affine square-root GARCH (SQGARCH) model originally proposed

Downloaded from https://www.cambridge.org/core. UNIVERSIDAD AUTONOMA METROPOLITANA, on 14 Nov 2026 at 21:01:13, subject to the Cambridge Core terms of use, available at https://www.cambridge.org/core/terms. https://doi.org/10.1017/S0266466626100607

by Ishida and Engle (2002) in a similar way.[6] We show that, irrespective of the convergence rates applied to the underlying parameters, the weak limits of both affine and non-affine specifications result in bivariate affine diffusions. Moreover, our asymptotic parametric scaling assumptions lead to the most complex dynamics and preserve the conditional moment structure of the underlying discrete-time model as the time step approaches zero. The weak limit of the Heston et al. (2024a) model remains a square-root diffusion driven by a Brownian motion stochastically correlated with the one from the returns. Conversely, our non-affine extension of Ishida and Engle's (2002) SQGARCH model converges weakly to Heston's (1993) model. Interestingly, if one were to employ the parametric scaling assumptions proposed in Heston and Nandi (2000), both models would converge to the same diffusion limit. This suggests that such rates might not be the most suitable to relate GARCH and SV models to diffusion models. Our results therefore indicate that the canonical affine classes of models popularized in discrete and continuous time are not analogous to one another.

The effect of using alternative convergence rates is also investigated numerically by computing European call option prices based on the Heston et al.'s (2024a) model across various moneyness levels and maturities. Overall, we find that our convergence rates yield the *best* limiting prices in the sense that they are the closest to their discrete-time counterparts evaluated at daily frequency. Such a feature is important as it may enable the interchange between discrete- and continuous-time settings for pricing and hedging purposes. The sensitivity of these prices is further examined relative to three key factors: the shape of the pricing kernel, the correlation between the innovations driving the returns and conditional variance processes, and the magnitude of the asymmetry parameter. Our analysis reveals that both the non-monotonic pricing kernel and the correlation coefficient significantly affect the convergence of option prices.

The remainder of this article is organized as follows. Section 2 introduces a general affine GARCH component option pricing framework which includes two well-known special cases—Gaussian and inverse Gaussian innovations. Using a distributional invariant assumption on the convergence rates of the model parameters, we derive the weak limits of both GARCH component models under the physical and risk-neutral measures in Section 3. Section 4 discusses alternative convergence rates and provides a comprehensive characterization of all possible diffusion limits for two new classes of GARCH models that feature SV. Numerical illustrations on the impact of different convergence rates on option prices are presented in Section 5. Section 6 concludes.

[6]While many of the discrete-time SV models proposed in the literature rely on modeling the (log) variance with an autoregressive process driven by independent and identically distributed (Gaussian) innovations (see, e.g., Taylor, 1986, 1994; Andersen, 1994; Harvey, Ruiz, and Shephard, 1994; Meddahi and Renault, 2004), another approach is to incorporate SV into a GARCH framework by replacing the driving noise from the conditional variance equation with a different innovation process correlated with that of the returns (see, e.g., Pitt, Malik, and Doucet, 2014). The advantage of making such an adjustment to Heston and Nandi's (2000) model is that it preserves its affine property and it has been shown to be very effective in improving the option pricing performance (see, e.g., Heston et al., 2024a).

Downloaded from https://www.cambridge.org/core. UNIVERSIDAD AUTONOMA METROPOLITANA, on 14 Nov 2026 at 21:01:13, subject to the Cambridge Core terms of use, available at https://www.cambridge.org/core/terms. https://doi.org/10.1017/S0266466626100607

2. AFFINE VOLATILITY COMPONENT MODELS, SPECIAL CASES, AND THEIR RELATIONSHIPS

This section introduces a general discrete-time option pricing framework based on affine GARCH dynamics with two variance components and investigates the relationship between two popular models nested in this setting: the first being driven by Gaussian innovations, and the second by inverse Gaussian innovations. Our focus on two variance factors is motivated by the affine option pricing literature in discrete time that we aim to encompass, in particular the component models of Christoffersen et al. (2008) and Babaoğlu et al. (2018). A two-factor setting is sufficient for this purpose and is also consistent with the empirical evidence that volatility contains a transitory short-run component and a more persistent long-run component (see, e.g., Engle and Lee, 1999).

We consider an n-indexed discrete-time market defined over a set of equally spaced trading dates $\mathcal{T}^{(n)} = \{k\tau \mid k = 0, 1, \ldots, nT\}$, where $\tau = 1/n > 0$ is the discretization step. When $n = 1$, we recover the classical discrete-time setting with integer time steps (i.e., $\tau = 1$). The uncertainty is modeled by a filtered probability space $\left(\Omega^{(n)}, \mathcal{F}^{(n)}, \mathbb{F}^{(n)}, \mathbb{P}^{(n)}\right)$, where $\mathbb{F}^{(n)} = \left\{\mathcal{F}_{k\tau}^{(n)}\right\}_{k=0}^{nT}$ is the filtration constructed from the σ-algebras $\mathcal{F}_{k\tau}^{(n)}$ denoting the information available to investors at time $k\tau$ and $\mathbb{P}^{(n)}$ represents the physical measure. The market consists of a risk-free and a risky asset whose price processes are denoted by $B^{(n)} = \left\{B_{k\tau}^{(n)}\right\}_{k=0}^{nT}$ and $S^{(n)} = \left\{S_{k\tau}^{(n)}\right\}_{k=0}^{nT}$, respectively. We denote the logarithm of the risky asset price process by $Y^{(n)} = \left\{Y_{k\tau}^{(n)}\right\}_{k=0}^{nT}$, so that $Y_{k\tau}^{(n)} = \log\left(S_{k\tau}^{(n)}\right)$. The difference $\Delta Y_{(k+1)\tau}^{(n)} = Y_{(k+1)\tau}^{(n)} - Y_{k\tau}^{(n)}$ thus represents the risky asset's log-return (henceforth return) from time $k\tau$ to $(k+1)\tau$. The risk-free asset price at time $k\tau$ is assumed to be given by $B_{k\tau}^{(n)} = e^{rk\tau}$, where r represents the constant continuously compounded risk-free rate. We further assume that the risky asset's returns have the following n-augmented dynamics under measure $\mathbb{P}^{(n)}$:

$$\Delta Y_{(k+1)\tau}^{(n)} = r\tau + F^{\mathcal{D}}\left(h_{k\tau}^{(n)}; \lambda(\tau)\right) + \sqrt{\tau} z_{(k+1)\tau}^{(n)}, \qquad z_{(k+1)\tau}^{(n)} \,\Big|\, \mathcal{F}_{k\tau}^{(n)} \sim \mathcal{D}\left(0, h_{k\tau}^{(n)}\right), \tag{1}$$

$$h_{(k+1)\tau}^{(n)} = s_{(k+1)\tau}^{(n)} + q_{(k+1)\tau}^{(n)}, \tag{2}$$

$$\Delta s_{(k+1)\tau}^{(n)} = -\left(1 - \phi_s(\tau)\right) s_{k\tau}^{(n)} + \alpha_s(\tau)\, G^{\mathcal{D}}\left(z_{(k+1)\tau}^{(n)}, h_{k\tau}^{(n)}; \gamma_s(\tau)\right), \tag{3}$$

$$\Delta q_{(k+1)\tau}^{(n)} = \left(1 - \phi_q(\tau)\right)\left(\sigma^2(\tau) - q_{k\tau}^{(n)}\right) + \alpha_q(\tau)\, G^{\mathcal{D}}\left(z_{(k+1)\tau}^{(n)}, h_{k\tau}^{(n)}; \gamma_q(\tau)\right). \tag{4}$$

Here, we set $\mathcal{F}_{k\tau}^{(n)} = \sigma\left(z_{l\tau}^{(n)} \,\middle|\, l \le k\right)$, so that $\mathbb{F}^{(n)}$ is the natural filtration generated by the innovation process $z^{(n)} = \left\{z_{k\tau}^{(n)}\right\}_{k=0}^{nT}$. We assume that $z_{(k+1)\tau}^{(n)}$ is a random variable following a generic distribution $\mathcal{D}$ with mean zero and variance $h_{k\tau}^{(n)}$ conditionally

Downloaded from https://www.cambridge.org/core. UNIVERSIDAD AUTONOMA METROPOLITANA, on 14 Nov 2026 at 21:01:13, subject to the Cambridge Core terms of use, available at https://www.cambridge.org/core/terms. https://doi.org/10.1017/S0266466626100607

on $\mathcal{F}_{k\tau}^{(n)}$ and under measure $\mathbb{P}^{(n)}$. The function $F^{\mathcal{D}}$ in Equation (1) represents the conditional mean excess return or equity risk premium. It is specified to depend on the conditional variance $h_{k\tau}^{(n)}$ and an equity risk premium parameter, denoted by $\lambda(\tau)$, which varies with the discretization step τ.

The conditional variance $h_{k\tau}^{(n)}$ is decomposed into two components, $s_{k\tau}^{(n)}$ and $q_{k\tau}^{(n)}$, following GARCH(1,1) dynamics given by Equations (3) and (4), respectively, where $\Delta s_{(k+1)\tau}^{(n)} = s_{(k+1)\tau}^{(n)} - s_{k\tau}^{(n)}$ and $\Delta q_{(k+1)\tau}^{(n)} = q_{(k+1)\tau}^{(n)} - q_{k\tau}^{(n)}$. These dynamics rely on parameters that are dependent on the discretization step τ: $\boldsymbol{\phi}(\tau) = \begin{bmatrix} \phi_s(\tau) & \phi_q(\tau) \end{bmatrix}^\top$ is the vector of persistence parameters for $s_{k\tau}^{(n)}$ and $q_{k\tau}^{(n)}$, respectively, satisfying $0 < \phi_s(\tau) < \phi_q(\tau) < 1$ for any $\tau > 0$, $\boldsymbol{\alpha}(\tau) = \begin{bmatrix} \alpha_s(\tau) & \alpha_q(\tau) \end{bmatrix}^\top$ is the vector of nonnegative ARCH parameters associated with these components, $\boldsymbol{\gamma}(\tau) = \begin{bmatrix} \gamma_s(\tau) & \gamma_q(\tau) \end{bmatrix}^\top$ is the vector of leverage parameters, and $\sigma^2(\tau) > 0$ represents the unconditional mean of $q_{k\tau}^{(n)}$, as well as of $h_{k\tau}^{(n)}$.[7] The function $G^{\mathcal{D}}$ is the GARCH variance driving noise function—a function of the return innovation process, the overall conditional variance, and the component-specific leverage parameter. We assume that

$$E^{\mathbb{P}^{(n)}}\left[G^{\mathcal{D}}\left(z_{(k+1)\tau}^{(n)}, h_{k\tau}^{(n)}; \gamma_u(\tau)\right) \middle| \mathcal{F}_{k\tau}^{(n)}\right] = 0,$$

for $u \in \{s, q\}$, so that $E^{\mathbb{P}^{(n)}}\left[s_{k\tau}^{(n)}\right] = 0$ and $E^{\mathbb{P}^{(n)}}\left[h_{k\tau}^{(n)}\right] = E^{\mathbb{P}^{(n)}}\left[q_{k\tau}^{(n)}\right] = \sigma^2(\tau)$.

The modeling framework of Equations (1)–(4) generalizes the component GARCH model of Engle and Lee (1999). Their specification is nested as a special case by setting $\tau = 1$, adopting Gaussian-distributed innovations, and specifying particular functional forms for $F^{\mathcal{D}}$ and $G^{\mathcal{D}}$. Following the terminology of Engle and Lee (1999), the decomposition $h_{k\tau}^{(n)} = s_{k\tau}^{(n)} + q_{k\tau}^{(n)}$ admits a natural interpretation in terms of short- and long-run variance components. In particular, the factor $s_{k\tau}^{(n)}$ represents the short-run component because it has zero unconditional mean and lower persistence than $q_{k\tau}^{(n)}$, as implied by the restriction $\phi_s(\tau) < \phi_q(\tau)$. It therefore captures relatively fast-moving transitory fluctuations in conditional variance. In contrast, $q_{k\tau}^{(n)}$ is interpreted as the long-run component because it has higher persistence and fluctuates around the long-run variance level $\sigma^2(\tau)$. This two-component structure is better able to capture the well-documented slow decay of the autocorrelation function of squared returns than a single-factor GARCH specification.

Remark 1. The one-component version of the above model is obtained by taking $\phi_q(\tau) = \alpha_q(\tau) = 0$, so that the long-run variance component is constant, that is, $q_{k\tau}^{(n)} = \sigma^2(\tau)$. Equation (3) can therefore be rewritten in terms of the conditional

[7] Leverage in our models is defined as the $\mathcal{F}_{k\tau}^{(n)}$-conditional correlation between the return increment $\Delta Y_{(k+1)\tau}^{(n)}$ and the variance component increment $\Delta u_{(k+1)\tau}^{(n)}$ with $u \in \{s, q\}$. It is the natural discrete-time analog of the instantaneous correlation between the Brownian motions driving returns and variance components in continuous-time SV models.

Downloaded from https://www.cambridge.org/core. UNIVERSIDAD AUTONOMA METROPOLITANA, on 14 Nov 2026 at 21:01:13, subject to the Cambridge Core terms of use, available at https://www.cambridge.org/core/terms. https://doi.org/10.1017/S0266466626100607

variance as

$$\Delta h^{(n)}_{(k+1)\tau} = (1-\phi(\tau))\left(\sigma^2(\tau) - h^{(n)}_{k\tau}\right) + \alpha(\tau)\, G^{\mathcal{D}}\left(z^{(n)}_{(k+1)\tau}, h^{(n)}_{k\tau}; \gamma(\tau)\right), \tag{5}$$

where $\phi(\tau), \alpha(\tau)$, and $\gamma(\tau)$ are the parameters of the conditional variance process.

2.1. Affine Assumptions

To establish an affine setting for the GARCH component modeling framework of Equations (1)–(4), we introduce the following assumption.

Assumption 1. For any real w and $\boldsymbol{v} = [\, v_1 \quad v_2 \,]^\top$, the one-step $\mathcal{F}^{(n)}_{k\tau}$-conditional joint cgf of $\Delta Y^{(n)}_{(k+1)\tau}$, $\Delta s^{(n)}_{(k+1)\tau}$, and $\Delta q^{(n)}_{(k+1)\tau}$ is affine in the state variables with the following representation under measure $\mathbb{P}^{(n)}$:

$$\begin{aligned}
&\mathcal{C}^{\mathbb{P}^{(n)}}_{\Delta Y^{(n)}_{(k+1)\tau}, \Delta s^{(n)}_{(k+1)\tau}, \Delta q^{(n)}_{(k+1)\tau}}\left(w, \boldsymbol{v} \,\middle|\, \mathcal{F}^{(n)}_{k\tau}\right) \\
&\quad = \log\left(E^{\mathbb{P}^{(n)}}\left[\exp\left(w\,\Delta Y^{(n)}_{(k+1)\tau} + v_1\,\Delta s^{(n)}_{(k+1)\tau} + v_2\,\Delta q^{(n)}_{(k+1)\tau}\right) \,\middle|\, \mathcal{F}^{(n)}_{k\tau}\right]\right) \\
&\quad = \mathcal{A}^{\mathcal{D}}(w, \boldsymbol{v}; \tau) + \mathcal{B}^{\mathcal{D}}_s(w, \boldsymbol{v}; \tau)\, s^{(n)}_{k\tau} + \mathcal{B}^{\mathcal{D}}_q(w, \boldsymbol{v}; \tau)\, q^{(n)}_{k\tau}.
\end{aligned} \tag{6}$$

The coefficients $\mathcal{A}^{\mathcal{D}}(w, \boldsymbol{v}; \tau)$ and $\mathcal{B}^{\mathcal{D}}_u(w, \boldsymbol{v}; \tau)$ depend on the discretization step τ and are real-valued functions that satisfy $\mathcal{A}^{\mathcal{D}}(0, \mathbf{0}; \tau) = \mathcal{B}^{\mathcal{D}}_u(0, \mathbf{0}; \tau) = 0$ for $u \in \{s, q\}$.

Assumption 1 will be satisfied in the context of Equations (1)–(4) if and only if the following two conditions are met:

1. The function $F^{\mathcal{D}}$ is affine in $s^{(n)}_{k\tau}$ and $q^{(n)}_{k\tau}$ conditionally on $\mathcal{F}^{(n)}_{k\tau}$.
2. The joint cgf of $z^{(n)}_{(k+1)\tau}$ and $G^{\mathcal{D}}$ is affine in $s^{(n)}_{k\tau}$ and $q^{(n)}_{k\tau}$ conditionally on $\mathcal{F}^{(n)}_{k\tau}$.

While the first condition can be easily imposed when specifying the mean return dynamics, the second property can only be satisfied within two special classes of GARCH component processes, namely, the Gaussian and inverse Gaussian classes which will be introduced in Section 2.2.

Furthermore, the valuation of derivatives requires the specification of a martingale measure, which is not unique under our modeling assumptions. To preserve the affine property inherent in Assumption 1 under the risk-neutral measure, we introduce an n-augmented exponential affine pricing kernel in $\Delta Y^{(n)}_{(k+1)\tau}$ and the conditional variance components $\Delta s^{(n)}_{(k+1)\tau}$ and $\Delta q^{(n)}_{(k+1)\tau}$.

Assumption 2. The risk-neutral probability measure denoted by $\mathbb{Q}^{(n)}$ is defined via the Radon–Nikodym derivative

$$\left.\frac{d\mathbb{Q}^{(n)}}{d\mathbb{P}^{(n)}}\right|_{\mathcal{F}^{(n)}_T} = \prod_{k=0}^{nT-1} \frac{\exp\left(\theta(\tau)\,\Delta Y^{(n)}_{(k+1)\tau} + \xi_s(\tau)\,\Delta s^{(n)}_{(k+1)\tau} + \xi_q(\tau)\,\Delta q^{(n)}_{(k+1)\tau}\right)}{\exp\left(\mathcal{C}^{\mathbb{P}^{(n)}}_{\Delta Y^{(n)}_{(k+1)\tau}, \Delta s^{(n)}_{(k+1)\tau}, \Delta q^{(n)}_{(k+1)\tau}}\left(\theta(\tau), \boldsymbol{\xi}(\tau) \mid \mathcal{F}^{(n)}_{k\tau}\right)\right)}, \tag{7}$$

Downloaded from https://www.cambridge.org/core. UNIVERSIDAD AUTONOMA METROPOLITANA, on 14 Nov 2026 at 21:01:13, subject to the Cambridge Core terms of use, available at https://www.cambridge.org/core/terms. https://doi.org/10.1017/S0266466626100607

where $\theta(\tau)$ and $\boldsymbol{\xi}(\tau) = \begin{bmatrix} \xi_s(\tau) & \xi_q(\tau) \end{bmatrix}^\top$ represent the equity and variance component risk preference parameters, respectively; these parameters are also known as the market prices of risk in the literature. A nonzero value of the variance component risk preference parameter leads to a non-monotonic pricing kernel. We assume that these preference parameters satisfy the following system of equations:

$$\mathcal{A}^{\mathcal{D}}(1+\theta(\tau),\boldsymbol{\xi}(\tau);\tau) = \mathcal{A}^{\mathcal{D}}(\theta(\tau),\boldsymbol{\xi}(\tau);\tau) + r\tau \tag{8}$$

$$\text{and} \quad \mathcal{B}_u^{\mathcal{D}}(1+\theta(\tau),\boldsymbol{\xi}(\tau);\tau) = \mathcal{B}_u^{\mathcal{D}}(\theta(\tau),\boldsymbol{\xi}(\tau);\tau), \qquad u \in \{s,q\}. \tag{9}$$

Equations (8) and (9) ensure that the discounted asset price is a martingale under $\mathbb{Q}^{(n)}$ and are referred to as the martingale (or no-arbitrage) constraints. They follow directly from the martingale restriction,

$$E^{\mathbb{Q}^{(n)}}\left[\exp\left(\Delta Y^{(n)}_{(k+1)\tau} - r\tau\right) \middle| \mathcal{F}^{(n)}_{k\tau}\right] = 1,$$

and the affine form of the cgf provided in Assumption 1. These equations do not by themselves fully identify the pricing kernel parameters; solving them typically yields a relationship between the risk preference parameters, and in particular allows one to express $\theta(\tau)$ as a function of $\boldsymbol{\xi}(\tau)$. The variance risk preference parameters $\boldsymbol{\xi}(\tau)$ are therefore not restricted by the martingale constraints and are left to be estimated from option prices, giving the pricing kernel the flexibility needed to better fit the option cross section. This is consistent with the variance-dependent pricing kernel approach of Christoffersen et al. (2013) and contrasts with the remaining model parameters, which can be identified using return data.[8]

2.2. Classes of Affine GARCH Models

This section presents two classes of affine GARCH component models. They are obtained as a special case of the general modeling framework introduced in Equations (1)–(4) by specifying the conditional distribution of the GARCH innovations $\mathcal{D}$ along with functions $F^{\mathcal{D}}$ and $G^{\mathcal{D}}$. In addition, we prove a limiting relationship between these two classes of models.

[8] Recently, Cheng, Renault, and Sangrey (2025) (see also Bandi and Renò, 2016; Han, Khrapov, and Renault, 2020) established that equity and volatility prices of risk parameters can both be identified from return data alone in the presence of leverage within an SV model where the volatility factor is contemporaneously latent. However, this result does not apply to our affine GARCH framework. Moreover, it is important to distinguish between $\lambda(\tau)$, which is the parameter entering the equity risk premium term $F^{\mathcal{D}}\left(h^{(n)}_{k\tau};\lambda(\tau)\right)$ in the return dynamics, and the equity risk preference parameter $\theta(\tau)$ appearing in the pricing kernel. While $\lambda(\tau)$ can be estimated from return data alone, $\theta(\tau)$ is determined by the martingale constraints and is uniquely identified only once $\boldsymbol{\xi}(\tau)$ is specified or estimated from derivative prices. In the special case of a monotonic pricing kernel (i.e., $\boldsymbol{\xi}(\tau) = \mathbf{0}$), $\theta(\tau)$ reduces to a function of the physical measure parameters and can thus be inferred from return data alone. However, when $\boldsymbol{\xi}(\tau) \neq \mathbf{0}$, $\theta(\tau)$ must be jointly determined alongside $\boldsymbol{\xi}(\tau)$ using derivative prices. Separate empirical identification of $\xi_s(\tau)$ and $\xi_q(\tau)$ depends on the estimation strategy adopted and may require a restriction such as $\xi_s(\tau) = \xi_q(\tau)$ to ensure identification.

Downloaded from https://www.cambridge.org/core. UNIVERSIDAD AUTONOMA METROPOLITANA, on 14 Nov 2026 at 21:01:13, subject to the Cambridge Core terms of use, available at https://www.cambridge.org/core/terms. https://doi.org/10.1017/S0266466626100607

2.2.1. *The Gaussian GARCH Component Model.* The Heston–Nandi GARCH component model, denoted by HN(C) in this article, was introduced by Christoffersen et al. (2008) to generalize the one-component model proposed by Heston and Nandi (2000). It is constructed based on a conditionally Gaussian assumption for the return innovation, that is, $\mathcal{D} = \mathcal{N}$. More specifically, we assume that

$$z^{(n)}_{(k+1)\tau} = \sqrt{h^{(n)}_{k\tau}}\,\epsilon^{(n)}_{(k+1)\tau}, \qquad \epsilon^{(n)}_{(k+1)\tau} \,\big|\, \mathcal{F}^{(n)}_{k\tau} \sim \mathcal{N}(0,1), \tag{10}$$

where $\epsilon^{(n)}_{(k+1)\tau}$ follows a standard Gaussian distribution, so that $z^{(n)}_{(k+1)\tau}$ is conditionally normally distributed with mean zero and variance $h^{(n)}_{k\tau}$. The functions $F^{\mathcal{N}}$ and $G^{\mathcal{N}}$ are given by

$$F^{\mathcal{N}}\left(h^{(n)}_{k\tau}; \lambda(\tau)\right) = \lambda(\tau)\, h^{(n)}_{k\tau}, \tag{11}$$

$$G^{\mathcal{N}}\left(z^{(n)}_{(k+1)\tau}, h^{(n)}_{k\tau}; \gamma_u(\tau)\right) = \frac{z^{(n)2}_{(k+1)\tau}}{h^{(n)}_{k\tau}} - 2\,\gamma_u(\tau)\, z^{(n)}_{(k+1)\tau} - 1, \tag{12}$$

for $u \in \{s, q\}$, respectively. Following Augustyniak et al. (2023), we show in Appendix A.1 that the n-augmented version of the HN(C) model belongs to the affine family introduced in Assumption 1. Moreover, as demonstrated in Appendix A.2.3, solving the martingale constraints (8) and (9) yields the following relationship between the risk preference parameters (see Equation (A.17)):

$$\theta(\tau) = -\frac{1}{2} - \frac{\lambda(\tau)}{\tau} + 2\boldsymbol{\xi}(\tau)^{\top}\left(\frac{\lambda(\tau)\boldsymbol{\alpha}(\tau)}{\tau} + \frac{\boldsymbol{\alpha}(\tau)\odot\boldsymbol{\gamma}(\tau)}{\sqrt{\tau}}\right).$$

2.2.2. *The Inverse Gaussian GARCH Component Model.* The inverse Gaussian GARCH component model, denoted by IG(C) henceforth, was introduced by Babaoğlu et al. (2018). It is an extension of the affine one-component GARCH model driven by inverse Gaussian innovations proposed by Christoffersen et al. (2006). We denote the inverse Gaussian distribution by $\mathcal{IG}$, and we define

$$z^{(n)}_{(k+1)\tau} = \eta\,\epsilon^{(n)}_{(k+1)\tau} - \frac{h^{(n)}_{k\tau}}{\eta}, \qquad \epsilon^{(n)}_{(k+1)\tau} \,\big|\, \mathcal{F}^{(n)}_{k\tau} \sim \mathcal{IG}\left(\frac{h^{(n)}_{k\tau}}{\eta^2}, \frac{h^{(n)}_{k\tau}}{\eta^2}\right),$$

where $\epsilon^{(n)}_{(k+1)\tau}$ has a single parameter inverse Gaussian distribution with conditional mean and variance equal to $h^{(n)}_{k\tau}/\eta^2$. It follows that $z^{(n)}_{(k+1)\tau}$ has a shifted inverse Gaussian distribution with mean zero and variance $h^{(n)}_{k\tau}$ conditionally on $\mathcal{F}^{(n)}_{k\tau}$. The skewness of the distribution of $\epsilon^{(n)}_{(k+1)\tau}$ is given by $3|\eta| \Big/ \sqrt{h^{(n)}_{k\tau}}$, so that η is usually called the skewness parameter. In practice, η is negative, so that although $\epsilon^{(n)}_{(k+1)\tau}$ is

Downloaded from https://www.cambridge.org/core. UNIVERSIDAD AUTONOMA METROPOLITANA, on 14 Nov 2026 at 21:01:13, subject to the Cambridge Core terms of use, available at https://www.cambridge.org/core/terms. https://doi.org/10.1017/S0266466626100607

a positive random variable, the term $z^{(n)}_{(k+1)\tau}$ can generate both positive and negative returns (see Christoffersen et al., 2006, for more details on the inverse Gaussian models). The IG(C) model relies on the following specifications for $F^{\mathcal{IG}}$ and $G^{\mathcal{IG}}$[9]:

$$F^{\mathcal{IG}}\left(h^{(n)}_{k\tau};\lambda(\tau)\right)=\left(\lambda(\tau)+\frac{\sqrt{\tau}}{\eta}-\frac{\tau}{\eta}\right)h^{(n)}_{k\tau}, \tag{13}$$

$$G^{\mathcal{IG}}\left(z^{(n)}_{(k+1)\tau},h^{(n)}_{k\tau};\gamma_u(\tau)\right)=\gamma_u(\tau)\frac{z^{(n)}_{(k+1)\tau}}{\eta}-\frac{\eta^3 h^{(n)}_{k\tau}z^{(n)}_{(k+1)\tau}}{\eta z^{(n)}_{(k+1)\tau}+h^{(n)}_{k\tau}}-\eta^4. \tag{14}$$

We again show in Appendix A.1 that the n-augmented version of the IG(C) model belongs to the affine class of Assumption 1. Moreover, Section SM.D.3 of the Supplementary Material establishes that the martingale constraints (8) and (9) result in the following relationship:

$$\theta(\tau)=\frac{1-2\boldsymbol{\xi}(\tau)^\top(\boldsymbol{\alpha}(\tau)\odot\boldsymbol{\gamma}(\tau))}{2\eta\sqrt{\tau}}-\frac{\left(\eta(\eta\lambda(\tau)-\tau)^2+2\sqrt{\tau}\left(1-2\eta^4\boldsymbol{\xi}(\tau)^\top\boldsymbol{\alpha}(\tau)\right)\right)^2}{8\eta\sqrt{\tau}(\eta\lambda(\tau)-\tau)^2\left(1-2\eta^4\boldsymbol{\xi}(\tau)^\top\boldsymbol{\alpha}(\tau)\right)}.$$

2.2.3. *Relationship between the Gaussian and Inverse Gaussian GARCH Models.* Proposition 1 shows that the HN(C) model can be obtained as a limiting case of the IG(C) model by letting the skewness parameter η go to zero under specific relationships between the parameters of the two models. The same result holds for one-component versions of these models.[10]

PROPOSITION 1. *For any fixed $k=0,\ldots,nT-1$, the $\mathcal{F}^{(n)}_{k\tau}$-conditional joint cgf of $\Delta Y^{(n)}_{(k+1)\tau}$, $\Delta s^{(n)}_{(k+1)\tau}$, and $\Delta q^{(n)}_{(k+1)\tau}$ in the IG(C) model converges to the corresponding joint cgf in the HN(C) model as η approaches zero, if the following parametric relationships hold between the two classes of models:*

$$\lambda^{\mathcal{IG}}(\tau)=\lambda^{\mathcal{N}}(\tau)-\frac{\sqrt{\tau}}{\eta}+\frac{\tau}{\eta},\qquad \sigma^{\mathcal{IG}}(\tau)=\sigma^{\mathcal{N}}(\tau),\qquad \boldsymbol{\phi}^{\mathcal{IG}}(\tau)=\boldsymbol{\phi}^{\mathcal{N}}(\tau),$$
$$\boldsymbol{\alpha}^{\mathcal{IG}}(\tau)=\eta^{-4}\boldsymbol{\alpha}^{\mathcal{N}}(\tau),\qquad \boldsymbol{\gamma}^{\mathcal{IG}}(\tau)=\eta^4\mathbf{1}-2\eta^5\boldsymbol{\gamma}^{\mathcal{N}}(\tau). \tag{15}$$

The superscripts $\mathcal{N}$ and $\mathcal{IG}$ on a parameter signify that the parameter corresponds to the HN(C) and IG(C) models, respectively.

Proof. See Section SM.D.1 of the Supplementary Material. □

[9]Note that, for notational consistency, we express the variance dynamics with respect to the noise $z^{(n)}_{(k+1)\tau}$ instead of $\epsilon^{(n)}_{(k+1)\tau}$, which differs from the usual representation used in Christoffersen et al. (2006) and Babaoğlu et al. (2018).

[10]A similar result was stated by Babaoğlu et al. (2018) for the case $\tau=1$. Based on a GARCH(2,2) representation for the two-component models, they argued that the HN(C) model can be recovered as a limiting case of the IG(C) model as η approaches zero but did not provide an explicit proof of this relationship.

Downloaded from https://www.cambridge.org/core. UNIVERSIDAD AUTONOMA METROPOLITANA, on 14 Nov 2026 at 21:01:13, subject to the Cambridge Core terms of use, available at https://www.cambridge.org/core/terms. https://doi.org/10.1017/S0266466626100607

3. MAIN RESULTS ON THE WEAK LIMITS UNDER THE PHYSICAL AND RISK-NEUTRAL MEASURES

This section presents weak diffusion limits of the affine GARCH component models introduced in Section 2 for Gaussian and inverse Gaussian specifications, under both physical and risk-neutral measures.

We denote by $\boldsymbol{X}^{(n)} = \{\boldsymbol{X}_{k\tau}^{(n)}\}_{k=0}^{nT}$ the discrete-time Markov process defined with respect to the filtration $\mathbb{F}^{(n)}$ representing the vector of our underlying processes of interest, that is, the vector $\boldsymbol{X}_{k\tau}^{(n)} = \left[\begin{array}{ccc} Y_{k\tau}^{(n)} & s_{k\tau}^{(n)} & q_{k\tau}^{(n)} \end{array}\right]^{\top}$ satisfying the dynamics of Equations (1)–(4) under measure $\boldsymbol{P}^{(n)}$.

The diffusion limits in this article are derived based on the weak convergence theorem of Markov processes to continuous-time diffusions (see Section SM.A of the Supplementary Material for details). First, we introduce the right-continuous with left limits (càdlàg) extension of the process $\boldsymbol{X}^{(n)}$:

$$\boldsymbol{X}_t^{(n)} = \boldsymbol{X}_{k\tau}^{(n)}, \qquad \text{for } k\tau \leq t < (k+1)\tau. \tag{16}$$

Assuming that $\boldsymbol{X}_0^{(n)}$ converges in distribution to a vector of random variables $\boldsymbol{X}_0$ as τ approaches zero, and provided that conditions (i)–(iii) of Theorem SM.1 in Section SM.A of the Supplementary Material are satisfied under a set of asymptotic scaling assumptions on the parameters, the process $\{\boldsymbol{X}_t^{(n)}\}_{t\in[0,T]}$ converges weakly to a three-dimensional diffusion process $\{\boldsymbol{X}_t\}_{t\in[0,T]}$, where $\boldsymbol{X}_t = \left[\begin{array}{ccc} Y_t & s_t & q_t \end{array}\right]^{\top}$. Specifically, the weak limit process satisfies the time-homogeneous stochastic differential equation (SDE)

$$d\boldsymbol{X}_t = \boldsymbol{A}(\boldsymbol{X}_t)\,dt + \boldsymbol{\Sigma}(\boldsymbol{X}_t)\,d\boldsymbol{W}_t. \tag{17}$$

Here, the process $\{\boldsymbol{W}_t\}_{t\in[0,T]}$ is a three-dimensional standard Brownian motion on the filtered probability space $(\Omega, \mathcal{F}, \mathbb{F}, \mathbb{P})$, such that $\boldsymbol{W}_t = \left[\begin{array}{ccc} W_{1,t} & W_{2,t} & W_{3,t} \end{array}\right]^{\top}$ and $W_i = \{W_{i,t}\}_{t\in[0,T]}$ are independent standard Brownian motions for $i = 1, 2, 3$.

We show that the weak limits of all affine discrete-time models considered in this study belong to the class of affine diffusion processes with coefficients having a specific representation as outlined below.[11] The drift coefficient $\boldsymbol{A}(\boldsymbol{X}_t)$ is a three-dimensional vector satisfying

$$\boldsymbol{A}(\boldsymbol{X}_t) = \boldsymbol{A}_0 + \boldsymbol{A}_1\boldsymbol{X}_t, \qquad \boldsymbol{A}_0 \in \mathbb{R}^3,\ \boldsymbol{A}_1 \in \mathbb{R}^{3\times 3}. \tag{18}$$

The diffusion coefficient $\boldsymbol{\Sigma}(\boldsymbol{X}_t)$ is a 3×3 lower triangular matrix which admits the decomposition

$$\boldsymbol{\Sigma}(\boldsymbol{X}_t) = \boldsymbol{\Gamma}\boldsymbol{V}(\boldsymbol{X}_t), \tag{19}$$

[11] The continuous-time process $\boldsymbol{X}$ which satisfies the SDE in Equation (17) is called affine if the $\mathcal{F}_t$-conditional cf of $\boldsymbol{X}_T$ has an exponential affine structure or equivalently if $\boldsymbol{A}(\boldsymbol{x})$ and $\boldsymbol{\Sigma}(\boldsymbol{x})\boldsymbol{\Sigma}^{\top}(\boldsymbol{x})$ are affine functions of $\boldsymbol{x}$. Following Filipović and Mayerhofer (2009), Section SM.B of the Supplementary Material presents necessary and sufficient conditions for a solution $\boldsymbol{X}$ of Equation (17) to be an affine process.

Downloaded from https://www.cambridge.org/core. UNIVERSIDAD AUTONOMA METROPOLITANA, on 14 Nov 2026 at 21:01:13, subject to the Cambridge Core terms of use, available at https://www.cambridge.org/core/terms. https://doi.org/10.1017/S0266466626100607

where $\mathbf{\Gamma}$ is a 3×3 lower triangular matrix of scalars and $\boldsymbol{V}(\boldsymbol{X}_t)$ is a 3×3 diagonal matrix with the i^{th} diagonal element having a square-root representation

$$V_i(\boldsymbol{X}_t) = \sqrt{v_{0,i} + \boldsymbol{v}_{1,i}^{\top} \boldsymbol{X}_t}, \tag{20}$$

with $v_{0,i} \in \mathbb{R}$ and $\boldsymbol{v}_{1,i} \in \mathbb{R}^3$ for any $i = 1, 2, 3$. Equation (17) admits a unique (strong) solution $\boldsymbol{X} = \{\boldsymbol{X}_t\}_{t \in [0,T]}$ under certain assumptions on the drift and diffusion coefficients (e.g., multidimensional Feller conditions). See Appendix A.2.2 for further details on these constraints in our specific setting.

The drift and diffusion coefficients in Equation (17) are model dependent, and we therefore augment them with the superscript $\mathcal{D}$ when referring to the weak limits of our Gaussian and inverse Gaussian specifications, that is, $\mathcal{D} = \mathcal{N}$ and $\mathcal{D} = \mathcal{IG}$, respectively. These coefficients are determined based on the scaling assumptions imposed on the discrete-time model parameters as the time step τ approaches zero.

3.1. Asymptotic Scaling Assumptions Imposed on the Parameters

The asymptotic scaling assumptions imposed on the parameters to derive the weak diffusion limits of the affine GARCH component models introduced in Section 2 are summarized in Assumption 3.

Assumption 3. The equity risk premium and conditional variance parameters of the HN(C) and IG(C) models satisfy the following limiting constraints as the time step τ approaches zero.

A. Convergence Rates Governing First-Order Conditional Moments of $\boldsymbol{X}^{(n)}$:

$$\lambda = \begin{cases} \lim\limits_{\tau \to 0} \tau^{-1} \lambda(\tau) & \text{for HN(C)} \\ \lim\limits_{\tau \to 0} \tau^{-1} \left(\lambda(\tau) + \dfrac{\sqrt{\tau}}{\eta} - \dfrac{\tau}{\eta} \right) & \text{for IG(C)} \end{cases},$$

$$\sigma^2 = \lim_{\tau \to 0} \sigma^2(\tau), \qquad \boldsymbol{\kappa} = \lim_{\tau \to 0} \tau^{-1} \left(\mathbf{1} - \boldsymbol{\phi}(\tau) \right).$$

B. Convergence Rates Governing Second-Order Conditional Moments of $\boldsymbol{X}^{(n)}$:

$$\boldsymbol{\alpha} = \lim_{\tau \to 0} \tau^{-\frac{1}{2}} \boldsymbol{\alpha}(\tau), \qquad \boldsymbol{\gamma} = \lim_{\tau \to 0} \boldsymbol{\gamma}(\tau).$$

All limits are assumed to be finite and in the following admissible ranges: $\lambda \in \mathbb{R}$, $\sigma^2 > 0$, $\boldsymbol{\kappa} > \mathbf{0}$, $\boldsymbol{\alpha} \geq \mathbf{0}$, and $\boldsymbol{\gamma} \in \mathbb{R}^2$.

First, notice that the first limiting constraint of Assumption 3A on the equity risk premium parameter $\lambda(\tau)$ is the only constraint that differs between the HN(C) and IG(C) specifications. Its role is to ensure that the risk premium term $F^{\mathcal{D}}$ in Equation (1) is of order $O(\tau)$ for both models, which guarantees the convergence of the first-order conditional moment of the return process. The remaining constraints of Assumption 3A govern the convergence of the first-order conditional moment

Downloaded from https://www.cambridge.org/core. UNIVERSIDAD AUTONOMA METROPOLITANA, on 14 Nov 2026 at 21:01:13, subject to the Cambridge Core terms of use, available at https://www.cambridge.org/core/terms. https://doi.org/10.1017/S0266466626100607

of the variance components, while Assumption 3B ensures the convergence of all quantities from the conditional covariance matrix of $\boldsymbol{X}^{(n)}$. Overall, Assumption 3 preserves the first- and second-order moment structure of the underlying discrete-time process as τ approaches zero, in the sense that the drift and covariance matrix of the diffusion limit process $\boldsymbol{X}$ exhibit the same functional representations as the corresponding conditional moments of $\boldsymbol{X}^{(n)}$ (see Appendix A.2.2 for more details).

We remark that it is straightforward to specify some functions $\lambda(\tau)$, $\sigma^2(\tau)$, $\boldsymbol{\phi}(\tau)$, $\boldsymbol{\alpha}(\tau)$, and $\boldsymbol{\gamma}(\tau)$ that satisfy the limiting constraints from Assumption 3. For example, we can set

$$\lambda(\tau) = \begin{cases} \tau\lambda & \text{for HN(C)} \\ \tau\left(\lambda + \dfrac{1}{\eta}\right) - \dfrac{\sqrt{\tau}}{\eta} & \text{for IG(C),} \end{cases}$$
$$\sigma^2(\tau) = \sigma^2, \quad \boldsymbol{\phi}(\tau) = \mathbf{1} - \tau\boldsymbol{\kappa}, \quad \boldsymbol{\alpha}(\tau) = \sqrt{\tau}\boldsymbol{\alpha}, \quad \boldsymbol{\gamma}(\tau) = \boldsymbol{\gamma}. \tag{21}$$

The convergence rates proposed in Assumption 3 align with those used by Nelson (1990) and Duan (1997) for establishing weak limits across a large plethora of non-affine GARCH models. In Section 4, we shall discuss the use of alternative convergence rates—including those previously adopted by the affine GARCH literature—for one-component Gaussian models. More specifically, we shall explain that the rates postulated in Assumption 3 lead to the most general diffusion dynamics and are the only ones capable of preserving the (conditional) moment structure of the underlying discrete-time affine process.

To conclude this section, we introduce a distributional invariant asymptotic constraint on the parameters governing the change of measure.

Assumption 4. The risk preference parameters in Equation (7) satisfy the following limiting relationship:

$$\boldsymbol{\xi} = \lim_{\tau \to 0} \boldsymbol{\xi}(\tau),$$

where $\boldsymbol{\xi} \in \mathbb{R}^2$ is finite.

Assumption 4 is required to establish the weak limits of the HN(C) and IG(C) models under the risk-neutral measure, or equivalently, the convergence of the Radon–Nikodym process.[12] As mentioned in Section 2.1, we can express $\theta(\tau)$ as a function of $\boldsymbol{\xi}(\tau)$ by solving Equations (8) and (9). Interestingly, the value of the equity risk preference parameter $\theta(\tau)$ is dependent on the discretization step and has a finite nonzero limit for both HN(C) and IG(C) models. For additional details, see Equations (A.17) and (A.18) in Appendix A.2.3 as well as Equations (SM.7) and (SM.8) in the Supplementary Material, respectively.

[12]Note that both types of convergence are equivalent for most discrete-time models and ensure the convergence of various derivative prices under mild continuity and uniform integrability constraints of the payoff function. The theoretical foundation for weak convergence of options prices and hedge ratios using the latter approach has been provided by Prigent (2003). Yet, the asymptotic results in the GARCH option pricing literature are typically based on deriving the weak limits of the underlying asset price process under a given risk-neutral measure, and this is also the approach used in our article.

Downloaded from https://www.cambridge.org/core. UNIVERSIDAD AUTONOMA METROPOLITANA, on 14 Nov 2026 at 21:01:13, subject to the Cambridge Core terms of use, available at https://www.cambridge.org/core/terms. https://doi.org/10.1017/S0266466626100607

3.2. Weak Limits

The key ingredient for the computation of the drift and diffusion terms in Equation (17) within an affine setting is the asymptotic evaluation of the cross-cumulants of the underlying discrete-time process. Specifically, we can obtain these coefficients by computing partial derivatives of the conditional cgf of $\Delta \boldsymbol{X}_{k\tau}^{(n)}$ evaluated at zero, and then taking their limits as τ approaches zero (see Appendix A.2.1 for more details). Although the dynamics of Equations (1)–(4) can also be used directly to compute the weak limits under the physical measure $\mathbb{P}^{(n)}$, our approach does not require the a priori derivation of the risk-neutral dynamics of $\Delta \boldsymbol{X}_{k\tau}^{(n)}$ for identifying the weak limits under $\mathbb{Q}^{(n)}$.

3.2.1. *Weak Limits under the Physical Measure.* The diffusion limits of the HN(C) and IG(C) models under the physical measure are presented in Proposition 2.[13]

PROPOSITION 2. *Assume that* $\left\{\boldsymbol{X}_{k\tau}^{(n)}\right\}_{k=0}^{nT}$ *follows the dynamics of Equations (1)–(4) under measure* $\mathbb{P}^{(n)}$*, that Assumption 3 holds, and let* $h_t = s_t + q_t$*. Then, as* τ *approaches zero, the process* $\{\boldsymbol{X}_t^{(n)}\}_{t\in[0,T]}$ *introduced in Equation (16) converges weakly to a three-dimensional diffusion process* $\{\boldsymbol{X}_t\}_{t\in[0,T]}$ *governed by the SDE of Equation (17),*

$$d\boldsymbol{X}_t = \boldsymbol{A}^{\mathcal{D}}(\boldsymbol{X}_t)\,dt + \boldsymbol{\Sigma}^{\mathcal{D}}(\boldsymbol{X}_t)\,d\boldsymbol{W}_t,$$

with drift and diffusion coefficients given by:

(i) *For the HN(C) model:*

$$\boldsymbol{A}^{\mathcal{N}}(\boldsymbol{X}_t) = \begin{bmatrix} r + \lambda h_t \\ -\kappa_s s_t \\ \kappa_q\left(\sigma^2 - q_t\right) \end{bmatrix}, \qquad \boldsymbol{\Sigma}^{\mathcal{N}}(\boldsymbol{X}_t) = \begin{bmatrix} \sqrt{h_t} & 0 & 0 \\ -2\alpha_s\gamma_s\sqrt{h_t} & \sqrt{2}\alpha_s & 0 \\ -2\alpha_q\gamma_q\sqrt{h_t} & \sqrt{2}\alpha_q & 0 \end{bmatrix}. \tag{22}$$

(ii) *For the IG(C) model:*

$$\boldsymbol{A}^{\mathcal{IG}}(\boldsymbol{X}_t) = \begin{bmatrix} r + \lambda h_t \\ -\kappa_s s_t \\ \kappa_q\left(\sigma^2 - q_t\right) \end{bmatrix}, \quad \boldsymbol{\Sigma}^{\mathcal{IG}}(\boldsymbol{X}_t) = \begin{bmatrix} \sqrt{h_t} & 0 & 0 \\ \dfrac{\alpha_s\left(\gamma_s - \eta^4\right)}{\eta}\sqrt{h_t} & \sqrt{2}\eta^4\alpha_s & 0 \\ \dfrac{\alpha_q\left(\gamma_q - \eta^4\right)}{\eta}\sqrt{h_t} & \sqrt{2}\eta^4\alpha_q & 0 \end{bmatrix}. \tag{23}$$

[13] These limits are identified from the convergence of the first two conditional moments of the underlying discrete-time process using Theorem SM.1 in the Supplementary Material. Whenever the coefficients of the limiting SDE are defined only on the state domain where the aggregate variance is positive (i.e., $h_t > 0$), the convergence is understood locally, up to the first exit from this domain. Equivalently, the convergence results apply to the corresponding stopped processes.

Downloaded from https://www.cambridge.org/core. UNIVERSIDAD AUTONOMA METROPOLITANA, on 14 Nov 2026 at 21:01:13, subject to the Cambridge Core terms of use, available at https://www.cambridge.org/core/terms. https://doi.org/10.1017/S0266466626100607

Proof. See Appendix A.2.2 and Section SM.D.2 of the Supplementary Material. □

The SDEs derived in Proposition 2 as the weak limits of the HN(C) and IG(C) models do not, in general, define SV models whose variance process can be guaranteed to remain nonnegative along all sample paths. This is due to the constant loading coefficient of the second Brownian motion in the limiting dynamics of the component factors s_t and q_t, which implies that these components cannot in general be constrained to be nonnegative with probability one. In particular, Appendix A.2.2 shows that the multidimensional Feller-type sufficient conditions of Duffie and Kan (1996) are generally not fully satisfied by the diffusion limits in Proposition 2. However, this issue is not specific to the limiting dynamics and is also present in the underlying discrete-time component GARCH models (see, e.g., Majewski et al., 2015; Oh and Park, 2023). Indeed, in these models, the short-run variance component can take negative values. In applications, however, the long-run component typically compensates for such movements so that the aggregate conditional variance remains positive along the realized path. The weak limiting result in Proposition 2 should therefore be interpreted as a local approximation on the domain where $h_t > 0$.

Moreover, both diffusion limits fit the continuous-time affine framework of Equations (18)–(20). For example, in the HN(C) case, the coefficients $\boldsymbol{A}_0$ and $\boldsymbol{A}_1$ from the drift term are given by

$$\boldsymbol{A}_0 = \begin{bmatrix} r \\ 0 \\ \kappa_q \sigma^2 \end{bmatrix}, \qquad \boldsymbol{A}_1 = \begin{bmatrix} 0 & \lambda & \lambda \\ 0 & -\kappa_s & 0 \\ 0 & 0 & -\kappa_q \end{bmatrix},$$

while the matrices $\boldsymbol{\Gamma}$ and $\boldsymbol{V}(\boldsymbol{X}_t)$ from the diffusion term decomposition are given by

$$\boldsymbol{\Gamma} = \begin{bmatrix} 1 & 0 & 0 \\ -2\alpha_s\gamma_s & \sqrt{2}\alpha_s & 0 \\ -2\alpha_q\gamma_q & \sqrt{2}\alpha_q & 0 \end{bmatrix},$$

$$\boldsymbol{V}(\boldsymbol{X}_t) = \begin{bmatrix} \sqrt{v_{0,1} + \boldsymbol{v}_{1,1}^\top \boldsymbol{X}_t} & 0 & 0 \\ 0 & \sqrt{v_{0,2} + \boldsymbol{v}_{1,2}^\top \boldsymbol{X}_t} & 0 \\ 0 & 0 & \sqrt{v_{0,3} + \boldsymbol{v}_{1,3}^\top \boldsymbol{X}_t} \end{bmatrix},$$

with $v_{0,1} = 0$ and $\boldsymbol{v}_{1,1} = \begin{bmatrix} 0 & 1 & 1 \end{bmatrix}^\top$, $v_{0,j} = 1$ and $\boldsymbol{v}_{1,j} = \begin{bmatrix} 0 & 0 & 0 \end{bmatrix}^\top$ for $j = 2, 3$, so that $V_1(\boldsymbol{X}_t) = \sqrt{h_t}$, $V_2(\boldsymbol{X}_t) = V_3(\boldsymbol{X}_t) = 1$. The drift and diffusion coefficients for the IG(C) limit have a similar structure.

Downloaded from https://www.cambridge.org/core. UNIVERSIDAD AUTONOMA METROPOLITANA, on 14 Nov 2026 at 21:01:13, subject to the Cambridge Core terms of use, available at https://www.cambridge.org/core/terms. https://doi.org/10.1017/S0266466626100607

In addition, both diffusion limits correspond to three-dimensional degenerate SV models.[14] Although the limiting SDE is written in the generic form of Equation (17) with a three-dimensional Brownian motion, the diffusion matrices $\boldsymbol{\Sigma}^{\mathcal{N}}(\boldsymbol{X}_t)$ and $\boldsymbol{\Sigma}^{\mathcal{IG}}(\boldsymbol{X}_t)$ are singular of rank two because their third column is identically zero. Hence, the third Brownian motion in the generic representation is redundant, and the limiting dynamics admit an equivalent formulation in terms of two independent Brownian motions only. However, this rank deficiency does not imply that one of the state equations becomes deterministic. The short- and long-run variance components are mean-reverting stochastic processes driven by two independent Brownian motions, one of which also drives the return process. The presence of a second Brownian motion in each variance component, and thus in the overall variance h_t, comes in contrast with previous findings on the weak limits of one-component affine Gaussian GARCH models. These contrasting results can be explained by the use of different sets of asymptotic scaling assumptions on the model parameters and will be further analyzed in Section 4.

Interestingly, the HN(C) diffusion limit in Equation (22) coincides with that of the IG(C) model in Equation (23) if and only if the following relationships hold:

$$\lambda^{\mathcal{IG}} = \lambda^{\mathcal{N}}, \qquad \boldsymbol{\kappa}^{\mathcal{IG}} = \boldsymbol{\kappa}^{\mathcal{N}}, \qquad \sigma^{\mathcal{IG}} = \sigma^{\mathcal{N}}, \qquad \boldsymbol{\alpha}^{\mathcal{IG}} = \eta^{-4}\boldsymbol{\alpha}^{\mathcal{N}},$$
$$\boldsymbol{\gamma}^{\mathcal{IG}} = \eta^4\mathbf{1} - 2\eta^5\boldsymbol{\gamma}^{\mathcal{N}}. \tag{24}$$

The relationships of Equation (24) are similar to those that ensure the convergence of the IG(C) model to the HN(C) model as η approaches zero in Proposition 1. Indeed, under the parametric scaling specifications of Equation (21), the relationships in Equation (15) are analogous to those of Equation (24).

3.2.2. *Weak Limits under the Risk-Neutral Measure.* Proposition 3 establishes the diffusion limits of the HN(C) and IG(C) models under the risk-neutral measure.

PROPOSITION 3. *Assume that* $\{\boldsymbol{X}_{k\tau}^{(n)}\}_{k=0}^{nT}$ *follows the dynamics of Equations (1)–(4) under measure* $\mathbb{P}^{(n)}$*, and that the risk-neutral probability measure* $\mathbb{Q}^{(n)}$ *is defined via the Radon–Nikodym derivative given in Assumption 2. Moreover, suppose that Assumptions 3 and 4 hold, and let* $h_t = s_t + q_t$*. Then, as* τ *approaches zero, the process* $\{\boldsymbol{X}_t^{(n)}\}_{t\in[0,T]}$ *converges weakly to a three-dimensional diffusion process* $\{\boldsymbol{X}_t\}_{t\in[0,T]}$ *governed by the following SDE:*

$$d\boldsymbol{X}_t = \tilde{\boldsymbol{A}}^{\mathcal{D}}(\boldsymbol{X}_t)\,dt + \tilde{\boldsymbol{\Sigma}}^{\mathcal{D}}(\boldsymbol{X}_t)\,d\tilde{\boldsymbol{W}}_t. \tag{25}$$

Here, $\{\tilde{\boldsymbol{W}}_t\}_{t\in[0,T]}$ *is a three-dimensional standard Brownian motion under the risk-neutral measure, the diffusion matrix satisfies* $\tilde{\boldsymbol{\Sigma}}^{\mathcal{D}}(\boldsymbol{X}_t) = \boldsymbol{\Sigma}^{\mathcal{D}}(\boldsymbol{X}_t)$*, where* $\boldsymbol{\Sigma}^{\mathcal{D}}(\boldsymbol{X}_t)$ *is obtained from Proposition 2, and the drift term is given by:*

[14] A p-dimensional diffusion process is non-degenerate if it is driven by p mutually independent Brownian motions and its associated covariance matrix is non-singular.

Downloaded from https://www.cambridge.org/core. UNIVERSIDAD AUTONOMA METROPOLITANA, on 14 Nov 2026 at 21:01:13, subject to the Cambridge Core terms of use, available at https://www.cambridge.org/core/terms. https://doi.org/10.1017/S0266466626100607

(i) *For the HN(C) model:*

$$\tilde{\boldsymbol{A}}^{\mathcal{N}}(\boldsymbol{X}_t) = \begin{bmatrix} r - \frac{1}{2}h_t \\ -\kappa_s s_t + 2\alpha_s\gamma_s\left(\lambda + \frac{1}{2}\right)h_t + 2\alpha_s\boldsymbol{\alpha}^\top\boldsymbol{\xi} \\ \kappa_q\left(\sigma^2 - q_t\right) + 2\alpha_q\gamma_q\left(\lambda + \frac{1}{2}\right)h_t + 2\alpha_q\boldsymbol{\alpha}^\top\boldsymbol{\xi} \end{bmatrix}. \tag{26}$$

(ii) *For the IG(C) model:*

$$\tilde{\boldsymbol{A}}^{\mathcal{IG}}(\boldsymbol{X}_t) = \begin{bmatrix} r - \frac{1}{2}h_t \\ -\kappa_s s_t - \frac{\alpha_s\left(\gamma_s - \eta^4\right)}{\eta}\left(\lambda + \frac{1}{2}\right)h_t + 2\eta^8\alpha_s\boldsymbol{\alpha}^\top\boldsymbol{\xi} \\ \kappa_q\left(\sigma^2 - q_t\right) - \frac{\alpha_q\left(\gamma_q - \eta^4\right)}{\eta}\left(\lambda + \frac{1}{2}\right)h_t + 2\eta^8\alpha_q\boldsymbol{\alpha}^\top\boldsymbol{\xi} \end{bmatrix}. \tag{27}$$

Proof. See Appendix A.2.3 and Section SM.D.3 of the Supplementary Material. □

The drift coefficients of Equations (26) and (27) satisfy the general form of Equation (18), while the diffusion matrices remain unchanged after the change of measure. Consequently, the affine property of our weak limit process is preserved under the risk-neutral measure $\mathbb{Q}$ implied by the exponential affine pricing kernel of Assumption 2. Although the diffusion limit derived in Proposition 3 belongs to the affine class, it differs from the continuous-time option pricing models that are typically used in practice, such as the one in Christoffersen et al. (2009) which consists of a two-factor Heston model with uncorrelated volatility components.

Furthermore, we note that the physical and risk-neutral dynamics of Propositions 2 and 3 are consistent with Girsanov's principle. Specifically, we can recover the risk-neutral drift dynamics of Equations (26) and (27) by applying the standard change of measure provided by Girsanov's theorem to the physical dynamics implied by Equations (22) and (23), respectively, for two particular choices of market prices of risk associated with the Brownian motions governing the variance component dynamics. Indeed, we can define the Radon–Nikodym derivative with respect to the two independent Brownian motions $\{W_{1,t}\}_{t\in[0,T]}$ and $\{W_{2,t}\}_{t\in[0,T]}$ from Proposition 2 via

$$\left.\frac{d\mathbb{Q}}{d\mathbb{P}}\right|_{\mathcal{F}_T} = \exp\left(-\sum_{i=1}^{2}\left(\int_0^T \nu_{i,t}\,dW_{i,t} + \frac{1}{2}\int_0^T \nu_{i,t}^2\,dt\right)\right),$$

which yields the risk-neutral dynamics of Proposition 3 if

$$\nu_{1,t} = \sqrt{h_t}\left(\lambda + \frac{1}{2}\right) \qquad \text{and} \qquad \nu_{2,t} = \begin{cases} -\sqrt{2}\boldsymbol{\alpha}^\top\boldsymbol{\xi} & \text{for HN(C)} \\ -\sqrt{2}\eta^4\boldsymbol{\alpha}^\top\boldsymbol{\xi} & \text{for IG(C).} \end{cases}$$

Downloaded from https://www.cambridge.org/core. UNIVERSIDAD AUTONOMA METROPOLITANA, on 14 Nov 2026 at 21:01:13, subject to the Cambridge Core terms of use, available at https://www.cambridge.org/core/terms. https://doi.org/10.1017/S0266466626100607

This result can be easily verified for each model by defining two independent standard Brownian motions under Q, $\{\tilde{W}_{1,t}\}_{t\in[0,T]}$ and $\{\tilde{W}_{2,t}\}_{t\in[0,T]}$, with dynamics given by $d\tilde{W}_{i,t} = dW_{i,t} + \nu_{i,t}\,dt$ for $i = 1, 2$. Thus, it comes as no surprise that, similarly to the physical measure case, the resulting risk-neutral diffusion limits of Equations (26) and (27) are identical if and only if the relationships of Equation (24) hold.

To conclude this section, we derive the cf of the risk-neutral diffusion limit obtained in Proposition 3. Such a function is typically required for the valuation of European-style derivatives in continuous time. Proposition 4 provides the $\mathcal{F}_t$-conditional risk-neutral cf of $\boldsymbol{X}_T$ associated with the HN(C) limit. The corresponding cf in the IG(C) case can be obtained in a similar way by using the parametric relationships of Equation (24).

PROPOSITION 4. *Assume that the three-dimensional diffusion process* $\{\boldsymbol{X}_t\}_{t\in[0,T]}$ *with* $\boldsymbol{X}_t = [\, Y_t \quad s_t \quad q_t \,]^\top$ *satisfies the SDE of Equation (25) with drift* $\tilde{\boldsymbol{A}}^{\mathcal{N}}(\boldsymbol{X}_t)$ *given in Equation (26) and diffusion matrix* $\tilde{\boldsymbol{\Sigma}}^{\mathcal{N}}(\boldsymbol{X}_t) = \boldsymbol{\Sigma}^{\mathcal{N}}(\boldsymbol{X}_t)$ *given in Proposition 2. Then, for any* $\boldsymbol{u} \in \mathbb{R}^3$, *the* $\mathcal{F}_t$*-conditional cf of* $\boldsymbol{X}_T$ *is*

$$\chi^{\mathbb{Q}}_{\boldsymbol{X}_T}(\boldsymbol{u}\,|\,\mathcal{F}_t) = E^{\mathbb{Q}}\left[\exp\left(\mathrm{i}\boldsymbol{u}^\top \boldsymbol{X}_T\right)\,\middle|\,\mathcal{F}_t\right] = \exp\left(\Phi(\boldsymbol{u}; T-t) + \boldsymbol{\Psi}(\boldsymbol{u}; T-t)^\top \boldsymbol{X}_t\right).$$

Here, $\Phi(\boldsymbol{u}; T-t)$ *and* $\boldsymbol{\Psi}(\boldsymbol{u}; T-t) = [\, \Psi_1(\boldsymbol{u}; T-t) \quad \Psi_2(\boldsymbol{u}; T-t) \quad \Psi_3(\boldsymbol{u}; T-t)]^\top$ *are complex-valued functions satisfying the following system of ordinary differential equations (ODEs):*

$$\begin{aligned}
\partial_t \Phi(\boldsymbol{u}; t) &= r\Psi_1(\boldsymbol{u}; t) + 2\alpha_s \boldsymbol{\alpha}^\top \boldsymbol{\xi} \Psi_2(\boldsymbol{u}; t) + \left(\kappa_q \sigma^2 + 2\alpha_q \boldsymbol{\alpha}^\top \boldsymbol{\xi}\right) \Psi_3(\boldsymbol{u}; t) \\
&\quad + \left(\alpha_s \Psi_2(\boldsymbol{u}; t) + \alpha_q \Psi_3(\boldsymbol{u}; t)\right)^2, \\
\partial_t \Psi_1(\boldsymbol{u}; t) &= 0, \\
\partial_t \Psi_2(\boldsymbol{u}; t) &= -\frac{1}{2}\Psi_1(\boldsymbol{u}; t) + \left(-\kappa_s + 2\alpha_s\gamma_s\left(\lambda + \frac{1}{2}\right)\right)\Psi_2(\boldsymbol{u}; t) \\
&\quad + 2\alpha_q\gamma_q\left(\lambda + \frac{1}{2}\right)\Psi_3(\boldsymbol{u}; t) \\
&\quad + \frac{1}{2}\left(\Psi_1(\boldsymbol{u}; t) - 2\left(\alpha_s\gamma_s\Psi_2(\boldsymbol{u}; t) + \alpha_q\gamma_q\Psi_3(\boldsymbol{u}; t)\right)\right)^2, \\
\partial_t \Psi_3(\boldsymbol{u}; t) &= -\frac{1}{2}\Psi_1(\boldsymbol{u}; t) + 2\alpha_s\gamma_s\left(\lambda + \frac{1}{2}\right)\Psi_2(\boldsymbol{u}; t) \\
&\quad + \left(-\kappa_q + 2\alpha_q\gamma_q\left(\lambda + \frac{1}{2}\right)\right)\Psi_3(\boldsymbol{u}; t) \\
&\quad + \frac{1}{2}\left(\Psi_1(\boldsymbol{u}; t) - 2\left(\alpha_s\gamma_s\Psi_2(\boldsymbol{u}; t) + \alpha_q\gamma_q\Psi_3(\boldsymbol{u}; t)\right)\right)^2,
\end{aligned}$$

subject to the boundary constraints $\Phi(\boldsymbol{u}; 0) = 0$ *and* $\boldsymbol{\Psi}(\boldsymbol{u}; 0) = \mathrm{i}\boldsymbol{u}$.

Downloaded from https://www.cambridge.org/core. UNIVERSIDAD AUTONOMA METROPOLITANA, on 14 Nov 2026 at 21:01:13, subject to the Cambridge Core terms of use, available at https://www.cambridge.org/core/terms. https://doi.org/10.1017/S0266466626100607

Proof. See Section SM.B of the Supplementary Material. □

We remark that although the second ODE can be solved explicitly (i.e., $\Psi_1(\boldsymbol{u};t) = \mathrm{i}u_1$), the remaining system of quadratic ODEs for the coefficients $\Psi_2(\boldsymbol{u};t)$ and $\Psi_3(\boldsymbol{u};t)$ does not generally admit a closed-form solution, so one has to rely on numerical approximations to compute these coefficients (e.g., Runge–Kutta method). Nevertheless, explicit solutions can be obtained in specific cases, such as when there are no leverage effects (i.e., $\gamma_s = \gamma_q = 0$) or in the single-component case. In the latter instance, the system of ODEs can be solved in a similar fashion as that of the model of Heston (1993).

3.3. A Numerical Illustration of the Weak Limits

We now illustrate the impact of weak convergence limits of discrete-time affine GARCH models driven by both Gaussian and inverse Gaussian innovations on option prices. Specifically, we compute European call prices for the HN(C) and IG(C) models introduced in Section 2, risk-neutralized with the pricing kernel from Assumption 2, for different values of the number of discretization points per day n. The corresponding diffusion limit prices are obtained using the risk-neutral dynamics derived in Proposition 3.

European option prices can be expressed in semi-closed-form using Laplace or Fourier inversion methods for all discrete- and continuous-time affine models introduced in Sections 2 and 3. Indeed, the price at time $t \in \mathcal{T}^{(1)}$ of a K-strike European call option with maturity T is given by the integral representation (see, e.g., Augustyniak et al., 2023)

$$\begin{aligned}\mathrm{C}(\boldsymbol{X}_t^{(n)};K,T) &= e^{-r(T-t)}\, E^{\mathbb{Q}^{(n)}}\left[\max\left(e^{Y_T^{(n)}} - K, 0\right)\middle|\, \mathcal{F}_t^{(n)}\right] \\ &= \frac{e^{-r(T-t)}}{2\pi\mathrm{i}} \int_{R-\mathrm{i}\infty}^{R+\mathrm{i}\infty} \frac{\exp\left(\mathcal{C}_{Y_T^{(n)}}^{\mathbb{Q}^{(n)}}\left(z\,\middle|\,\mathcal{F}_t^{(n)}\right)\right) K^{1-z}}{(z(z-1))}\, dz.\end{aligned}$$

Here, $\mathcal{C}_{Y_T^{(n)}}^{\mathbb{Q}^{(n)}}\left(z\,\middle|\,\mathcal{F}_t^{(n)}\right)$ is the cgf of $Y_T^{(n)}$ conditional on $\mathcal{F}_t^{(n)}$, $R > 1$ is a chosen constant, and the integration is performed along the vertical line $\{z \in \mathbb{C} : \mathrm{Re}(z) = R\}$ in the complex plane.[15] The corresponding continuous-time limit prices are computed based on a similar integral representation with the $\mathcal{F}_t$-conditional cf of $\boldsymbol{X}_T$ under the risk-neutral measure $\mathbb{Q}$ derived in Proposition 4.

The parameters for the HN(C) model at the daily frequency ($\tau = 1$) are taken from Augustyniak et al. (2023), where they were estimated from S&P 500 returns

[15]The computation of this cgf follows the procedure developed by Augustyniak et al. (2023) for general affine discrete-time settings and for completeness is illustrated in Section SM.C of the Supplementary Material. Moreover, we rely on the trapezoidal rule to numerically evaluate the above integral (see Černỳ, 2004, for details).

Downloaded from https://www.cambridge.org/core. UNIVERSIDAD AUTONOMA METROPOLITANA, on 14 Nov 2026 at 21:01:13, subject to the Cambridge Core terms of use, available at https://www.cambridge.org/core/terms. https://doi.org/10.1017/S0266466626100607

and options data over 1996–2018 using a sequential maximum likelihood estimation method. Parameters for other time steps are obtained based on the scaling constraints in Equation (21), and we assume that the variance risk preference parameters are invariant to the discretization step, setting $\boldsymbol{\xi}(\tau) = \boldsymbol{\xi}$ for all τ, which is consistent with the limiting behavior specified in Assumption 4. We consider two pricing kernels: a monotonic kernel with $\boldsymbol{\xi} = \mathbf{0}$ and a non-monotonic kernel with $\boldsymbol{\xi}$ estimated from market data following Augustyniak et al. (2023). All parameter values for the HN(C) model with $\tau = 1$ are reported in the note of Table 1. Moreover, the IG(C) parameters are obtained by setting $\eta = -0.01$ and applying the relationships from Proposition 1, so that the diffusion limits of both Gaussian and inverse Gaussian specifications coincide under the physical and risk-neutral measures. Unless stated otherwise, we assume an annualized risk-free rate of 2% (based on 252 trading days), an initial log-price $Y_t^{(n)} = \log(100)$, and initial values of the short- and long-run variance components equal to their respective unconditional means.

Table 1 reports the convergence of these European call option prices for three moneyness levels: in-the-money options ($K = 90$), at-the-money options ($K = 100$), and out-of-the-money options ($K = 110$), and three times to maturity: 3-month, 6-month, and 1-year. We notice that all discretized GARCH option prices converge smoothly to their corresponding diffusion limits. For any value of n, the HN(C) prices are consistently lower than the IG(C) counterparts, except for the shorter-term out-of-the-money options. As expected, when the constraints of Proposition 1 are satisfied, the weak limits of the HN(C) and IG(C) models are the same, and thus the limiting prices are identical, regardless of the shape of the pricing kernel (see, e.g., Panels A and C for monotonic pricing kernels, and Panels B and D for non-monotonic pricing kernels). The speed at which they converge to the limiting prices is however different—for the models exhibiting skewness, it generally takes more time for the prices to get closer to their limiting values.

The monotonic pricing kernel leads to limit prices that are less than those obtained with the non-monotonic pricing kernel, this being a by-product of the terms related to $\boldsymbol{\xi}$ in the drifts of Equations (26) and (27). Moreover, GARCH-based option prices computed at daily frequency (i.e., $\tau = 1$) are closer to their corresponding diffusion limit prices for monotonic pricing kernels. For example, for the HN(C) model in Panel A, the smallest (largest) absolute difference for monotonic pricing kernels is \$0.001 (\$0.015). In contrast, the smallest (largest) absolute difference for the non-monotonic counterparts is \$0.172 (\$0.752) as shown in Panel B. This feature can be explained by the nonzero variance risk-preference parameter $\boldsymbol{\xi}(\tau)$ assumed in the non-monotonic pricing kernels. Specifically, these kernels introduce a wedge between the physical and risk-neutral conditional variances for the discrete-time models, since $V^{\mathbb{Q}^{(n)}}[\Delta Y_{t+\tau}^{(n)} \mid \mathcal{F}_t^{(n)}] = \pi(\tau) V^{\mathbb{P}^{(n)}}[\Delta Y_{t+\tau}^{(n)} \mid \mathcal{F}_t^{(n)}]$, for $t \in \mathcal{T}^{(n)}$, with $\pi(\tau) > 1$. Thus, when $n = \tau = 1$, the GARCH conditional risk-neutral variance is larger than the physical one; however, in the limit, the discrepancy between the two variances vanishes, as

Downloaded from https://www.cambridge.org/core. UNIVERSIDAD AUTONOMA METROPOLITANA, on 14 Nov 2026 at 21:01:13, subject to the Cambridge Core terms of use, available at https://www.cambridge.org/core/terms. https://doi.org/10.1017/S0266466626100607

Downloaded from https://www.cambridge.org/core. UNIVERSIDAD AUTONOMA METROPOLITANA, on 14 Nov 2026 at 21:01:13, subject to the Cambridge Core terms of use, available at https://www.cambridge.org/core/terms. https://doi.org/10.1017/S0266466626100607

TABLE 1. Call option price convergence for the HN(C) and IG(C) models

Panel A: HN(C) model with a monotonic pricing kernel

	In-the-money ($K = 90$)			At-the-money ($K = 100$)			Out-of-the-money ($K = 110$)		
n	3-month	6-month	1-year	3-month	6-month	1-year	3-month	6-month	1-year
1	11.161	12.463	14.709	3.780	5.558	8.257	0.407	1.523	3.806
2^2	11.162	12.465	14.711	3.786	5.565	8.263	0.403	1.525	3.813
2^4	11.162	12.465	14.712	3.790	5.569	8.267	0.401	1.526	3.816
2^6	11.162	12.466	14.712	3.791	5.571	8.268	0.400	1.527	3.818
2^8	11.162	12.466	14.712	3.792	5.572	8.269	0.400	1.527	3.818
2^{10}	11.162	12.466	14.713	3.793	5.572	8.269	0.399	1.527	3.819
2^{12}	11.162	12.466	14.713	3.793	5.572	8.270	0.399	1.527	3.819
2^{14}	11.162	12.466	14.713	3.793	5.573	8.270	0.399	1.527	3.819
Limit	11.162	12.466	14.713	3.793	5.573	8.270	0.399	1.527	3.819

(Continued)

TABLE 1. (Continued)

Panel B: HN(C) model with a non-monotonic pricing kernel

	In-the-money ($K = 90$)			At-the-money ($K = 100$)			Out-of-the-money ($K = 110$)		
n	3-month	6-month	1-year	3-month	6-month	1-year	3-month	6-month	1-year
1	11.446	13.047	15.794	4.260	6.374	9.617	0.666	2.200	5.141
2^2	11.330	12.838	15.447	4.091	6.113	9.215	0.572	1.993	4.764
2^4	11.278	12.744	15.293	4.014	5.995	9.034	0.532	1.900	4.595
2^6	11.253	12.700	15.219	3.977	5.939	8.948	0.513	1.857	4.515
2^8	11.241	12.679	15.184	3.959	5.911	8.906	0.503	1.836	4.476
2^{10}	11.236	12.668	15.166	3.950	5.897	8.885	0.499	1.825	4.457
2^{12}	11.233	12.663	15.157	3.946	5.891	8.875	0.497	1.820	4.447
2^{14}	11.231	12.660	15.153	3.944	5.887	8.870	0.496	1.817	4.443
Limit	11.230	12.657	15.149	3.942	5.884	8.865	0.494	1.815	4.438

(Continued)

Downloaded from https://www.cambridge.org/core. UNIVERSIDAD AUTONOMA METROPOLITANA, on 14 Nov 2026 at 21:01:13, subject to the Cambridge Core terms of use, available at https://www.cambridge.org/core/terms. https://doi.org/10.1017/S0266466626100607

TABLE 1. (Continued)

Panel C: IG(C) model with a monotonic pricing kernel

	In-the-money ($K = 90$)			At-the-money ($K = 100$)			Out-of-the-money ($K = 110$)		
n	3-month	6-month	1-year	3-month	6-month	1-year	3-month	6-month	1-year
1	11.299	12.641	14.942	3.833	5.665	8.442	0.316	1.474	3.872
2^2	11.233	12.555	14.829	3.815	5.621	8.358	0.357	1.501	3.847
2^4	11.198	12.511	14.771	3.805	5.597	8.314	0.378	1.515	3.833
2^6	11.180	12.489	14.742	3.799	5.585	8.292	0.388	1.521	3.826
2^8	11.171	12.478	14.728	3.796	5.579	8.281	0.394	1.524	3.823
2^{10}	11.167	12.472	14.720	3.795	5.576	8.276	0.396	1.526	3.821
2^{12}	11.164	12.469	14.717	3.794	5.574	8.273	0.398	1.527	3.820
2^{14}	11.163	12.468	14.715	3.794	5.574	8.271	0.398	1.527	3.820
Limit	11.162	12.466	14.713	3.793	5.573	8.270	0.399	1.527	3.819

(Continued)

Downloaded from https://www.cambridge.org/core. UNIVERSIDAD AUTONOMA METROPOLITANA, on 14 Nov 2026 at 21:01:13, subject to the Cambridge Core terms of use, available at https://www.cambridge.org/core/terms. https://doi.org/10.1017/S0266466626100607

TABLE 1. (Continued)

Panel D: IG(C) model with a non-monotonic pricing kernel

	In-the-money ($K = 90$)			At-the-money ($K = 100$)			Out-of-the-money ($K = 110$)		
n	3-month	6-month	1-year	3-month	6-month	1-year	3-month	6-month	1-year
1	11.607	13.252	16.067	4.315	6.495	9.835	0.552	2.159	5.243
2^2	11.408	12.938	15.580	4.122	6.175	9.323	0.521	1.976	4.815
2^4	11.316	12.794	15.358	4.031	6.027	9.088	0.507	1.893	4.621
2^6	11.272	12.725	15.252	3.986	5.954	8.975	0.501	1.853	4.528
2^8	11.251	12.691	15.200	3.964	5.919	8.919	0.498	1.834	4.483
2^{10}	11.240	12.674	15.174	3.953	5.901	8.892	0.496	1.824	4.460
2^{12}	11.235	12.666	15.161	3.947	5.893	8.878	0.495	1.819	4.449
2^{14}	11.232	12.662	15.155	3.944	5.888	8.871	0.495	1.817	4.443
Limit	11.230	12.657	15.149	3.942	5.884	8.865	0.494	1.815	4.438

Note: This table reports European call option prices for the two-component HN(C) and IG(C) models for various strike prices and times to maturity as a function of the number of discretization points per day n. The HN(C) model parameters are $\lambda = 2.1190$, $\sigma^2 = 1.2150 \times 10^{-4}$, $\phi_s = 0.87662$, $\alpha_s = 2.5842 \times 10^{-6}$, $\gamma_s = 3.6089 \times 10^2$, $\phi_q = 0.98939$, $\alpha_q = 1.8801 \times 10^{-6}$, and $\gamma_q = 1.3387 \times 10^2$. The IG(C) model parameters are obtained using the relationships from Proposition 1 and assuming $\eta = -0.01$. A monotonic pricing kernel is considered in Panels A and C and corresponds to $\boldsymbol{\xi} = \begin{bmatrix} 0 & 0 \end{bmatrix}^\top$, while a non-monotonic pricing kernel is considered in Panels B and D and is obtained with $\boldsymbol{\xi} = \begin{bmatrix} 2.2798 \times 10^3 & 3.7886 \times 10^4 \end{bmatrix}^\top$.

Downloaded from https://www.cambridge.org/core. UNIVERSIDAD AUTONOMA METROPOLITANA, on 14 Nov 2026 at 21:01:13, subject to the Cambridge Core terms of use, available at https://www.cambridge.org/core/terms. https://doi.org/10.1017/S0266466626100607

$\lim_{\tau\to 0}\pi(\tau)=1$.[16] Note that one way to reduce the gap between the GARCH prices and their diffusion limits under non-monotonic pricing kernels is to set $\lim_{\tau\to 0}\pi(\tau)=\pi\neq 1$, which can be achieved using an alternative convergence rate for $\boldsymbol{\xi}(\tau)$ different from the one introduced in Assumption 4.[17] However, this modification would result in risk-neutral dynamics for the diffusion limits which can no longer be linked to the physical ones via Girsanov's theorem. Finally, we remark that the differences between GARCH option prices computed at daily frequency and their diffusion limits generally increase for the IG(C) models due to the presence of η, which is associated with a nonzero conditional skewness for the returns of the discrete-time models (see Panels C and D).

3.4. A Discussion of Possible Jump Limits

The weak limits derived in Propositions 2 and 3 for both the HN(C) and IG(C) models under the physical and risk-neutral measures are pure diffusion processes, driven by continuous Brownian motions. While diffusion-based SV models have long been the workhorse of continuous-time option pricing, there is compelling empirical and theoretical evidence that jumps play a significant role in modeling asset returns and option valuation (see, e.g., Bakshi et al., 1997; Andersen et al., 2002; Eraker, 2004; Broadie et al., 2007; Andersen et al., 2015; Bollerslev and Todorov, 2023). It is therefore natural to ask whether jump or jump-diffusion processes can arise as weak limits of the discrete-time affine GARCH models studied in this article, and under what conditions. The goal of this section is to address this question, first by reviewing the limited number of contributions in the literature that have tackled this problem, and then by discussing how a candidate jump limit may be constructed within our framework.

Despite the extensive literature on the continuous-time limits of GARCH processes, the derivation of jump or jump-diffusion limits from discrete-time GARCH models has received comparatively little attention. For example, Duan et al. (2006) extend the diffusion approximation framework of Nelson (1990) and Duan (1997) to a class of GARCH-Jump models in which the standard Gaussian innovation is augmented with a Poisson random sum of Gaussian random variables. By allowing the jump intensity and the mean and variance of the Gaussian components to scale appropriately with the time step, they show that their GARCH-Jump approximating sequence converges to a bivariate jump-diffusion process in which

[16] We can show that the conditional variance scaling factors for the HN(C) and IG(C) models are given by

$$\pi^{\mathcal{N}}(\tau)=\frac{1}{1-2\boldsymbol{\alpha}(\tau)^{\top}\boldsymbol{\xi}(\tau)},\qquad \pi^{\mathcal{IG}}(\tau)=\sqrt{\frac{1-2\eta^{4}\boldsymbol{\xi}(\tau)^{\top}\boldsymbol{\alpha}(\tau)}{\left(1-2\eta\sqrt{\tau}\theta(\tau)-2\boldsymbol{\xi}(\tau)^{\top}\left(\boldsymbol{\alpha}(\tau)\odot\boldsymbol{\gamma}(\tau)\right)\right)^{3}}},$$

where $\theta(\tau)$ is given in Equation (SM.7) in the Supplementary Material. It is easy to show that under the convergence rates from Assumptions 3 and 4, we have $\lim_{\tau\to 0}\pi^{\mathcal{D}}(\tau)=1$, for $\mathcal{D}\in\{\mathcal{N},\mathcal{IG}\}$.

[17] For example, for the HN(C) model, one can assume that $\lim_{\tau\to 0}\sqrt{\tau}\boldsymbol{\xi}(\tau)=\boldsymbol{\xi}$, which leads to $\lim_{\tau\to 0}\pi(\tau)=1/\left(1-2\boldsymbol{\alpha}^{\top}\boldsymbol{\xi}\right)=\pi$.

Downloaded from https://www.cambridge.org/core. UNIVERSIDAD AUTONOMA METROPOLITANA, on 14 Nov 2026 at 21:01:13, subject to the Cambridge Core terms of use, available at https://www.cambridge.org/core/terms. https://doi.org/10.1017/S0266466626100607

both asset returns and variance exhibit correlated jump components alongside a diffusive element. Their limiting models nest the pure diffusion limits of Duan (1997), when the jump component is suppressed. Kallsen and Vesenmayer (2009) take a different approach and consider the weak limit of the standard GARCH(1,1) process toward a continuous-time GARCH (COGARCH) process driven by a general Lévy process, with volatility responding to its purely discontinuous quadratic variation. Their derivation relies on a random thinning mechanism and, in contrast with Nelson (1990), the resulting limit features a single underlying source of randomness. However, both Duan et al. (2006) and Kallsen and Vesenmayer (2009) depart from the affine framework and their weak limits are also not in general affine processes.

At least to our knowledge, Christoffersen et al. (2006) is the only study which presents a potential weak limit which includes jumps for an affine GARCH model driven by non-Gaussian innovations, more specifically for their inverse Gaussian GARCH process which is also nested by our general setting. Their analysis provides useful intuition for the type of limit one might expect. We note, however, that the specific assumptions used in their discussion differ from those that would be required for proving a functional weak convergence result in the sense of Nelson (1990) for diffusions or Jacod and Shiryaev (2003) for general semimartingales, and it is worth clarifying these differences. First, their candidate limit is formulated in terms of a rescaled variance-rate process, and the conditions required to establish functional weak convergence are not formally verified. Second, the coefficient of the inverse innovation term in the conditional variance equation is set at 0, rather than as a function of the discretization step. As previously mentioned, for the discretized GARCH model to be internally consistent across sampling frequencies and to recover the unrestricted original daily model at $\tau = 1$, the parameters of the approximating sequence should depend on τ in a manner that is compatible with Assumption 3 or a *jump-diffusion-limit* analog. These observations motivate the alternative limiting constraints on the underlying model parameters that we advocate in this section, which are designed to satisfy both requirements simultaneously.

We now turn to the question of whether jump limits can arise from the affine models of Equations (1)–(4). In the Gaussian setting, under the model specifications and asymptotic scaling assumptions considered in this article, Condition (iii) of Theorem SM.1 in Section SM.A of the Supplementary Material is satisfied. This condition ensures that the increments of the approximating process do not generate jumps in the limit, and the resulting limiting processes therefore have continuous sample paths. Consequently, within the class of Gaussian affine GARCH approximating sequences and parameter scalings considered here, no jump component arises in the continuous-time limit.

The situation is richer in the inverse Gaussian setting. As shown in Proposition 2, under the scaling assumption of the IG innovations from Equation (1) and the asymptotic constraints from Assumption 3, Condition (iii) of Theorem SM.1 in Section SM.A of the Supplementary Material also holds true. Together with

Downloaded from https://www.cambridge.org/core. UNIVERSIDAD AUTONOMA METROPOLITANA, on 14 Nov 2026 at 21:01:13, subject to the Cambridge Core terms of use, available at https://www.cambridge.org/core/terms. https://doi.org/10.1017/S0266466626100607

the first- and second-order conditional moment limits, this condition leads to a Brownian diffusion limit. To obtain a jump component in the returns limit, one must instead scale the innovation process so that the $\mathcal{F}_{k\tau}^{(n)}$-conditional cgf of $\Delta Y_{(k+1)\tau}^{(n)}$ is *linear* in τ to leading order. This is the standard *Lévy-type* scaling, and it requires us to deviate from the modeling assumption made in Equation (1). Specifically, we remove the $\sqrt{\tau}$ scaling in front of the innovation process and allow the IG degrees of freedom parameter to be time-dependent so that the linearity property is satisfied, while preserving the affine structure. Under these specifications, the risky asset's returns have the following dynamics under $\mathbb{P}^{(n)}$:

$$\Delta Y_{(k+1)\tau}^{(n)} = r\tau + \left(\lambda(\tau) - \frac{\tau}{\eta}\right) h_{k\tau}^{(n)} + \eta \epsilon_{(k+1)\tau}^{(n)}, \quad \epsilon_{(k+1)\tau}^{(n)} \,\Big|\, \mathcal{F}_{k\tau}^{(n)} \sim \mathcal{IG}\left(\frac{\tau h_{k\tau}^{(n)}}{\eta^2}, \frac{\tau h_{k\tau}^{(n)}}{\eta^2}\right), \tag{28}$$

$$\Delta s_{(k+1)\tau}^{(n)} = -(1-\phi_s(\tau))\, s_{k\tau}^{(n)} + \alpha_s(\tau)\gamma_s(\tau)\left(\epsilon_{(k+1)\tau}^{(n)} - \frac{\tau h_{k\tau}^{(n)}}{\eta^2}\right) + \alpha_s(\tau)\left(\frac{\left(h_{k\tau}^{(n)}\right)^2}{\epsilon_{(k+1)\tau}^{(n)}} - \frac{\eta^2 h_{k\tau}^{(n)}}{\tau} - \frac{\eta^4}{\tau^2}\right), \tag{29}$$

$$\Delta q_{(k+1)\tau}^{(n)} = \left(1-\phi_q(\tau)\right)\left(\sigma^2(\tau) - q_{k\tau}^{(n)}\right) + \alpha_q(\tau)\gamma_q(\tau)\left(\epsilon_{(k+1)\tau}^{(n)} - \frac{\tau h_{k\tau}^{(n)}}{\eta^2}\right) + \alpha_q(\tau)\left(\frac{\left(h_{k\tau}^{(n)}\right)^2}{\epsilon_{(k+1)\tau}^{(n)}} - \frac{\eta^2 h_{k\tau}^{(n)}}{\tau} - \frac{\eta^4}{\tau^2}\right). \tag{30}$$

Here, the innovation $\epsilon_{(k+1)\tau}^{(n)}$ follows a single parameter inverse Gaussian distribution with mean and variance equal to $\tau h_{k\tau}^{(n)}/\eta^2$ conditionally on $\mathcal{F}_{k\tau}^{(n)}$, which satisfy the condition that both quantities scale at the same rate $\mathcal{O}(\tau)$. Moreover, the $\mathcal{F}_{k\tau}^{(n)}$-conditional cgf of $\epsilon_{(k+1)\tau}^{(n)}$ admits the following linear representation under $\mathbb{P}^{(n)}$:

$$\mathcal{C}_{\epsilon_{(k+1)\tau}^{(n)}}^{\mathbb{P}^{(n)}}\left(w \,\middle|\, \mathcal{F}_{k\tau}^{(n)}\right) = \tau \frac{h_{k\tau}^{(n)}}{\eta^2}\left(1 - \sqrt{1-2w}\right), \qquad w < \frac{1}{2}. \tag{31}$$

It is easy to verify that under the cgf specification from Equation (31), Condition (iii) of Theorem SM.1 in Section SM.A of the Supplementary Material is no longer satisfied. To identify a plausible candidate jump limit for the above process, we consider asymptotic assumptions on the underlying parameters that differ from those used to derive the diffusion limits. Specifically, we impose the following scaling rates:

$$\lambda = \lim_{\tau\to 0} \tau^{-1}\lambda(\tau), \quad \sigma^2 = \lim_{\tau\to 0}\sigma^2(\tau), \quad \boldsymbol{\kappa} = \lim_{\tau\to 0}\tau^{-1}(\mathbf{1} - \boldsymbol{\phi}(\tau)),$$
$$\boldsymbol{\alpha} = \lim_{\tau\to 0}\tau^{-p}\boldsymbol{\alpha}(\tau), \quad \boldsymbol{\gamma} = \lim_{\tau\to 0}\tau^{p}\boldsymbol{\gamma}(\tau),$$

Downloaded from https://www.cambridge.org/core. UNIVERSIDAD AUTONOMA METROPOLITANA, on 14 Nov 2026 at 21:01:13, subject to the Cambridge Core terms of use, available at https://www.cambridge.org/core/terms. https://doi.org/10.1017/S0266466626100607

for some $p > 5/2$. We notice that while the convergence rates for the long-run variance parameter $\sigma^2(\tau)$ and persistence $\boldsymbol{\phi}(\tau)$ are the same as in Assumption 3, those driving the variance of variance process are significantly different. The exponent p is not uniquely determined: any $p > 5/2$ yields the same candidate limit below. Indeed, the product $\boldsymbol{\alpha}(\tau) \odot \boldsymbol{\gamma}(\tau)$ converges to a finite limit for every p, and, whenever the corresponding limit is nonzero, the ϵ channel contributes a jump to the variance dynamics, whereas the conditional variance per unit time of the centered $1/\epsilon$ channel is of order $\mathcal{O}\left(\tau^{2p-5}\right)$ and therefore vanishes. Since only this product enters the limiting dynamics, the individual exponents are not separately identified. At the boundary $p = 5/2$, the centered $1/\epsilon$ channel instead contributes a non-degenerate Gaussian component, whereas for $p < 5/2$, its conditional variance per unit time diverges. Under these assumptions, the limiting conditional characteristics suggest that the (càdlàg) extension of the process $\boldsymbol{X}_{k\tau}^{(n)} = \begin{bmatrix} Y_{k\tau}^{(n)} & s_{k\tau}^{(n)} & q_{k\tau}^{(n)} \end{bmatrix}^\top$ that follows the dynamics from Equations (28) to (30) has the candidate limit $\boldsymbol{X}_t = \begin{bmatrix} Y_t & s_t & q_t \end{bmatrix}^\top$, which satisfies the following SDEs:

$$dY_t = \left(r + \lambda h_{t-} - \frac{h_{t-}}{\eta} \right) dt + \eta dL_t, \tag{32}$$

$$ds_t = \left(-\kappa_s s_{t-} - \frac{\alpha_s \gamma_s}{\eta^2} h_{t-} \right) dt + \alpha_s \gamma_s dL_t, \tag{33}$$

$$dq_t = \left(\kappa_q \left(\sigma^2 - q_{t-} \right) - \frac{\alpha_q \gamma_q}{\eta^2} h_{t-} \right) dt + \alpha_q \gamma_q dL_t. \tag{34}$$

Here, L_t is a state-dependent pure-jump process of inverse Gaussian type whose jump measure has compensator $h_{t-}\eta^{-2}\nu_{\mathcal{IG}}(dx)\,dt$, where $\nu_{\mathcal{IG}}$ denotes the unit inverse Gaussian Lévy measure. A rigorous proof of the corresponding weak convergence result would follow the prescription of Theorem IX.3.39 from Jacod and Shiryaev (2003). However, since the focus of our article is on diffusion limits, we leave the rigorous treatment of this convergence result, including its numerical implementation and empirical analysis, for future research.

Several features of the candidate limiting dynamics in Equations (32)–(34) are noteworthy. First, similarly to the candidate limit discussed by Christoffersen et al. (2006), all three state variables Y_t, s_t, and q_t are driven by the same jump process L_t. However, this common source of randomness does not imply market completeness, because the continuum of possible jump-size risks need not be spanned by the traded risky asset. Second, the candidate limiting process is a pure-jump process with no diffusion component. Although pure-jump processes are theoretically tractable and have been used in the option pricing literature, they tend to be less flexible than jump-diffusion models for fitting implied volatility surfaces. A more flexible structure is already available within the same modeling framework at the boundary rate $p = 5/2$, for which the variance components acquire an additional Gaussian component and the candidate limit becomes a jump-diffusion; the returns, however, remain purely discontinuous under any of

Downloaded from https://www.cambridge.org/core. UNIVERSIDAD AUTONOMA METROPOLITANA, on 14 Nov 2026 at 21:01:13, subject to the Cambridge Core terms of use, available at https://www.cambridge.org/core/terms. https://doi.org/10.1017/S0266466626100607

these scalings, since the innovation enters Equation (28) only through $\epsilon^{(n)}_{(k+1)\tau}$. A possible way to enrich the return dynamics is therefore to augment the return equation with an independent Gaussian diffusion component, similarly to the approach of Duan et al. (2006) for their jump-GARCH option pricing model. Such a modification, however, would require a separate analysis of the affine property and of the corresponding limiting and risk-neutral dynamics.

An affine alternative that could allow for a richer jump-diffusion limiting structure has been proposed in discrete time by Ornthanalai (2014), who introduces a class of Lévy GARCH models in which the returns are modeled with the sum of a Gaussian and a pure-jump Lévy component with time-homogeneous parameters that follow Heston and Nandi (2000) dynamics, which is required for preserving the affine property. Because the variance dynamics are driven only by the Gaussian part, this specification can be viewed as a hybrid GARCH-SV model with heavy-tailed innovations. Using the same intuition as above, the resulting limit would be a jump-diffusion process for the returns driven by two independent sources of randomness—a Brownian motion and a Lévy process—and with no jumps in the time-homogeneous factors. Unlike in the *jump-driven* IG limiting case, this setting allows for more general pricing kernels which can incorporate equity, volatility, and jump risk aversion coefficients, yielding a more empirically appealing continuous-time model for option pricing. This is a natural direction for future research and some of the results derived in this article provide the key building block for such an extension.

4. REVISITING THE RELATIONSHIP BETWEEN DISCRETE AND CONTINUOUS-TIME AFFINE MODELS

This section relates the affine GARCH weak limit derived in Section 3 to the one obtained by Heston and Nandi (2000). Specifically, we investigate the impact of using different parametric convergence rates on the resulting diffusion limit. We extend our analysis to include two new categories of GARCH models that feature SV, aiming to understand the connection between affine models in discrete and continuous time. Moreover, we explain why the asymptotic scaling assumptions postulated in Assumption 3 are the most natural ones to consider for relating GARCH models to diffusion processes through weak convergence.

For the sake of exposition, we focus our analysis in this section on the limiting behavior of one-component Gaussian models under the physical measure. To simplify the notation, we remove the distribution superscript $\mathcal{N}$ henceforth. In addition, the underlying discrete-time process $\boldsymbol{X}^{(n)} = \{\boldsymbol{X}^{(n)}_{k\tau}\}_{k=0}^{nT}$ is now assumed to be two-dimensional with $\boldsymbol{X}^{(n)}_{k\tau} = \begin{bmatrix} Y^{(n)}_{k\tau} & h^{(n)}_{k\tau} \end{bmatrix}^\top$, so that its weak limit $\boldsymbol{X}_t = \begin{bmatrix} Y_t & h_t \end{bmatrix}^\top$ represents the solution of the SDE in Equation (17), where $\{\boldsymbol{W}_t\}_{t\in[0,T]}$ is now a two-dimensional standard Brownian motion, $\boldsymbol{A}(\boldsymbol{X}_t)$ is a two-dimensional vector of drift terms, and $\boldsymbol{\Sigma}(\boldsymbol{X}_t)$ is a 2×2 lower triangular matrix containing the

Downloaded from https://www.cambridge.org/core. UNIVERSIDAD AUTONOMA METROPOLITANA, on 14 Nov 2026 at 21:01:13, subject to the Cambridge Core terms of use, available at https://www.cambridge.org/core/terms. https://doi.org/10.1017/S0266466626100607

diffusion terms; both $\boldsymbol{A}(\boldsymbol{X}_t)$ and $\boldsymbol{\Sigma}(\boldsymbol{X}_t)$ adhere to the affine structure of Equations (18)–(20).

4.1. Revisiting the Heston and Nandi (2000) Diffusion Limit

Following Remark 1, the discretized one-component affine Gaussian GARCH model of Heston and Nandi (2000), denoted henceforth by HN, is obtained by setting $\phi(\tau) = \phi_s(\tau)$, $\alpha(\tau) = \alpha_s(\tau)$, $\gamma(\tau) = \gamma_s(\tau)$, and assuming $\phi_q(\tau) = \alpha_q(\tau) = 0$, so that $q_{k\tau}^{(n)} = \sigma^2(\tau)$ and $s_{k\tau}^{(n)} = h_{k\tau}^{(n)} - \sigma^2(\tau)$. Corollary 1 provides the diffusion limit of the HN model that is obtained as a special case of Proposition 2.

COROLLARY 1. *Assume that* $\{\boldsymbol{X}_{k\tau}^{(n)}\}_{k=0}^{nT}$ *follows the dynamics of the discretized HN model under measure* $\mathbb{P}^{(n)}$. *Further suppose that the limiting parameter scaling constraints in Assumption 3 hold. Then, as* τ *approaches zero, the process* $\{\boldsymbol{X}_t^{(n)}\}_{t\in[0,T]}$ *converges weakly to a two-dimensional diffusion process* $\{\boldsymbol{X}_t\}_{t\in[0,T]}$ *governed by the following SDEs:*

$$dY_t = (r + \lambda h_t)\, dt + \sqrt{h_t}\, dW_{1,t}, \tag{35}$$

$$dh_t = \kappa\left(\sigma^2 - h_t\right) dt - 2\alpha\gamma\sqrt{h_t}\, dW_{1,t} + \sqrt{2}\alpha\, dW_{2,t}. \tag{36}$$

Here, $\{W_{1,t}\}_{t\in[0,T]}$ *and* $\{W_{2,t}\}_{t\in[0,T]}$ *are two independent standard Brownian motions on* $(\Omega, \mathcal{F}, \mathbb{F}, \mathbb{P})$.

Proof. The diffusion limit of the HN model can be obtained directly from Equation (22) by assuming $q_t = \sigma^2$, so that $dq_t = 0$ and $dh_t = ds_t$, and letting $\kappa = \kappa_s$, $\alpha = \alpha_s$, and $\gamma = \gamma_s$. □

In contrast to the component case of Proposition 2, the HN limit presented in Corollary 1 is a non-degenerate diffusion process. The conditional variance dynamics of Equation (36) contain two sources of noise, which is a result commonly obtained when deriving diffusion limits in non-affine (one-component) GARCH settings under similar convergence rates for the underlying parameters (see, e.g., Nelson, 1990; Duan, 1997). Note that Equation (36) can be reformulated using a single Brownian motion as follows:

$$dh_t = \kappa\left(\sigma^2 - h_t\right) dt + \alpha\sqrt{2 + 4\gamma^2 h_t}\, dW'_{2,t}. \tag{37}$$

Here, $W'_2 = \{W'_{2,t}\}_{t\in[0,T]}$ is a Brownian motion that exhibits a stochastic correlation with the Brownian motion governing the return dynamics, such that $d\langle W_1, W'_2\rangle_t = -\dfrac{2\gamma\sqrt{h_t}}{\sqrt{2+4\gamma^2 h_t}}\, dt$. This limit is also consistent with the result from Han et al. (2020), who obtained a similar CIR-type limit for a discrete-time affine SV model under comparable asymptotic assumptions, with their scaling implied by the temporal aggregation property of the integrated volatility process.

Downloaded from https://www.cambridge.org/core. UNIVERSIDAD AUTONOMA METROPOLITANA, on 14 Nov 2026 at 21:01:13, subject to the Cambridge Core terms of use, available at https://www.cambridge.org/core/terms. https://doi.org/10.1017/S0266466626100607

It is important to highlight that the HN limit presented in Corollary 1 differs from the one derived by Heston and Nandi (2000), which corresponds to a two-dimensional degenerate diffusion where returns and volatility dynamics are driven by the same Brownian motion. Specifically, the Heston and Nandi (2000) diffusion limit comprises the same dynamics for the return process as in Equation (35), but involves a simpler SDE for the variance dynamics:

$$dh_t = \kappa\left(\sigma^2 - h_t\right)dt - 2\alpha\gamma\sqrt{h_t}\,dW_{1,t}. \tag{38}$$

This diffusion limit corresponds to a special case of the model of Heston (1993) that is driven by perfectly (negatively) correlated Brownian motions with a volatility of volatility parameter equal to $2\alpha\gamma$. The disparity between our limit and that established by Heston and Nandi (2000) can be explained by the fact that the latter limit was derived assuming different limiting constraints for the parameters $\alpha(\tau)$ and $\gamma(\tau)$; specifically, they used[18]

$$\alpha = \lim_{\tau\to 0}\tau^{-1}\alpha(\tau) \quad \text{and} \quad \gamma = \lim_{\tau\to 0}\tau^{\frac{1}{2}}\gamma(\tau). \tag{39}$$

These constraints, in contrast to those in Assumption 3B, imply different scaling behaviors for $\alpha(\tau)$ and $\alpha(\tau)\gamma(\tau)$, with rates of τ and $\tau^{1/2}$, respectively. This discrepancy leads to an asymmetry in the loadings of the affine GARCH driving noise function as τ approaches zero, altering the limiting dynamics. To understand this, consider the expression representing the noise driving the conditional variance dynamics in the HN model as per Equation (5):

$$\alpha(\tau)\,G^{\mathcal{N}}\left(z^{(n)}_{(k+1)\tau}, h^{(n)}_{k\tau}; \gamma(\tau)\right) = \alpha(\tau)\left(\frac{z^{(n)2}_{(k+1)\tau}}{h^{(n)}_{k\tau}} - 1\right) - 2\alpha(\tau)\gamma(\tau)z^{(n)}_{(k+1)\tau}. \tag{40}$$

This equation involves linear and quadratic functions of the innovation that are multiplied by $\alpha(\tau)\gamma(\tau)$ and $\alpha(\tau)$, respectively. If $\alpha(\tau)$ scales faster to zero than $\alpha(\tau)\gamma(\tau)$, the linear noise component $-2\alpha(\tau)\gamma(\tau)z^{(n)}_{(k+1)\tau}$ dominates over the quadratic one, leading to an asymptotic setting where the return and variance dynamics are both driven by a linear function of the innovation $z^{(n)}_{(k+1)\tau}$. This explains why the Heston and Nandi (2000) diffusion limit contains a single Brownian motion driving both returns and variance dynamics, while our limit includes an additional Brownian motion that accounts for the quadratic noise component in Equation (40).

We remark that if there is no leverage effect in the HN model (i.e., $\gamma = 0$), the Heston and Nandi (2000) diffusion limit exhibits a deterministic variance process, akin to the non-affine GARCH(1,1) weak limit derived by Corradi (2000). In fact, the scaling assumption of τ^{-1} for $\alpha(\tau)$ made by Heston and Nandi (2000) aligns

[18]Note that the convergence rates considered by Heston and Nandi (2000) are slightly different and do not allow one to recover the original HN model when $\tau = 1$. Badescu et al. (2019) provide an alternative parametric scaling specification that is consistent with (39) and leads to the same diffusion limit.

Downloaded from https://www.cambridge.org/core. UNIVERSIDAD AUTONOMA METROPOLITANA, on 14 Nov 2026 at 21:01:13, subject to the Cambridge Core terms of use, available at https://www.cambridge.org/core/terms. https://doi.org/10.1017/S0266466626100607

with that of Corradi (2000), while our assumption of $\tau^{-1/2}$ is in line with Nelson (1990) and Duan (1997).

Furthermore, it can be shown that $\alpha(\tau)$ and $\alpha(\tau)\gamma(\tau)$ must scale at the rate $\tau^{1/2}$ to preserve the second-order moment structure of the underlying affine GARCH dynamics in the limit (see Appendix A.2.2 for more details). For example, the conditional variance of variance function in the HN model is $V^{\mathbb{P}^{(n)}}[h^{(n)}_{t+\tau} \mid \mathcal{F}^{(n)}_t] = 2\alpha^2(\tau) + 4\alpha^2(\tau)\gamma^2(\tau)h^{(n)}_t$, for $t \in \mathcal{T}^{(n)}$. In our limit, the instantaneous variance of variance function implied by Equation (36) is $2\alpha^2 + 4\alpha^2\gamma^2 h_t$, while it is $4\alpha^2\gamma^2 h_t$ in the Heston and Nandi (2000) limit. The absence of the term $2\alpha^2$ in their limit is due to the asymmetric scaling behavior of $\alpha(\tau)\gamma(\tau)$ and $\alpha(\tau)$, as previously discussed. Another difference between the dynamics in Equations (36) and (38) is that the latter are driven by three free parameters instead of four.[19]

4.2. Characterization of Weak Limits for a New Discrete-Time Affine GARCH Stochastic Volatility Model

The fact that different diffusion limits can be derived under distinct parametric convergence rates motivates us to study the diffusion processes that can be obtained as a limit of an affine discrete-time process. To this end, we consider a generalization of the HN model that was recently proposed by Heston et al. (2024a), and refer to it as the Heston–Nandi SV model, henceforth denoted by HNSV.

We introduce this model under a modified parametrization that fits the general discrete-time framework presented in Section 2. The discretized HNSV dynamics under the physical measure $\mathbb{P}^{(n)}$ are given by

$$\Delta Y^{(n)}_{(k+1)\tau} = r\tau + \lambda(\tau)\, h^{(n)}_{k\tau} + \sqrt{\tau}\sqrt{h^{(n)}_{k\tau}}\,\epsilon^{(n)}_{(k+1)\tau}, \tag{41}$$

$$\begin{aligned}\Delta h^{(n)}_{(k+1)\tau} = {} & \left(1-\phi(\tau)\right)\left(\sigma^2(\tau) - h^{(n)}_{k\tau}\right) \\ & + \alpha(\tau)\left(\psi^{(n)2}_{(k+1)\tau} - 2\gamma(\tau)\sqrt{h^{(n)}_{k\tau}}\,\psi^{(n)}_{(k+1)\tau} - 1\right).\end{aligned} \tag{42}$$

Here, $\left(\epsilon^{(n)}_{(k+1)\tau}, \psi^{(n)}_{(k+1)\tau}\right)$ follows an $\mathcal{F}^{(n)}_{k\tau}$-conditional bivariate standard Gaussian distribution with correlation coefficient ρ. Apart from the parameter ρ, this model shares the same parameters as the HN model, namely, $\lambda(\tau)$, $\phi(\tau)$, $\sigma^2(\tau)$, $\alpha(\tau)$, and $\gamma(\tau)$, which are defined analogously as in Section 2. It can be interpreted as an HN process in which the innovation driving the variance dynamics is correlated with—but no longer the same as—the one driving returns. Clearly, the HN model is recovered as a special case when $\rho = 1$. Moreover, Section SM.D.4 of the Supplementary Material confirms that the HNSV model satisfies the affine

[19] Indeed, only the product $\alpha\gamma$ is statistically identifiable in Equation (38), resulting in one fewer degree of freedom in the diffusion limit of Heston and Nandi (2000) compared to its discrete-time counterpart (and to our limit).

Downloaded from https://www.cambridge.org/core. UNIVERSIDAD AUTONOMA METROPOLITANA, on 14 Nov 2026 at 21:01:13, subject to the Cambridge Core terms of use, available at https://www.cambridge.org/core/terms. https://doi.org/10.1017/S0266466626100607

property of Assumption 1. Consequently, this process is akin to a continuous-time SV model driven by two correlated Brownian motions and is thus a perfect candidate for studying the limiting relationship between affine models in discrete and continuous time.

To relate Equations (41) and (42) to the modeling framework introduced in Section 2, note that Equation (41) is identical to Equation (1) with $F^{\mathcal{D}}\left(h_{k\tau}^{(n)};\lambda(\tau)\right) = F^{\mathcal{N}}\left(h_{k\tau}^{(n)};\lambda(\tau)\right) = \lambda(\tau)\,h_{k\tau}^{(n)}$ as in Equation (11). In addition, Equation (42) can be expressed in the form of Equation (5), that is,

$$\Delta h_{(k+1)\tau}^{(n)} = \left(1-\phi(\tau)\right)\left(\sigma^2(\tau)-h_{k\tau}^{(n)}\right)+\alpha(\tau)G^{\mathcal{D}}\left(w_{(k+1)\tau}^{(n)},h_{k\tau}^{(n)};\gamma(\tau)\right), \tag{43}$$

where the function $G^{\mathcal{D}}$ is now expressed in terms of a new innovation, $w_{(k+1)\tau}^{(n)} = \sqrt{h_{k\tau}^{(n)}}\,\psi_{(k+1)\tau}^{(n)}$, as follows:

$$\begin{aligned} G^{\mathcal{D}}\left(w_{(k+1)\tau}^{(n)},h_{k\tau}^{(n)};\gamma(\tau)\right) &= G^{\mathcal{N}}\left(w_{(k+1)\tau}^{(n)},h_{k\tau}^{(n)};\gamma(\tau)\right) \\ &= \frac{w_{(k+1)\tau}^{(n)\,2}}{h_{k\tau}^{(n)}} - 2\gamma(\tau)\,w_{(k+1)\tau}^{(n)} - 1. \end{aligned} \tag{44}$$

Although $G^{\mathcal{D}}$ is a function of a new innovation, its functional form is identical to the one we considered for the Gaussian class of affine GARCH models introduced in Section 2.

Throughout the remainder of this section, we assume that the parameters of the discretized HNSV model satisfy Assumption 3A. However, Assumption 3B is replaced by Assumption 5, which comprises all power-law convergence rates for $\alpha(\tau)$ and $\gamma(\tau)$ that result in a diffusion matrix with finite entries.

Assumption 5. The parameters $\alpha(\tau)$ and $\gamma(\tau)$ of the discretized HNSV model satisfy the following asymptotic relationships:

$$\alpha = \lim_{\tau\to 0}\tau^{-\left(\frac{1}{2}+\delta_1\right)}\alpha(\tau), \qquad \gamma = \lim_{\tau\to 0}\tau^{-\delta_2}\gamma(\tau),$$

where $\delta_1 \geq 0$ and $\delta_2 \geq -\delta_1$.

The asymptotic relationships that were postulated in Assumption 3B are the slowest convergence rates that can be considered for $\alpha(\tau)$ and $\gamma(\tau)$, that is, they can be obtained by setting $\delta_1 = \delta_2 = 0$ in Assumption 5. The convergence rates employed by Heston and Nandi (2000) and given in Equation (39) correspond to the case $\delta_1 = 1/2$ and $\delta_2 = -1/2$. Proposition 5 provides a characterization of the HNSV diffusion limits that can be obtained under all possible combinations of δ_1 and δ_2.

PROPOSITION 5. *Assume that* $\left\{\boldsymbol{X}_{k\tau}^{(n)}\right\}_{k=0}^{nT}$ *follows the discretized HNSV dynamics from Equations (41) and (42) under measure* $\mathbb{P}^{(n)}$*, and Assumptions 3A and 5 hold.*

Downloaded from https://www.cambridge.org/core. UNIVERSIDAD AUTONOMA METROPOLITANA, on 14 Nov 2026 at 21:01:13, subject to the Cambridge Core terms of use, available at https://www.cambridge.org/core/terms. https://doi.org/10.1017/S0266466626100607

Then, as τ approaches zero, the process $\{\boldsymbol{X}_t^{(n)}\}_{t\in[0,T]}$ converges weakly to a two-dimensional diffusion process $\{\boldsymbol{X}_t\}_{t\in[0,T]}$ governed by the following SDEs:

$$dY_t = (r+\lambda h_t)\,dt + \sqrt{h_t}\,dW_{1,t}$$

and

$$dh_t = \begin{cases} \kappa\left(\sigma^2 - h_t\right)dt - 2\alpha\gamma\rho\sqrt{h_t}\,dW_{1,t} \\ \quad +\sqrt{2\alpha^2 + 4\alpha^2\gamma^2\left(1-\rho^2\right)}\,h_t\,dW_{2,t} & \text{if } \delta_1 = 0 \text{ and } \delta_2 = 0 \\ \kappa\left(\sigma^2 - h_t\right)dt - 2\alpha\gamma\rho\sqrt{h_t}\,dW_{1,t} \\ \quad +2\alpha\gamma\sqrt{1-\rho^2}\sqrt{h_t}\,dW_{2,t} & \text{if } \delta_1 > 0 \text{ and } \delta_2 = -\delta_1 \\ \kappa\left(\sigma^2 - h_t\right)dt + \sqrt{2}\alpha\,dW_{2,t} & \text{if } \delta_1 = 0 \text{ and } \delta_2 > 0 \\ \kappa\left(\sigma^2 - h_t\right)dt & \text{if } \delta_1 > 0 \text{ and } \delta_2 > -\delta_1. \end{cases}$$

Here, $\{W_{1,t}\}_{t\in[0,T]}$ and $\{W_{2,t}\}_{t\in[0,T]}$ are two independent standard Brownian motions on $(\Omega, \mathcal{F}, \mathbb{F}, \mathbb{P})$.

Proof. See Section SM.D.4 of the Supplementary Material. □

First, we observe that all weak limits derived in Proposition 5 belong to the class of affine diffusion processes. The diffusion limit with the most general variance dynamics emerges when both δ_1 and δ_2 are equal to zero, which corresponds to the setting of Assumption 3B. In this scenario, $\alpha(\tau)$ and $\alpha(\tau)\,\gamma(\tau)$ both scale at the rate $\tau^{1/2}$, which allows us to preserve the effects of the linear and quadratic components of the noise function asymptotically, as discussed in Section 4.1. The other three cases result in either the linear or quadratic noise components vanishing in the limit. This occurs when the scaling rates of $\alpha(\tau)$ or $\alpha(\tau)\,\gamma(\tau)$ exceed $\tau^{1/2}$. In particular, in the last case (i.e., $\delta_1 > 0$ and $\delta_2 > -\delta_1$), the noise elements completely vanish, leading to a deterministic variance process—a structure that is not consistent with the underlying HNSV dynamics. In the third case (i.e., $\delta_1 = 0$ and $\delta_2 > 0$), the variance dynamics follow an Ornstein–Uhlenbeck process that is uncorrelated with the return dynamics. Since the GARCH leverage effect parameter γ does not appear in the limiting dynamics, this case fails to capture a fundamental characteristic in the structure of the HNSV model. The second case (i.e., $\delta_1 > 0$ and $\delta_2 = -\delta_1$) leads to the classical Heston (1993) model where return and variance dynamics are driven by two correlated Brownian motions with a constant correlation coefficient.[20] This result can be viewed as a generalization

[20] Let $\rho' = -\rho$ and $W_2' = \{W_{2,t}'\}_{t\in[0,T]}$, with $dW_{2,t}' = \rho'\,dW_{1,t} + \sqrt{1-\rho'^2}\,dW_{2,t}$, so that W_1 and W_2' are two correlated Brownian motions with correlation coefficient ρ'. Then, the variance dynamics for the case $\delta_1 > 0$ and $\delta_2 = -\delta_1$ can be expressed in terms of $W_{2,t}'$ as follows:

$$dh_t = \kappa\left(\sigma^2 - h_t\right)dt + 2\alpha\gamma\sqrt{h_t}\,dW_{2,t}', \tag{45}$$

which corresponds to a square-root process with a volatility of volatility parameter equal to $2\alpha\gamma$.

Downloaded from https://www.cambridge.org/core. UNIVERSIDAD AUTONOMA METROPOLITANA, on 14 Nov 2026 at 21:01:13, subject to the Cambridge Core terms of use, available at https://www.cambridge.org/core/terms. https://doi.org/10.1017/S0266466626100607

of the Heston and Nandi (2000) limit for the HN model since the latter is obtained as a special case by taking $\rho = 1$. However, the underlying parametric convergence rates lead to a diffusion process that does not have the same variance of variance structure as the HNSV model, similarly to our discussion for the HN model in Section 4.1.

The dynamics of the variance process obtained in Proposition 5 for the case $\delta_1 = \delta_2 = 0$ can be reformulated using a single Brownian motion as in Equation (37). However, the stochastic correlation between the Brownian motions W_1 and W_2' has now a more flexible form as it is a function of the new parameter ρ, that is, $d\langle W_1, W_2' \rangle_t = -\rho \dfrac{2\gamma\sqrt{h_t}}{\sqrt{2+4\gamma^2 h_t}}\, dt$. We remark that nonzero γ and ρ are necessary to induce a leverage effect in both continuous- and discrete-time dynamics. This entails that simply having correlated innovations affecting return and variance dynamics is not enough for generating a leverage effect; the γ parameter plays a critical role. Moreover, the instantaneous variance of variance function in this model is not directly proportional to h_t as in the model of Heston (1993). Consequently, this diffusion limit has somewhat more complex variance dynamics compared to Heston's (1993) model, and features five parameters instead of four. This additional flexibility may explain why Heston et al. (2024a) found that the HNSV model slightly outperformed Heston's model in an empirical experiment.

4.3. Relating Continuous-Time Canonical Affine Stochastic Volatility Models to GARCH Processes

Section 4.2 showed that the affine SV model of Heston (1993), which assumes a constant correlation, cannot be obtained as a weak limit of a discrete-time affine model from the GARCH class without making specific asymptotic scaling assumptions on the parameters that alter the moment structure of the process as the time step approaches zero.[21]

Ishida and Engle (2002) introduce an SQGARCH model that converges weakly to Heston's model using parametric scaling assumptions that are consistent with Nelson (1990) and those in Assumption 3. However, there is a caveat—this SQGARCH model does not satisfy Assumption 1 and is therefore not affine. In other words, the canonical (one-factor) affine classes of models popularized in discrete and continuous time are not analogous to one another from the point of view of weak convergence.

More generally, Ishida and Engle (2002) show that the CEV SV diffusion process (see, e.g., Jones, 2003, and the references therein), which encompasses the models of Hull and White (1987) and Heston (1993), can be obtained as a weak

[21] Interestingly, if one were to apply a Milstein discretization scheme to Heston's model, then one would obtain a restricted HNSV model in which the parameters $\alpha(\tau)$ and $\gamma(\tau)$ are a function of a single parameter—the volatility of volatility parameter in the Heston model. However, such a discretization scheme would entail that the respective scaling rates of $\alpha(\tau)$ and $\alpha(\tau)\gamma(\tau)$ are τ and $\tau^{1/2}$, respectively, which causes a mismatch between the second-order moment structures of the underlying discrete- and continuous-time processes, as explained in Section 4.2.

Downloaded from https://www.cambridge.org/core. UNIVERSIDAD AUTONOMA METROPOLITANA, on 14 Nov 2026 at 21:01:13, subject to the Cambridge Core terms of use, available at https://www.cambridge.org/core/terms. https://doi.org/10.1017/S0266466626100607

limit of a GARCH class of processes, which they introduced as CEVGARCH. The variance dynamics of this process obey the general form of Equation (5) with a variance driving noise function given by

$$G^{\mathcal{D}}\left(z^{(n)}_{(k+1)\tau}, h^{(n)}_{k\tau}; \gamma(\tau)\right) = \left(h^{(n)}_{k\tau}\right)^{p}\left(\frac{z^{(n)2}_{(k+1)\tau}}{h^{(n)}_{k\tau}} - 2\gamma(\tau)\frac{z^{(n)}_{(k+1)\tau}}{\sqrt{h^{(n)}_{k\tau}}} - 1\right), \tag{46}$$

where $p \geq 0$. The SQGARCH is obtained as a special case for $p = 1/2$. When $p = 1$, the variance dynamics correspond to the non-linear asymmetric GARCH of Engle and Ng (1993). This model has been proposed for option valuation by Duan (1995) and is now the standard non-affine GARCH model used in the option pricing literature.

Just as the HN model can be extended to HNSV, we consider here a generalization of the CEVGARCH model that allows the return and variance equations to be driven by different innovations. We refer to this generalization as the CEVSV model. Its discretized dynamics under the physical measure $\mathbb{P}^{(n)}$ are given by

$$\Delta Y^{(n)}_{(k+1)\tau} = r\tau + \lambda(\tau)\, h^{(n)}_{k\tau} + \sqrt{\tau}\sqrt{h^{(n)}_{k\tau}}\,\epsilon^{(n)}_{(k+1)\tau}, \tag{47}$$

$$\begin{aligned}\Delta h^{(n)}_{(k+1)\tau} = &\left(1-\phi(\tau)\right)\left(\sigma^2(\tau) - h^{(n)}_{k\tau}\right)\\ &+\alpha(\tau)\left(h^{(n)}_{k\tau}\right)^{p}\left(\psi^{(n)2}_{(k+1)\tau} - 2\gamma(\tau)\,\psi^{(n)}_{(k+1)\tau} - 1\right).\end{aligned} \tag{48}$$

Here, $\left(\epsilon^{(n)}_{(k+1)\tau}, \psi^{(n)}_{(k+1)\tau}\right)$ follows an $\mathcal{F}^{(n)}_{k\tau}$-conditional bivariate standard Gaussian distribution with correlation coefficient ρ. The CEVGARCH model of Ishida and Engle (2002) is obtained as a special case of CEVSV by taking $\rho = 1$. Unlike the previous models considered, the CEVSV specification is generally non-affine. Section SM.D.5 of the Supplementary Material shows that it is non-affine for every $p > 0$. When $p = 0$, the model is affine only if $\rho\gamma(\tau) = 0$, apart from the trivial case $\alpha(\tau) = 0$. Proposition 6 provides a characterization of the CEVSV diffusion limits across all possible combinations of δ_1 and δ_2 in Assumption 5.

PROPOSITION 6. *Assume that* $\left\{\boldsymbol{X}^{(n)}_{k\tau}\right\}_{k=0}^{nT}$ *follows the dynamics of the discretized CEVSV dynamics from Equations (47) and (48) under measure* $\mathbb{P}^{(n)}$*, and Assumptions 3A and 5 hold. Then, as* τ *approaches zero, the process* $\{\boldsymbol{X}^{(n)}_t\}_{t\in[0,T]}$ *converges weakly to a two-dimensional diffusion process* $\{\boldsymbol{X}_t\}_{t\in[0,T]}$ *governed by the following SDEs:*

$$dY_t = (r + \lambda h_t)\, dt + \sqrt{h_t}\, dW_{1,t}$$

Downloaded from https://www.cambridge.org/core. UNIVERSIDAD AUTONOMA METROPOLITANA, on 14 Nov 2026 at 21:01:13, subject to the Cambridge Core terms of use, available at https://www.cambridge.org/core/terms. https://doi.org/10.1017/S0266466626100607

and

$$dh_t = \begin{cases} \kappa\left(\sigma^2 - h_t\right) dt - 2\alpha\gamma\rho h_t^p \, dW_{1,t} & \\ \quad + \sqrt{2\alpha^2 + 4\alpha^2\gamma^2\left(1-\rho^2\right)} h_t^p \, dW_{2,t} & \text{if } \delta_1 = 0 \text{ and } \delta_2 = 0 \\ \kappa\left(\sigma^2 - h_t\right) dt - 2\alpha\gamma\rho h_t^p \, dW_{1,t} & \\ \quad + 2\alpha\gamma\sqrt{1-\rho^2} h_t^p \, dW_{2,t} & \text{if } \delta_1 > 0 \text{ and } \delta_2 = -\delta_1 \\ \kappa\left(\sigma^2 - h_t\right) dt + \sqrt{2}\alpha h_t^p \, dW_{2,t} & \text{if } \delta_1 = 0 \text{ and } \delta_2 > 0 \\ \kappa\left(\sigma^2 - h_t\right) dt & \text{if } \delta_1 > 0 \text{ and } \delta_2 > -\delta_1. \end{cases}$$

Here, $\{W_{1,t}\}_{t\in[0,T]}$ *and* $\{W_{2,t}\}_{t\in[0,T]}$ *are two independent standard Brownian motions on* $(\Omega, \mathcal{F}, \mathbb{F}, \mathbb{P})$.

Proof. See Section SM.D.5 of the Supplementary Material. □

When $\delta_1 = \delta_2 = 0$, the diffusion limit of the CEVSV model corresponds to the CEV SV model studied by Jones (2003) and is no more general than that obtained for the CEVGARCH assuming $\rho = 1$. Indeed, we can express the variance dynamics as follows:

$$dh_t = \kappa\left(\sigma^2 - h_t\right) dt + \sqrt{2\alpha^2 + 4\alpha^2\gamma^2} h_t^p \left(\rho' \, dW_{1,t} + \sqrt{1-\rho'^2} \, dW_{2,t}\right), \tag{49}$$

where $\rho' = -2\gamma\rho \Big/ \left(\sqrt{2+4\gamma^2}\right)$. This indicates that the parameters γ and ρ are not identifiable in the continuous-time dynamics, implying that the diffusion limit assuming $\rho = 1$ can exhibit dynamics indistinguishable from those with a general ρ. This is in contrast to the weak limit of the HNSV model, where all parameters are identifiable and which is not equivalent to its GARCH counterpart's limit. Moreover, we note that nonzero γ and ρ are necessary to induce a leverage effect in both continuous- and discrete-time dynamics, similarly to the HNSV setting.

The weak limits of the CEVSV model belong to the class of affine diffusion processes for $p = 1/2$, and also for $p = 0$ when the return–variance covariance vanishes (see Section SM.D.5 of the Supplementary Material for more details).[22] This indicates that the transition from a non-affine GARCH model to an affine process in continuous time is more the exception than the norm. For the case $\delta_1 = \delta_2 = 0$, the HNSV and CEVSV with $p = 1/2$ converge to distinct processes. Specifically, the CEVSV diffusion limit with $p = 1/2$ corresponds to the model of Heston (1993) with an instantaneous variance of variance function $(2\alpha^2 + 4\alpha^2\gamma^2)h_t$, whereas the HNSV limit is a non-standard affine SV model that features a stochastic correlation between return and variance dynamics and a variance of variance function $2\alpha^2 + 4\alpha^2\gamma^2 h_t$.

[22] When $p = 1$, the CEVSV diffusion limits correspond to a mean reverting version of the Hull and White (1987) SV model, sometimes referred to as the GARCH diffusion model. Further setting $\rho = 1$ and $\gamma = 0$, we have that the case $\delta_1 = \delta_2 = 0$ aligns with the standard GARCH(1,1) limit derived by Nelson (1990), while the case $\delta_1 > 0$ and $\delta_2 = -\delta_1$ matches the limiting deterministic variance process obtained by Corradi (2000).

Downloaded from https://www.cambridge.org/core. UNIVERSIDAD AUTONOMA METROPOLITANA, on 14 Nov 2026 at 21:01:13, subject to the Cambridge Core terms of use, available at https://www.cambridge.org/core/terms. https://doi.org/10.1017/S0266466626100607

Interestingly, when $p = 1/2$, the case $\delta_1 > 0$ and $\delta_2 = -\delta_1$ yields the same Heston (1993) diffusion limit for the HNSV and CEVSV models. Hence, despite their different GARCH variance noise functions—one affine and the other non-affine—these two specifications are asymptotically indistinguishable under these scaling assumptions. This suggests that these convergence rates may not be the most suitable for relating GARCH models to diffusion processes through weak convergence.

Finally, we note that both models considered in this section are special cases of the SR-SARV(1) class of Meddahi and Renault (2004), which is closed under temporal aggregation with cross-frequency formulas available for the latent factor dynamics. However, when leverage is present, as is the case with both our specifications, Meddahi and Renault (2004) show that the moment structure of the aggregated process differs from that of the original model. Moreover, closed-form expressions for cross-frequency formulas in terms of the observable parameters are not available, in contrast to the symmetric weak GARCH(1,1) where Alexander and Lazar (2021) show that the Drost and Nijman (1993) formulas uniquely determine the convergence rates as $\tau \to 0$. For our models, no such unique scaling is implied, and characterizing the full class of admissible diffusion limits is therefore one of the contributions of this article.

5. NUMERICAL ILLUSTRATIONS

This section complements our theoretical results by providing a detailed numerical assessment of the alternative diffusion limits derived for one-component models as well as a calibration exercise. We first examine how different choices of convergence rates affect option prices and their limiting behavior, with particular attention to the role of the pricing kernel, correlation structure, and asymmetry in the variance dynamics. We then turn to an empirical investigation using observed option data to assess the performance of the proposed limit relative to both its discrete-time counterpart and an SV benchmark.

5.1. Alternative Limits for One-Component Models

This section discusses the effect of using the alternative convergence rates of Assumption 5 on option prices constructed based on the most general one-component affine Gaussian model considered in Section 4—the HNSV model—and on its diffusion limits.[23] Recall that the weak limits derived in Section 3 rely on $\delta_1 = \delta_2 = 0$, denoted by (1) in this section. Following Proposition 5, however, it is possible to change the value of these two convergence rates by using alternative specifications for δ_1 and δ_2. Specifically, we consider three additional cases in this illustration: (2) $\delta_1 = \frac{1}{2}$ and $\delta_2 = -\frac{1}{2}$ (corresponding to the Heston and Nandi limit),

[23]The numerical implementation follows a similar approach to the one described in Section 3.3 for the two-component models by taking $s_t^{(n)} = 0$ and $q_t^{(n)} = \sigma^2(\tau)$. Note that the $\mathcal{F}_t$-conditional cf of $\boldsymbol{X}_T$ under $\mathbb{Q}$ is derived for the weak limits of the HNSV model using the same approach as in Proposition 4.

Downloaded from https://www.cambridge.org/core. UNIVERSIDAD AUTONOMA METROPOLITANA, on 14 Nov 2026 at 21:01:13, subject to the Cambridge Core terms of use, available at https://www.cambridge.org/core/terms. https://doi.org/10.1017/S0266466626100607

(3) $\delta_1 = 0$ and $\delta_2 = \frac{1}{2}$, and (4) $\delta_1 = \frac{1}{2}$ and $\delta_2 = \frac{1}{2}$. The HNSV model is implemented using the corresponding HN parameters estimated in Table SM.1 of Augustyniak et al. (2023), together with two specific values for the correlation between the two driving noise processes: $\rho = 0.7867$ consistent with the parameter estimated jointly from returns, VIX, and options by Heston et al. (2024a), and $\rho = 1$ corresponding to the HN model. We compute one-year European call option prices as a function of the number of discretization points per day for three moneyness levels: in-the-money options ($K = 90$), at-the-money options ($K = 100$), and out-of-the-money options ($K = 110$). As in Section 3.3, we also investigate the impact of the shape of the pricing kernel on convergence of option prices using two different values for the variance risk-preference parameter ξ. The results are reported in Table 2.

When $n = 1$, the prices obtained with the four convergence rate cases are identical—as expected. As soon as n increases, however, the prices become different. Their limiting values are also significantly different, which emphasizes that using different convergence rate parameters produces distinct option prices for the limiting diffusions because the underlying GARCH models converge to different diffusion limits under both the physical and risk-neutral measures. Overall, we notice that the option prices based on the weak limits obtained with the standard convergence rates from Assumption 3B are the closest to those of the underlying discrete-time model in all but one of the cases considered—in line with our theoretical results developed in Sections 3 and 4.[24] This observation thus offers another numerical justification for choosing these rates over the alternative choices from Assumption 5.

We now examine the impact on option prices of the above convergence rates relative to three key factors: the shape of the pricing kernel (monotonic vs. non-monotonic), the correlation between the innovations driving the returns and conditional variance processes (HNSV vs. HN), and the magnitude of the asymmetry parameter γ.

Panels A and C of Table 2 report the monotonic pricing kernel cases; as expected, the limit prices obtained with (1) are the closest to those obtained with the GARCH model, with the maximum absolute difference being \$0.008 for HNSV and \$0.012 for HN. The difference is slightly larger when using the Heston and Nandi (2000) convergence rates in (2); it is however significantly larger when using the rates in (3) and (4). These differences in the limit are a by-product of the dynamics given by Proposition 5 and the values of the risk-neutral long-run variance and speed of mean reversion for each limiting diffusion process.[25] Specifically, the risk-neutral

[24] This property is only violated for out-of-the-money HN-based options with the non-monotonic pricing kernel for which the limit prices obtained with the convergence rates (3) are closer to the daily HN counterparts than those obtained with (1).

[25] Note that Proposition 5 only illustrates the physical dynamics of the HNSV diffusion limits. While the variance of variance remains unchanged after the change of measure, the risk-neutral drifts are computed using a similar approach as in Proposition 3. The expressions for the risk-neutral long-run variance level $\tilde{\sigma}^2$ and speed of mean reversion $\tilde{\kappa}$ for each convergence rate are as follows: (1) $\tilde{\kappa} = \kappa - 2\alpha\gamma\left(\rho\left(\lambda + \frac{1}{2}\right) + 2\alpha\gamma\xi\left(1-\rho^2\right)\right)$ and $\tilde{\sigma}^2 = \frac{\kappa\sigma^2 + 2\xi\alpha^2}{\tilde{\kappa}}$, (2)

Downloaded from https://www.cambridge.org/core. UNIVERSIDAD AUTONOMA METROPOLITANA, on 14 Nov 2026 at 21:01:13, subject to the Cambridge Core terms of use, available at https://www.cambridge.org/core/terms. https://doi.org/10.1017/S0266466626100607

TABLE 2. Call option prices for the HNSV and HN models under different convergence rates

Panel A: HNSV model and a monotonic pricing kernel

	In-the-money ($K = 90$)				At-the-money ($K = 100$)				Out-of-the-money ($K = 110$)			
n	(1)	(2)	(3)	(4)	(1)	(2)	(3)	(4)	(1)	(2)	(3)	(4)
1	14.532	14.532	14.532	14.532	8.135	8.135	8.135	8.135	3.812	3.812	3.812	3.812
2^2	14.533	14.536	14.295	14.167	8.139	8.146	8.034	7.973	3.815	3.822	3.901	3.934
2^4	14.533	14.537	14.165	14.065	8.141	8.149	7.968	7.917	3.817	3.824	3.930	3.950
2^6	14.534	14.537	14.097	14.040	8.142	8.150	7.930	7.902	3.817	3.824	3.940	3.953
2^8	14.534	14.537	14.063	14.033	8.142	8.150	7.911	7.899	3.818	3.824	3.944	3.953
2^{10}	14.534	14.537	14.046	14.031	8.142	8.150	7.901	7.898	3.818	3.825	3.946	3.953
2^{12}	14.534	14.537	14.037	14.031	8.143	8.150	7.895	7.897	3.818	3.825	3.947	3.953
2^{14}	14.534	14.537	14.033	14.031	8.143	8.150	7.893	7.897	3.818	3.825	3.947	3.953
Limit	14.534	14.537	14.029	14.031	8.143	8.150	7.891	7.897	3.818	3.825	3.948	3.953

(Continued)

Downloaded from https://www.cambridge.org/core. UNIVERSIDAD AUTONOMA METROPOLITANA, on 14 Nov 2026 at 21:01:13, subject to the Cambridge Core terms of use, available at https://www.cambridge.org/core/terms. https://doi.org/10.1017/S0266466626100607

TABLE 2. (Continued)

Panel B: HNSV model and a non-monotonic pricing kernel

	In-the-money ($K = 90$)				At-the-money ($K = 100$)				Out-of-the-money ($K = 110$)			
n	(1)	(2)	(3)	(4)	(1)	(2)	(3)	(4)	(1)	(2)	(3)	(4)
1	18.516	18.516	18.516	18.516	12.723	12.723	12.723	12.723	8.192	8.192	8.192	8.192
2^2	17.930	17.239	15.265	14.410	12.104	11.303	9.263	8.292	7.615	6.802	5.083	4.238
2^4	17.671	16.973	14.692	14.107	11.830	11.004	8.662	7.974	7.360	6.512	4.603	4.004
2^6	17.550	16.910	14.511	14.049	11.701	10.932	8.481	7.915	7.240	6.443	4.475	3.965
2^8	17.491	16.894	14.440	14.035	11.638	10.914	8.414	7.902	7.182	6.425	4.432	3.956
2^{10}	17.461	16.890	14.409	14.032	11.607	10.909	8.386	7.898	7.154	6.421	4.416	3.954
2^{12}	17.447	16.889	14.394	14.031	11.592	10.908	8.374	7.898	7.139	6.420	4.409	3.954
2^{14}	17.440	16.889	14.387	14.031	11.584	10.908	8.368	7.897	7.132	6.420	4.406	3.953
Limit	17.433	16.889	14.381	14.031	11.577	10.908	8.362	7.897	7.126	6.420	4.403	3.953

(Continued)

Downloaded from https://www.cambridge.org/core. UNIVERSIDAD AUTONOMA METROPOLITANA, on 14 Nov 2026 at 21:01:13, subject to the Cambridge Core terms of use, available at https://www.cambridge.org/core/terms. https://doi.org/10.1017/S0266466626100607

TABLE 2. (Continued)

Panel C: HN model and a monotonic pricing kernel

	In-the-money ($K = 90$)				At-the-money ($K = 100$)				Out-of-the-money ($K = 110$)			
n	(1)	(2)	(3)	(4)	(1)	(2)	(3)	(4)	(1)	(2)	(3)	(4)
1	14.670	14.670	14.670	14.670	8.208	8.208	8.208	8.208	3.765	3.765	3.765	3.765
2^2	14.672	14.675	14.368	14.204	8.214	8.222	8.075	7.994	3.770	3.778	3.885	3.928
2^4	14.673	14.676	14.202	14.075	8.217	8.226	7.989	7.923	3.773	3.782	3.924	3.949
2^6	14.673	14.676	14.116	14.042	8.218	8.227	7.941	7.904	3.775	3.783	3.938	3.952
2^8	14.673	14.676	14.072	14.034	8.219	8.227	7.916	7.899	3.775	3.783	3.943	3.953
2^{10}	14.673	14.676	14.051	14.032	8.219	8.227	7.903	7.898	3.776	3.783	3.946	3.953
2^{12}	14.673	14.676	14.039	14.031	8.220	8.227	7.897	7.897	3.776	3.783	3.947	3.953
2^{14}	14.673	14.676	14.034	14.031	8.220	8.227	7.894	7.897	3.776	3.783	3.947	3.953
Limit	14.673	14.676	14.029	14.031	8.220	8.227	7.891	7.897	3.776	3.783	3.948	3.953

(Continued)

Downloaded from https://www.cambridge.org/core. UNIVERSIDAD AUTONOMA METROPOLITANA, on 14 Nov 2026 at 21:01:13, subject to the Cambridge Core terms of use, available at https://www.cambridge.org/core/terms. https://doi.org/10.1017/S0266466626100607

Downloaded from https://www.cambridge.org/core. UNIVERSIDAD AUTONOMA METROPOLITANA, on 14 Nov 2026 at 21:01:13, subject to the Cambridge Core terms of use, available at https://www.cambridge.org/core/terms. https://doi.org/10.1017/S0266466626100607

TABLE 2. (Continued)

Panel D: HN and a non-monotonic pricing kernel

	In-the-money ($K = 90$)				At-the-money ($K = 100$)				Out-of-the-money ($K = 110$)			
n	(1)	(2)	(3)	(4)	(1)	(2)	(3)	(4)	(1)	(2)	(3)	(4)
1	15.610	15.610	15.610	15.610	9.385	9.385	9.385	9.385	4.908	4.908	4.908	4.908
2^2	15.305	14.880	14.982	14.397	9.029	8.484	8.875	8.250	4.576	4.030	4.669	4.175
2^4	15.167	14.726	14.676	14.121	8.868	8.290	8.618	7.984	4.427	3.843	4.539	4.008
2^6	15.101	14.689	14.527	14.053	8.791	8.243	8.490	7.919	4.356	3.798	4.472	3.967
2^8	15.069	14.679	14.453	14.037	8.753	8.231	8.426	7.903	4.321	3.787	4.437	3.957
2^{10}	15.054	14.677	14.417	14.032	8.734	8.228	8.394	7.899	4.304	3.784	4.420	3.954
2^{12}	15.046	14.677	14.399	14.031	8.725	8.227	8.378	7.898	4.295	3.783	4.412	3.954
2^{14}	15.042	14.676	14.390	14.031	8.720	8.227	8.370	7.897	4.291	3.783	4.407	3.953
Limit	15.040	14.676	14.381	14.031	8.717	8.227	8.362	7.897	4.286	3.783	4.403	3.953

Note: This table reports one-year European call option prices for the HNSV and HN models for various strike prices as a function of the number of discretization points per day n. The HNSV model is based on $\rho = 0.7867$ and the HN model corresponds to $\rho = 1$. The other parameters are $\lambda = 2.1257$, $\sigma^2 = 1.2007 \times 10^{-4}$, $\phi = 0.9671$, $\alpha = 4.4440 \times 10^{-6}$, and $\gamma = 1.8927 \times 10^2$. A monotonic pricing kernel is considered in Panels A and C and corresponds to $\xi = 0$, while a non-monotonic pricing kernel is considered in Panels B and D and is obtained with $\xi = 1.6252 \times 10^4$. We rely on the following convergence rates for the parameters in Assumption 5: (1) $\delta_1 = \delta_2 = 0$, (2) $\delta_1 = \frac{1}{2}$, $\delta_2 = -\frac{1}{2}$, (3) $\delta_1 = 0$, $\delta_2 = \frac{1}{2}$, and (4) $\delta_1 = \frac{1}{2}$, $\delta_2 = \frac{1}{2}$.

variance drifts for (1) and (2) are identical under the monotonic pricing kernel, and therefore the small deviation in option prices is attributed exclusively to the difference in the variance-of-variance dynamics. The larger discrepancies between option prices computed based on (1) and (2) against (3) and (4) are mostly due to the form of the risk-neutral drift of the variance process, which changes for (1) and (2), but stays at its physical measure level for (3) and (4).

For non-monotonic pricing kernels (i.e., Panels B and D), we observe larger prices when $n = 1$; these prices decrease as n increases. As explained in Section 3.3, this pattern is caused by having larger risk-neutral conditional variances compared to the physical ones in the discrete-time models, with their ratio converging to one as n approaches infinity. As expected, the proposed rates in (1) lead to limit prices that are the closest to their GARCH counterparts, but the differences relative to the other three convergence rates are now substantial. For example, for out-of-the-money options, the differences between the HNSV and its diffusion limit prices are \$1.066 for (1), \$1.772 for (2), \$3.789 for (3), and \$4.239 for (4). The main factor which triggers these differences is the presence of the positive variance risk-preference parameter ξ which impacts both the (risk-neutral) long-run level and speed of mean reversion of the variance process. For example, the differences in limit prices based on (1) and (2), which were rather small for monotonic pricing kernels, are now significant because the risk-neutral long-run variance level implied by (1) is larger than that obtained with (2), despite both convergence rates sharing the same mean reversion rate (see Footnote 25). In other words, when accounting for variance risk in the pricing kernel, the Heston and Nandi (2000) convergence rates cannot capture the same asymptotic behavior of the risk-neutral long-run variance of the underlying HNSV model in contrast to our rates from Assumption 3B.

We now turn our attention to the effect of using different convergence rates with respect to the correlation parameter ρ. On the one hand, we notice that for monotonic pricing kernels, ρ does not have a large overall impact on option prices. Moreover, in the limit, it only impacts the prices obtained based on the rates used in (1) and (2). The convergence rates (3) and (4), on the other hand, are not affected by ρ, and option prices based on their limiting diffusions are identical for the HNSV and HN models. On the other hand, ρ has a significant effect on option prices in the non-monotonic pricing kernel case. Specifically, there is a strong negative relationship between option prices and ρ; for example, $\rho = 1$ leads to a substantial overall decrease in option prices relative to the case where $\rho = 0.7867$, the largest differences being documented for $n = 1$. For the diffusion limits, this drop is still significant but occurs only for (1) and (2). This can be explained by a decrease in the risk-neutral long-run variance level and increase in the speed of mean reversion for these two cases when $\rho = 1$ (see again Footnote 25); as stated above, ρ does not

$\tilde{\kappa} = \kappa - 2\alpha\gamma\left(\rho\left(\lambda + \frac{1}{2}\right) + 2\alpha\gamma\xi\left(1-\rho^2\right)\right)$ and $\tilde{\sigma}^2 = \frac{\kappa\sigma^2}{\tilde{\kappa}}$, (3) $\tilde{\kappa} = \kappa$ and $\tilde{\sigma}^2 = \frac{\kappa\sigma^2 + 2\xi\alpha^2}{\tilde{\kappa}}$, and (4) $\tilde{\kappa} = \kappa$ and $\tilde{\sigma}^2 = \sigma^2$.

Downloaded from https://www.cambridge.org/core. UNIVERSIDAD AUTONOMA METROPOLITANA, on 14 Nov 2026 at 21:01:13, subject to the Cambridge Core terms of use, available at https://www.cambridge.org/core/terms. https://doi.org/10.1017/S0266466626100607

affect the diffusion prices resulting from (3) and (4). However, under these rates, the HNSV option prices converge very fast to their diffusion level, a substantial drop in prices occurring from $n = 1$ to $n = 2^2$ for all moneyness levels considered. Consequently, HN-based option prices are closer to their continuous-time limit counterparts relative to the HNSV models, in addition to being less sensitive to the choice of the convergence rate.

Finally, we investigate the behavior of the option prices based on the four convergence rates relative to different levels of the asymmetry parameter γ. Figure 1 reports a graphical representation of the call option price convergence for in-the-money, at-the-money, and out-of-the-money options and four different values of γ, decreasing from $\gamma = 189.27$ in Panel A to $\gamma = 0$ in Panel D. For these four cases, we report the option prices for the four convergence rates considered above, that is, (1)–(4). There is a positive relationship between the call option prices and the value of γ—this is a by-product of a rise in the variance of variance and the risk-neutral long-run variance levels. In addition, we notice that the prices obtained with the diffusion limit in (1) are the closest to the original GARCH prices obtained when $n = 1$, and this for all values of γ considered in the figure. When $\gamma = 0$, the prices obtained with rates (1) and (3) are overlapping; this observation is consistent with the results of Proposition 5 and the expressions of the risk-neutral drift terms from Footnote 25. The same conclusion can be obtained for the convergence rates in (2) and (4). Interestingly, as γ decreases from 189.27 to 0, we observe that the limit prices calculated using (1) and (2) approach those of (3) and (4), respectively.

Collectively, these results suggest that when implementing continuous-time approximations to discrete-time option pricing models, the choice of parametric convergence rates is consequential: rates that preserve the conditional moment structure of the daily model yield the smallest pricing errors, while alternative rates can introduce systematic deviations that are amplified when the pricing kernel is non-monotonic or the leverage parameter γ is large.

5.2. Empirical Calibrations

The empirical exercise of this section is designed to assess the empirical usefulness of our proposed diffusion limit. To this end, we compare the fit of the HN model with that of our diffusion limit specification obtained by setting $\delta_1 = \delta_2 = 0$ using real option data. In addition, we include the Heston (1993) model as a benchmark. This framework allows us to compare the cross-sectional fitting ability of the proposed diffusion limit with that of the original discrete-time model and a more flexible SV model.

We retrieve the option data from OptionMetrics on the Wharton Research Data Services website. They span from January 1, 1996 to August 31, 2023. We apply a number of standard data filters, resulting in a final sample of 659,454 option prices observed over 1,429 Wednesdays. Specifically, we exclude options with non-positive trading volume or open interest, retain only those with bid prices

Downloaded from https://www.cambridge.org/core. UNIVERSIDAD AUTONOMA METROPOLITANA, on 14 Nov 2026 at 21:01:13, subject to the Cambridge Core terms of use, available at https://www.cambridge.org/core/terms. https://doi.org/10.1017/S0266466626100607

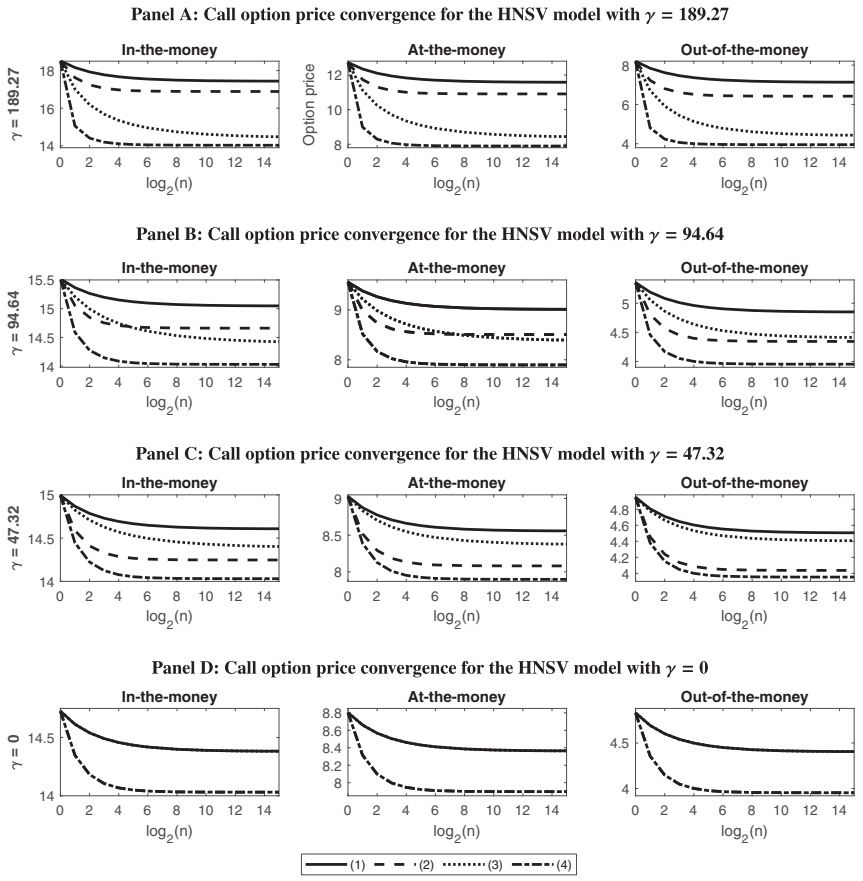


FIGURE 1. Call option price convergence for the HNSV model for different values of γ.
Note: This figure reports one-year European call option prices for the HNSV model for various strike prices and different values of the asymmetry parameter γ, as a function of the number of discretization points per day n. The parameters are $\lambda = 2.1257$, $\sigma^2 = 1.2007 \times 10^{-4}$, $\phi = 0.9671$, $\alpha = 4.4440 \times 10^{-6}$, and $\rho = 0.7867$. A non-monotonic pricing kernel with $\xi = 1.6252 \times 10^4$ is considered. We rely on the following convergence rates for the parameters in Assumption 5: (1) $\delta_1 = \delta_2 = 0$, (2) $\delta_1 = \frac{1}{2}$, $\delta_2 = -\frac{1}{2}$, (3) $\delta_1 = 0$, $\delta_2 = \frac{1}{2}$, and (4) $\delta_1 = \frac{1}{2}$, $\delta_2 = \frac{1}{2}$.

strictly lower than ask prices and with mid-quote prices exceeding the bid-ask spread, and focus on options with maturities between one week and one year. We also remove observations with missing implied volatility or underlying price data, as well as those that violate no-arbitrage conditions. Finally, we restrict the sample to standard monthly options, excluding weekly contracts.

The comparison considers a calibration exercise in which we estimate the parameters of each model on a weekly basis. Specifically, on each Wednesday, we calibrate the model parameters by minimizing the implied volatility root

Downloaded from https://www.cambridge.org/core. UNIVERSIDAD AUTONOMA METROPOLITANA, on 14 Nov 2026 at 21:01:13, subject to the Cambridge Core terms of use, available at https://www.cambridge.org/core/terms. https://doi.org/10.1017/S0266466626100607

TABLE 3. Summary statistics of implied volatility root mean squared errors across different specifications

	HN model	HN limit	Heston model
Moments			
Average	0.0108	0.0104	0.0088
Standard deviation	0.0065	0.0097	0.0063
Quantiles			
5^{th}	0.0040	0.0043	0.0036
25^{th}	0.0062	0.0064	0.0052
Median	0.0088	0.0085	0.0070
75^{th}	0.0137	0.0118	0.0100
95^{th}	0.0241	0.0227	0.0209

Note: This table reports implied volatility root mean squared error (IVRMSE) for the HN model, our HN limit, and the Heston model. The HN limit uses $\delta_1 = \delta_2 = 0$ for the convergence rate parameters in Assumption 5. Moments and quantiles are obtained from a sample of IVRMSEs calculated on each Wednesday from January 1996 to August 2023. The option data are retrieved from OptionMetrics on the Wharton Research Data Services website. We apply a number of standard data filters, resulting in a final sample of 659,454 option prices observed over 1,429 Wednesdays.

mean squared error (IVRMSE) across the cross section of observed options. This approach allows the parameters to vary over time, thus capturing changes in market conditions over the nearly 28 years of our sample.

Table 3 reports the mean and standard deviation of the weekly IVRMSEs, along with relevant quantiles of their empirical distribution, for each of the three models. The results show that, when calibrated separately, the diffusion limit of the HN model achieves a cross-sectional fit similar to that of its discrete-time counterpart, indicating that the limiting specification retains comparable empirical flexibility. Given that the Heston model offers greater flexibility than both the HN specification and its diffusion limit, we expect it to perform better on average, and our results are consistent with this expectation.

Figure 2 supplements the results of Table 3 by reporting the time series of the IVRMSEs for the three models on a semi-logarithmic plot with a logarithmic y-axis to improve readability. Overall, the Heston model exhibits lower IVRMSEs on average, indicating a better average fit over the sample. In contrast, the HN model and our proposed diffusion limit closely track each other over time, indicating that the two specifications have similar cross-sectional fitting performance.

6. CONCLUDING REMARKS

This article investigates the relationship between canonical affine option pricing models in discrete and continuous time, shedding light on the discrepancies between existing results in the literature by establishing novel diffusion limits

Downloaded from https://www.cambridge.org/core. UNIVERSIDAD AUTONOMA METROPOLITANA, on 14 Nov 2026 at 21:01:13, subject to the Cambridge Core terms of use, available at https://www.cambridge.org/core/terms. https://doi.org/10.1017/S0266466626100607

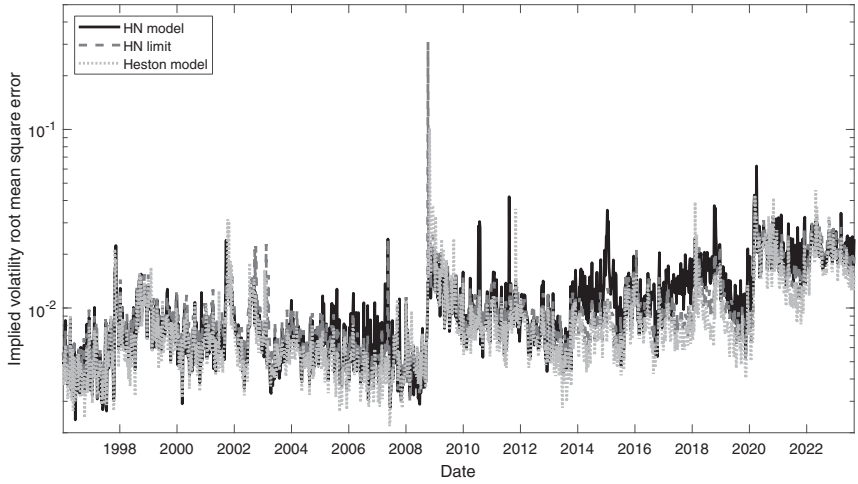


FIGURE 2. Time series of implied volatility root mean squared errors across different specifications. *Note*: This figure reports the time series of the implied volatility root mean squared error (IVRMSE) for the HN model (black solid line), our HN limit (dashed dark gray line), and the Heston model (dotted light gray line). The IVRMSEs are reported on a logarithmic scale to improve readability. The HN limit uses $\delta_1 = \delta_2 = 0$ for the convergence rate parameters in Assumption 5. IVRMSEs are calculated on each Wednesday from January 1996 to August 2023. The option data are retrieved from OptionMetrics on the Wharton Research Data Services website. We apply a number of standard data filters, resulting in a final sample of 659,454 option prices observed over 1,429 Wednesdays.

for various classes of GARCH and SV models. Using a general modeling framework which incorporates multi-component volatility, fat tails, and non-monotonic pricing kernels, we first derive weak limits for two classes of affine GARCH component models driven by Gaussian and inverse Gaussian innovations, and risk-neutralized with an exponential linear pricing kernel. These limits coincide if some relationships between the two models' parameters are satisfied. When restricted to a single volatility component, our limits generalize the result of Heston and Nandi (2000) in the Gaussian case and provide an alternative pathway to obtain the inverse Gaussian limiting process of Christoffersen et al. (2006). In contrast to these studies, which recover limiting processes governed by a single noise, our weak limits correspond to two-dimensional non-degenerate diffusions driven by stochastically correlated Brownian motions. This discrepancy arises due to the use of different asymptotic assumptions on the model parameters, leading to our subsequent contribution: the characterization of all possible limits for two classes of affine and non-affine discrete-time SV models. Interestingly, both specifications converge to affine diffusion limits and our asymptotic rates lead to the most complex dynamics sharing the same statistical properties as their discrete-time counterparts. Numerical experiments involving European options suggest that our limiting diffusions provide the closest prices to their daily discrete-time

Downloaded from https://www.cambridge.org/core. UNIVERSIDAD AUTONOMA METROPOLITANA, on 14 Nov 2026 at 21:01:13, subject to the Cambridge Core terms of use, available at https://www.cambridge.org/core/terms. https://doi.org/10.1017/S0266466626100607

counterparts. In addition, we find that the correlation between the underlying innovations and the shape of the pricing kernel are the two main determinants of the convergence behavior.

Our work can be extended in several possible ways. For example, weak limits can be further generalized to other discrete-time affine frameworks including jumps or information on the realized variance (RV), such as the Lévy GARCH model of Ornthanalai (2014), the generalized affine RV model of Christoffersen et al. (2014), the heterogeneous autoregressive gamma model of Corsi, Fusari, and La Vecchia (2013), and its extensions (see, e.g., Majewski et al., 2015; Alitab et al., 2020; Bormetti et al., 2020). While we primarily discuss applications to European option pricing, our weak limits could also be considered to examine the convergence of hedge ratios or optimal portfolio policies, as well as for pricing other derivatives (e.g., exotic options and volatility derivatives). Finally, our results linking discrete-time non-affine models to affine diffusions should be further investigated both theoretically and empirically. A potential area for future research could involve leveraging this relationship to enhance the efficiency of pricing and hedging in non-affine discrete-time settings using established methods and closed-form solutions available for affine diffusions.

A. APPENDIX

A.1. Affine Representations for the Discretized HN(C) and IG(C) Models

Following straightforward algebraic manipulations, we can show that for the HN(C) case, the $\mathcal{F}_{k\tau}^{(n)}$-conditional joint cgf of $\Delta Y_{(k+1)\tau}^{(n)}$, $\Delta s_{(k+1)\tau}^{(n)}$, and $\Delta q_{(k+1)\tau}^{(n)}$ evaluated at w and $\boldsymbol{v} = [\, v_1 \quad v_2 \,]^\top$ follows Equation (6) with the following one-step coefficients:

$$\mathcal{A}^{\mathcal{N}}(w, \boldsymbol{v}; \tau) = wr\tau + v_2\sigma^2(\tau)\left(1 - \phi_q(\tau)\right) - \boldsymbol{v}^\top \boldsymbol{\alpha}(\tau) - \frac{1}{2}\log\left(1 - 2\boldsymbol{v}^\top \boldsymbol{\alpha}(\tau)\right), \tag{A.1}$$

$$\mathcal{B}_s^{\mathcal{N}}(w, \boldsymbol{v}; \tau) = w\lambda(\tau) - v_1\left(1 - \phi_s(\tau)\right) + \frac{\left(w\sqrt{\tau} - 2\boldsymbol{v}^\top\left(\boldsymbol{\alpha}(\tau) \odot \boldsymbol{\gamma}(\tau)\right)\right)^2}{2\left(1 - 2\boldsymbol{v}^\top \boldsymbol{\alpha}(\tau)\right)}, \tag{A.2}$$

$$\mathcal{B}_q^{\mathcal{N}}(w, \boldsymbol{v}; \tau) = w\lambda(\tau) - v_2\left(1 - \phi_q(\tau)\right) + \frac{\left(w\sqrt{\tau} - 2\boldsymbol{v}^\top\left(\boldsymbol{\alpha}(\tau) \odot \boldsymbol{\gamma}(\tau)\right)\right)^2}{2\left(1 - 2\boldsymbol{v}^\top \boldsymbol{\alpha}(\tau)\right)}, \tag{A.3}$$

where $\odot$ represents the Hadamard (element-wise) product.

Similarly, for the IG(C) model, the $\mathcal{F}_{k\tau}^{(n)}$-conditional joint cgf of $\Delta Y_{(k+1)\tau}^{(n)}$, $\Delta s_{(k+1)\tau}^{(n)}$, and $\Delta q_{(k+1)\tau}^{(n)}$ follows Equation (6) with

$$\mathcal{A}^{\mathcal{IG}}(w, \boldsymbol{v}; \tau) = wr\tau + v_2\sigma^2(\tau)\left(1 - \phi_q(\tau)\right) - \eta^4 \boldsymbol{v}^\top \boldsymbol{\alpha}(\tau) - \frac{1}{2}\log\left(1 - 2\eta^4 \boldsymbol{v}^\top \boldsymbol{\alpha}(\tau)\right), \tag{A.4}$$

Downloaded from https://www.cambridge.org/core. UNIVERSIDAD AUTONOMA METROPOLITANA, on 14 Nov 2026 at 21:01:13, subject to the Cambridge Core terms of use, available at https://www.cambridge.org/core/terms. https://doi.org/10.1017/S0266466626100607

$$\mathcal{B}_s^{\mathcal{IG}}(w,\boldsymbol{v};\tau) = w\left(\lambda(\tau)-\frac{\tau}{\eta}\right) - v_1\left(1-\phi_s(\tau)\right) - \boldsymbol{v}^\top\left(\eta^2\boldsymbol{\alpha}(\tau)+\frac{1}{\eta^2}\left(\boldsymbol{\alpha}(\tau)\odot\boldsymbol{\gamma}(\tau)\right)\right) + \frac{1}{\eta^2}\left(1-\sqrt{\left(1-2\eta^4\boldsymbol{v}^\top\boldsymbol{\alpha}(\tau)\right)\left(1-2w\eta\sqrt{\tau}-2\boldsymbol{v}^\top\left(\boldsymbol{\alpha}(\tau)\odot\boldsymbol{\gamma}(\tau)\right)\right)}\right), \tag{A.5}$$

$$\mathcal{B}_q^{\mathcal{IG}}(w,\boldsymbol{v};\tau) = w\left(\lambda(\tau)-\frac{\tau}{\eta}\right) - v_2\left(1-\phi_q(\tau)\right) - \boldsymbol{v}^\top\left(\eta^2\boldsymbol{\alpha}(\tau)+\frac{1}{\eta^2}\left(\boldsymbol{\alpha}(\tau)\odot\boldsymbol{\gamma}(\tau)\right)\right) + \frac{1}{\eta^2}\left(1-\sqrt{\left(1-2\eta^4\boldsymbol{v}^\top\boldsymbol{\alpha}(\tau)\right)\left(1-2w\eta\sqrt{\tau}-2\boldsymbol{v}^\top\left(\boldsymbol{\alpha}(\tau)\odot\boldsymbol{\gamma}(\tau)\right)\right)}\right). \tag{A.6}$$

A.2. Proofs of Propositions 2 and 3

The proofs of Propositions 2 and 3 rely on the weak convergence theorem for Markov processes stated by Nelson (1990) and restated as Theorem SM.1 in the Supplementary Material. Applying this theorem requires verifying three conditions. Conditions (i) and (ii) concern the limiting drift vector and covariance matrix per unit of time. Specifically, for any fixed $\boldsymbol{x}$ and any given time $k\tau$, one must show that

$$\lim_{\tau\to 0}\frac{1}{\tau}E\left[\Delta\boldsymbol{X}^{(n)}_{(k+1)\tau}\;\middle|\;\boldsymbol{X}^{(n)}_{k\tau}=\boldsymbol{x}\right]=\boldsymbol{A}(\boldsymbol{x}),$$

$$\lim_{\tau\to 0}\frac{1}{\tau}C\left[\Delta\boldsymbol{X}^{(n)}_{(k+1)\tau},\Delta\boldsymbol{X}^{(n)}_{(k+1)\tau}\;\middle|\;\boldsymbol{X}^{(n)}_{k\tau}=\boldsymbol{x}\right]=\boldsymbol{\Sigma}(\boldsymbol{x})\,\boldsymbol{\Sigma}(\boldsymbol{x})^\top,$$

where we use the fact, noted in Nelson (1990), that the difference between the conditional second-moment matrix and the conditional covariance matrix vanishes as $\tau\to 0$, so that it suffices to work with the latter. Since the conditional first- and second-moment functions are affine in $\boldsymbol{x}$, convergence of the coefficients in their affine representations implies uniform convergence over compact subsets of the state domain, as required by conditions (i) and (ii). Condition (iii) imposes a bound on conditional moments of order $2+\delta$ for some $\delta>0$, which ensures that large increments are negligible asymptotically and hence that the sample paths of the limiting process are continuous with probability one.

Before turning to the specific proofs, we present in Appendix A.2.1 a general method for computing the required conditional mean vector and covariance matrix of $\Delta\boldsymbol{X}^{(n)}_{(k+1)\tau}$ and their limits per unit of time. The method exploits the affine structure of the $\mathcal{F}^{(n)}_{k\tau}$-conditional cgf stated in Assumption 1 and applies regardless of the distributional specification $\mathcal{D}$ or the underlying probability measure. For brevity, the approach is illustrated under the physical measure as the procedure under the risk-neutral measure is entirely analogous and is therefore omitted.

A.2.1. *A General Method for the Computation of the Drift and Diffusion Terms.* The first- and second-order conditional moments of $\Delta\boldsymbol{X}^{(n)}_{(k+1)\tau}=\left[\Delta Y^{(n)}_{(k+1)\tau}\;\;\Delta s^{(n)}_{(k+1)\tau}\;\;\Delta q^{(n)}_{(k+1)\tau}\right]^\top$ are recovered from the joint cumulants of the process, which are obtained as partial derivatives of the $\mathcal{F}^{(n)}_{k\tau}$-conditional joint cgf of $\Delta\boldsymbol{X}^{(n)}_{(k+1)\tau}$

Downloaded from https://www.cambridge.org/core. UNIVERSIDAD AUTONOMA METROPOLITANA, on 14 Nov 2026 at 21:01:13, subject to the Cambridge Core terms of use, available at https://www.cambridge.org/core/terms. https://doi.org/10.1017/S0266466626100607

evaluated at $\mathbf{0}$. Specifically, for any real vector $\boldsymbol{x} = \begin{bmatrix} x_1 & x_2 & x_3 \end{bmatrix}^\top$ and $l, m \in \{1,2,3\}$, we have

$$E^{P^{(n)}}\left[\Delta \boldsymbol{X}^{(n)}_{(k+1)\tau,l} \middle| \mathcal{F}^{(n)}_{k\tau}\right] = \left.\frac{\partial \mathcal{C}^{\mathbb{P}^{(n)}}_{\Delta \boldsymbol{X}^{(n)}_{(k+1)\tau}}\left(\boldsymbol{x} \middle| \mathcal{F}^{(n)}_{k\tau}\right)}{\partial x_l}\right|_{\boldsymbol{x}=\mathbf{0}},$$

$$C^{P^{(n)}}\left[\Delta \boldsymbol{X}^{(n)}_{(k+1)\tau,l}, \Delta \boldsymbol{X}^{(n)}_{(k+1)\tau,m} \middle| \mathcal{F}^{(n)}_{k\tau}\right] = \left.\frac{\partial^2 \mathcal{C}^{\mathbb{P}^{(n)}}_{\Delta \boldsymbol{X}^{(n)}_{(k+1)\tau}}\left(\boldsymbol{x} \middle| \mathcal{F}^{(n)}_{k\tau}\right)}{\partial x_l \partial x_m}\right|_{\boldsymbol{x}=\mathbf{0}},$$

where $\mathcal{C}^{\mathbb{P}^{(n)}}\left(\boldsymbol{x} \middle| \mathcal{F}^{(n)}_{k\tau}\right)$ is the cgf of $\Delta \boldsymbol{X}^{(n)}_{(k+1)\tau}$, which admits the affine representation of Equation (6) from Assumption 1. By this affine structure, computing partial derivatives of this cgf reduces to differentiating its coefficients $\mathcal{A}^{\mathcal{D}}$ and $\mathcal{B}^{\mathcal{D}}_u$ for $u \in \{s,q\}$.

We introduce the following notation for the first- and second-order partial derivatives for the coefficients of the $\mathcal{F}^{(n)}_{k\tau}$-conditional cgf of $\Delta \boldsymbol{X}^{(n)}_{(k+1)\tau}$ from Assumption 1 evaluated at $w = 0$ and $\boldsymbol{v} = \mathbf{0}$. For any nonnegative integers i,j,k with $1 \le i+j+k \le 2$, and $u \in \{s,q\}$, we let

$$\mathcal{A}^{\mathcal{D}}_{i,j,k}(\tau) = \left.\frac{\partial^{i+j+k}\mathcal{A}^{\mathcal{D}}(w,\boldsymbol{v};\tau)}{\partial w^i \partial v_1^j \partial v_2^k}\right|_{w=0,\boldsymbol{v}=\mathbf{0}}, \tag{A.7}$$

$$\mathcal{B}^{\mathcal{D}}_{u,i,j,k}(\tau) = \left.\frac{\partial^{i+j+k}\mathcal{B}^{\mathcal{D}}_u(w,\boldsymbol{v};\tau)}{\partial w^i \partial v_1^j \partial v_2^k}\right|_{w=0,\boldsymbol{v}=\mathbf{0}}. \tag{A.8}$$

The drift vector and the covariance matrix of the weak limit are then obtained by dividing these quantities by τ and passing to the limit. This is achieved by computing

$$\mathcal{A}^{\mathcal{D}}_{i,j,k} = \lim_{\tau\to 0}\frac{\mathcal{A}^{\mathcal{D}}_{i,j,k}(\tau)}{\tau}, \qquad \mathcal{B}^{\mathcal{D}}_{u,i,j,k} = \lim_{\tau\to 0}\frac{\mathcal{B}^{\mathcal{D}}_{u,i,j,k}(\tau)}{\tau}, \qquad u \in \{s,q\}, \tag{A.9}$$

using the convergence rates assumed for the model parameters. Note that these rates have been chosen such that these limits exist and are finite, that is, $\mathcal{A}^{\mathcal{D}}_{i,j,k} < \infty$ and $\mathcal{B}^{\mathcal{D}}_{u,i,j,k} < \infty$. By the affine form of the cgf, the drift coefficient of Equation (17) is given by

$$\boldsymbol{A}^{\mathcal{D}}(\boldsymbol{X}_t) = \begin{bmatrix} \mathcal{A}^{\mathcal{D}}_{1,0,0} + \mathcal{B}^{\mathcal{D}}_{s,1,0,0}s_t + \mathcal{B}^{\mathcal{D}}_{q,1,0,0}q_t \\ \mathcal{A}^{\mathcal{D}}_{0,1,0} + \mathcal{B}^{\mathcal{D}}_{s,0,1,0}s_t + \mathcal{B}^{\mathcal{D}}_{q,0,1,0}q_t \\ \mathcal{A}^{\mathcal{D}}_{0,0,1} + \mathcal{B}^{\mathcal{D}}_{s,0,0,1}s_t + \mathcal{B}^{\mathcal{D}}_{q,0,0,1}q_t \end{bmatrix}. \tag{A.10}$$

The 3×3 positive semidefinite matrix of asymptotic second-order cross-cumulants is denoted by $\boldsymbol{B}^{\mathcal{D}}(\boldsymbol{X}_t) = \left(B^{\mathcal{D}}_{rl}(\boldsymbol{X}_t)\right)$, with $r,l \in \{1,2,3\}$. Since under both cgf specifications of Appendix A.1, we have $\mathcal{B}^{\mathcal{D}}_{s,i,j,k} = \mathcal{B}^{\mathcal{D}}_{q,i,j,k}$, for any $i+j+k=2$, each entry of matrix $\boldsymbol{B}^{\mathcal{D}}(\boldsymbol{X}_t)$ is linear in h_t, so that

$$\boldsymbol{B}^{\mathcal{D}}(\boldsymbol{X}_t) = \begin{bmatrix} \mathcal{A}^{\mathcal{D}}_{2,0,0} + \mathcal{B}^{\mathcal{D}}_{u,2,0,0}h_t & \mathcal{A}^{\mathcal{D}}_{1,1,0} + \mathcal{B}^{\mathcal{D}}_{u,1,1,0}h_t & \mathcal{A}^{\mathcal{D}}_{1,0,1} + \mathcal{B}^{\mathcal{D}}_{u,1,0,1}h_t \\ \mathcal{A}^{\mathcal{D}}_{1,1,0} + \mathcal{B}^{\mathcal{D}}_{u,1,1,0}h_t & \mathcal{A}^{\mathcal{D}}_{0,2,0} + \mathcal{B}^{\mathcal{D}}_{u,0,2,0}h_t & \mathcal{A}^{\mathcal{D}}_{0,1,1} + \mathcal{B}^{\mathcal{D}}_{u,0,1,1}h_t \\ \mathcal{A}^{\mathcal{D}}_{1,0,1} + \mathcal{B}^{\mathcal{D}}_{u,1,0,1}h_t & \mathcal{A}^{\mathcal{D}}_{0,1,1} + \mathcal{B}^{\mathcal{D}}_{u,0,1,1}h_t & \mathcal{A}^{\mathcal{D}}_{0,0,2} + \mathcal{B}^{\mathcal{D}}_{u,0,0,2}h_t \end{bmatrix}. \tag{A.11}$$

Downloaded from https://www.cambridge.org/core. UNIVERSIDAD AUTONOMA METROPOLITANA, on 14 Nov 2026 at 21:01:13, subject to the Cambridge Core terms of use, available at https://www.cambridge.org/core/terms. https://doi.org/10.1017/S0266466626100607

Using the Cholesky decomposition of matrix $\boldsymbol{B}^{\mathcal{D}}(\boldsymbol{X}_t) = \left(\boldsymbol{\Sigma}^{\mathcal{D}}(\boldsymbol{X}_t)\right)\left(\boldsymbol{\Sigma}^{\mathcal{D}}(\boldsymbol{X}_t)\right)^{\top}$, where $\boldsymbol{\Sigma}^{\mathcal{D}}(\boldsymbol{X}_t)$ is a lower triangular matrix representing the diffusion of the GARCH weak limit of Equation (17), we obtain

$$\boldsymbol{\Sigma}^{\mathcal{D}}(\boldsymbol{X}_t) = \begin{pmatrix} \sqrt{B^{\mathcal{D}}_{11}(\boldsymbol{X}_t)} & 0 & 0 \\ \dfrac{B^{\mathcal{D}}_{21}(\boldsymbol{X}_t)}{\Sigma^{\mathcal{D}}_{11}(\boldsymbol{X}_t)} & \sqrt{B^{\mathcal{D}}_{22}(\boldsymbol{X}_t) - \left(\Sigma^{\mathcal{D}}_{21}(\boldsymbol{X}_t)\right)^2} & 0 \\ \dfrac{B^{\mathcal{D}}_{31}(\boldsymbol{X}_t)}{\Sigma^{\mathcal{D}}_{11}(\boldsymbol{X}_t)} & \dfrac{B^{\mathcal{D}}_{32}(\boldsymbol{X}_t) - \Sigma^{\mathcal{D}}_{31}(\boldsymbol{X}_t)\Sigma^{\mathcal{D}}_{21}(\boldsymbol{X}_t)}{\Sigma^{\mathcal{D}}_{22}(\boldsymbol{X}_t)} & \sqrt{B^{\mathcal{D}}_{33}(\boldsymbol{X}_t) - \left(\Sigma^{\mathcal{D}}_{31}(\boldsymbol{X}_t)\right)^2 - \left(\Sigma^{\mathcal{D}}_{32}(\boldsymbol{X}_t)\right)^2}. \end{pmatrix} \tag{A.12}$$

A.2.2. *Proof of Proposition 2.* The proof follows the approach described at the start of this appendix and proceeds by verifying conditions (i)–(iii) of Theorem SM.1 in the Supplementary Material. Conditions (i) and (ii) are established from the limiting conditional mean and covariance matrix of $\Delta \boldsymbol{X}^{(n)}_{(k+1)\tau}$, while condition (iii) is verified separately. We first derive the weak limit for the HN(C) model. The corresponding derivation for the IG(C) model follows in a similar way and is provided in Section SM.D.2 of the Supplementary Material.

Following the methodology of Appendix A.2.1 and using the definitions of Equations (A.7) and (A.8), we proceed by evaluating the partial derivatives of the step dependent coefficients of Equations (A.1)–(A.3) at $w = 0$ and $\boldsymbol{v} = \boldsymbol{0}$ and compute their limits per discretization step under the constraints from Assumption 3A. For any $u \in \{s, q\}$, we obtain the following first-order quantities:

$$\begin{aligned}
\mathcal{A}^{\mathcal{N}}_{1,0,0} &= \lim_{\tau\to 0} \frac{\mathcal{A}^{\mathcal{N}}_{1,0,0}(\tau)}{\tau} = \lim_{\tau\to 0} \frac{r\tau}{\tau} = r, \\
\mathcal{A}^{\mathcal{N}}_{0,1,0} &= \lim_{\tau\to 0} \frac{\mathcal{A}^{\mathcal{N}}_{0,1,0}(\tau)}{\tau} = \lim_{\tau\to 0} \frac{0}{\tau} = 0, \\
\mathcal{A}^{\mathcal{N}}_{0,0,1} &= \lim_{\tau\to 0} \frac{\mathcal{A}^{\mathcal{N}}_{0,0,1}(\tau)}{\tau} = \lim_{\tau\to 0} \frac{\sigma^2(\tau)\left(1-\phi_q(\tau)\right)}{\tau} = \kappa_q\sigma^2, \\
\mathcal{B}^{\mathcal{N}}_{u,1,0,0} &= \lim_{\tau\to 0} \frac{\mathcal{B}^{\mathcal{N}}_{u,1,0,0}(\tau)}{\tau} = \lim_{\tau\to 0} \frac{\lambda(\tau)}{\tau} = \lambda, \\
\mathcal{B}^{\mathcal{N}}_{s,0,1,0} &= \lim_{\tau\to 0} \frac{\mathcal{B}^{\mathcal{N}}_{s,0,1,0}(\tau)}{\tau} = \lim_{\tau\to 0} \frac{\phi_s(\tau)-1}{\tau} = -\kappa_s, \\
\mathcal{B}^{\mathcal{N}}_{s,0,0,1} &= \lim_{\tau\to 0} \frac{\mathcal{B}^{\mathcal{N}}_{s,0,0,1}(\tau)}{\tau} = \lim_{\tau\to 0} \frac{0}{\tau} = 0, \\
\mathcal{B}^{\mathcal{N}}_{q,0,1,0} &= \lim_{\tau\to 0} \frac{\mathcal{B}^{\mathcal{N}}_{q,0,1,0}(\tau)}{\tau} = \lim_{\tau\to 0} \frac{0}{\tau} = 0, \\
\mathcal{B}^{\mathcal{N}}_{q,0,0,1} &= \lim_{\tau\to 0} \frac{\mathcal{B}^{\mathcal{N}}_{q,0,0,1}(\tau)}{\tau} = \lim_{\tau\to 0} \frac{\phi_q(\tau)-1}{\tau} = -\kappa_q.
\end{aligned}$$

Downloaded from https://www.cambridge.org/core. UNIVERSIDAD AUTONOMA METROPOLITANA, on 14 Nov 2026 at 21:01:13, subject to the Cambridge Core terms of use, available at https://www.cambridge.org/core/terms. https://doi.org/10.1017/S0266466626100607

Replacing the above quantities into the general drift term of Equation (A.10) allows us to obtain

$$\boldsymbol{A}^{\mathcal{N}}(\boldsymbol{X}_t) = \begin{bmatrix} r + \lambda h_t \\ -\kappa_s s_t \\ -\kappa_q \left(q_t - \sigma^2 \right) \end{bmatrix}.$$

Next, for $u \in \{s, q\}$, we compute the limits of the second-order derivatives per discretization step using the convergence rates of Assumption 3B:

$$\begin{aligned}
\mathcal{A}^{\mathcal{N}}_{2,0,0} &= \lim_{\tau \to 0} \frac{\mathcal{A}^{\mathcal{N}}_{2,0,0}(\tau)}{\tau} = \lim_{\tau \to 0} \frac{0}{\tau} = 0, \\
\mathcal{A}^{\mathcal{N}}_{1,1,0} &= \lim_{\tau \to 0} \frac{\mathcal{A}^{\mathcal{N}}_{1,1,0}(\tau)}{\tau} = \lim_{\tau \to 0} \frac{0}{\tau} = 0, \\
\mathcal{A}^{\mathcal{N}}_{1,0,1} &= \lim_{\tau \to 0} \frac{\mathcal{A}^{\mathcal{N}}_{1,0,1}(\tau)}{\tau} = \lim_{\tau \to 0} \frac{0}{\tau} = 0, \\
\mathcal{A}^{\mathcal{N}}_{0,2,0} &= \lim_{\tau \to 0} \frac{\mathcal{A}^{\mathcal{N}}_{0,2,0}(\tau)}{\tau} = \lim_{\tau \to 0} \frac{2\alpha_s^2(\tau)}{\tau} = 2\alpha_s^2, \\
\mathcal{A}^{\mathcal{N}}_{0,1,1} &= \lim_{\tau \to 0} \frac{\mathcal{A}^{\mathcal{N}}_{0,1,1}(\tau)}{\tau} = \lim_{\tau \to 0} \frac{2\alpha_s(\tau)\alpha_q(\tau)}{\tau} = 2\alpha_s\alpha_q, \\
\mathcal{A}^{\mathcal{N}}_{0,0,2} &= \lim_{\tau \to 0} \frac{\mathcal{A}^{\mathcal{N}}_{0,0,2}(\tau)}{\tau} = \lim_{\tau \to 0} \frac{2\alpha_q^2(\tau)}{\tau} = 2\alpha_q^2, \\
\mathcal{B}^{\mathcal{N}}_{u,2,0,0} &= \lim_{\tau \to 0} \frac{\mathcal{B}^{\mathcal{N}}_{u,2,0,0}(\tau)}{\tau} = \lim_{\tau \to 0} \frac{\tau}{\tau} = 1, \\
\mathcal{B}^{\mathcal{N}}_{u,1,1,0} &= \lim_{\tau \to 0} \frac{\mathcal{B}^{\mathcal{N}}_{u,1,1,0}(\tau)}{\tau} = \lim_{\tau \to 0} \frac{-2\sqrt{\tau}\alpha_s(\tau)\gamma_s(\tau)}{\tau} = -2\alpha_s\gamma_s, \\
\mathcal{B}^{\mathcal{N}}_{u,1,0,1} &= \lim_{\tau \to 0} \frac{\mathcal{B}^{\mathcal{N}}_{u,1,0,1}(\tau)}{\tau} = \lim_{\tau \to 0} \frac{-2\sqrt{\tau}\alpha_q(\tau)\gamma_q(\tau)}{\tau} = -2\alpha_q\gamma_q, \\
\mathcal{B}^{\mathcal{N}}_{u,0,2,0} &= \lim_{\tau \to 0} \frac{\mathcal{B}^{\mathcal{N}}_{u,0,2,0}(\tau)}{\tau} = \lim_{\tau \to 0} \frac{4\alpha_s^2(\tau)\gamma_s^2(\tau)}{\tau} = 4\alpha_s^2\gamma_s^2, \\
\mathcal{B}^{\mathcal{N}}_{u,0,1,1} &= \lim_{\tau \to 0} \frac{\mathcal{B}^{\mathcal{N}}_{u,0,1,1}(\tau)}{\tau} = \lim_{\tau \to 0} \frac{4\alpha_s(\tau)\alpha_q(\tau)\gamma_s(\tau)\gamma_q(\tau)}{\tau} = 4\alpha_s\alpha_q\gamma_s\gamma_q, \\
\mathcal{B}^{\mathcal{N}}_{u,0,0,2} &= \lim_{\tau \to 0} \frac{\mathcal{B}^{\mathcal{N}}_{u,0,0,2}(\tau)}{\tau} = \lim_{\tau \to 0} \frac{4\alpha_q^2(\tau)\gamma_q^2(\tau)}{\tau} = 4\alpha_q^2\gamma_q^2.
\end{aligned}$$

Plugging these into the matrix of asymptotic second-order cross-cumulants of Equation (A.11) leads to

$$\boldsymbol{B}^{\mathcal{N}}(\boldsymbol{X}_t) = \begin{bmatrix} h_t & -2\alpha_s\gamma_s h_t & -2\alpha_q\gamma_q h_t \\ -2\alpha_s\gamma_s h_t & 2\alpha_s^2 + 4\alpha_s^2\gamma_s^2 h_t & 2\alpha_s\alpha_q + 4\alpha_s\alpha_q\gamma_s\gamma_q h_t \\ -2\alpha_q\gamma_q h_t & 2\alpha_s\alpha_q + 4\alpha_s\alpha_q\gamma_s\gamma_q h_t & 2\alpha_q^2 + 4\alpha_q^2\gamma_q^2 h_t \end{bmatrix}. \tag{A.13}$$

Downloaded from https://www.cambridge.org/core. UNIVERSIDAD AUTONOMA METROPOLITANA, on 14 Nov 2026 at 21:01:13, subject to the Cambridge Core terms of use, available at https://www.cambridge.org/core/terms. https://doi.org/10.1017/S0266466626100607

Performing the Cholesky decomposition of the covariance matrix of Equation (A.13) as outlined in Equation (A.12), we obtain the diffusion term

$$\boldsymbol{\Sigma}^{\mathcal{N}}(\boldsymbol{X}_t) = \begin{bmatrix} \sqrt{h_t} & 0 & 0 \\ -2\alpha_s\gamma_s\sqrt{h_t} & \sqrt{2}\alpha_s & 0 \\ -2\alpha_q\gamma_q\sqrt{h_t} & \sqrt{2}\alpha_q & 0 \end{bmatrix}.$$

The resulting limit is a degenerate diffusion driven by two mutually independent Brownian motions W_1 and W_2. This is a consequence of the diffusion matrix $\boldsymbol{\Sigma}^{\mathcal{N}}(\boldsymbol{X}_t)$ having a unique representation along with a column of zeros—a direct consequence of the matrix $\boldsymbol{B}^{\mathcal{N}}(\boldsymbol{X}_t)$ being singular and of rank two.

Next, we need to verify Condition (iii) of Theorem SM.1 in Section SM.A of the Supplementary Material that there exists a $\delta > 0$ such that

$$\limsup_{\tau \to 0,\ \boldsymbol{x} \le c} \tau^{-1} E\left[\left| \Delta X^{(n)}_{(k+1)\tau,i} \right|^{2+\delta} \middle| \boldsymbol{X}^{(n)}_{k\tau} = \boldsymbol{x} \right] = 0.$$

Indeed, if we let $\delta = 2$ and take the fourth-order derivatives of the moment generating function of $\Delta \boldsymbol{X}^{(n)}_{(k+1)\tau} = \left[\begin{array}{ccc} \Delta Y^{(n)}_{(k+1)\tau} & \Delta s^{(n)}_{(k+1)\tau} & \Delta q^{(n)}_{(k+1)\tau} \end{array} \right]^\top$ conditional on $\mathcal{F}^{(n)}_{k\tau}$, we can show that

$$\tau^{-1} E\left[\left| \Delta Y^{(n)}_{(k+1)\tau} \right|^4 \middle| \mathcal{F}^{(n)}_{k\tau} \right] = L^{\mathcal{N}}_Y \tau + \mathcal{O}(\tau),$$
$$\tau^{-1} E\left[\left| \Delta s^{(n)}_{(k+1)\tau} \right|^4 \middle| \mathcal{F}^{(n)}_{k\tau} \right] = L^{\mathcal{N}}_s \tau + \mathcal{O}(\tau),$$
$$\tau^{-1} E\left[\left| \Delta q^{(n)}_{(k+1)\tau} \right|^4 \middle| \mathcal{F}^{(n)}_{k\tau} \right] = L^{\mathcal{N}}_q \tau + \mathcal{O}(\tau),$$

where $L^{\mathcal{N}}_Y$, $L^{\mathcal{N}}_s$, and $L^{\mathcal{N}}_q$ are finite quantities which depend on $\boldsymbol{X}^{(n)}_{k\tau}$ and its diffusion limit parameters, specifically we have $L^{\mathcal{N}}_Y = 3\left(h^{(n)}_{k\tau}\right)^2$ and $L^{\mathcal{N}}_u = 12\alpha_u^4\left(5 + 20\gamma_u^2 h_{k\tau} + 4\gamma_u^4\left(h^{(n)}_{k\tau}\right)^2\right)$, for $u \in \{s, q\}$.

We now proceed to verify if the multidimensional Feller constraints of Duffie and Kan (1996) are satisfied by the HN(C) diffusion limit. A sufficient condition for the existence and uniqueness of a (strong) solution to our diffusion limit is given below.

Condition 1. (Sufficient Condition for the Existence of a Solution of the Affine SDE)

A. For all $\boldsymbol{x}$ such that $V_i(\boldsymbol{x}) = 0$, we have $\boldsymbol{v}^\top_{1,i}\left(\boldsymbol{A}_0 + \boldsymbol{A}^{\mathcal{N}}_1 \boldsymbol{x}\right) > \frac{1}{2}\boldsymbol{v}^\top_{1,i}\boldsymbol{\Gamma}^{\mathcal{N}}\left(\boldsymbol{\Gamma}^{\mathcal{N}}\right)^\top \boldsymbol{v}_{1,i}$.

B. For all j, if $\left(\boldsymbol{v}^\top_{1,i}\boldsymbol{\Gamma}^{\mathcal{N}}\right)_j \neq 0$, then $V_i(\boldsymbol{x})$ and $V_j(\boldsymbol{x})$ are proportional.

Part A of Condition 1 ensures that each volatility process $V_i(\boldsymbol{x})$ has a strong positive drift at the boundary $V_i(\boldsymbol{x}) = 0$. The above inequality typically imposes a constraint on the model parameters, as explained below. First, we notice that when $i = 2, 3$, $V_i(\boldsymbol{x}) = 1 > 0$, so we only need to analyze the case when $i = 1$. The boundary constraint corresponds to having $s_t = -q_t$, so the inequality in Part A becomes

$$q_t\left(\kappa_s - \kappa_q\right) + \kappa_q\sigma^2 > \left(\alpha_s + \alpha_q\right)^2 + 2\left(\alpha_s\gamma_s + \alpha_q\gamma_q\right)^2.$$

Downloaded from https://www.cambridge.org/core. UNIVERSIDAD AUTONOMA METROPOLITANA, on 14 Nov 2026 at 21:01:13, subject to the Cambridge Core terms of use, available at https://www.cambridge.org/core/terms. https://doi.org/10.1017/S0266466626100607

Since $\kappa_s > \kappa_q$, the preceding inequality is satisfied on the portion of the boundary where $q_t > 0$ whenever

$$\kappa_q \sigma^2 > \left(\alpha_s + \alpha_q\right)^2 + 2\left(\alpha_s \gamma_s + \alpha_q \gamma_q\right)^2.$$

For the one-component HN limit, the corresponding restriction in Part A reduces to $\kappa\sigma^2 > \alpha^2 + 2\alpha^2\gamma^2$. Although these parameter restrictions may limit the flexibility of the models, they could be imposed during estimation. According to Duffie and Kan (1996), Part B of Condition 1 implies that whenever the i^{th} volatility is at zero, it cannot be driven "negative" by dependence on other nonzero volatilities. This condition is automatically satisfied for $i = 2, 3$, so we only need to verify the case $i = 1$. We notice that $\left(\boldsymbol{v}_{1,1}^{\top} \boldsymbol{\Gamma}^{\mathcal{N}}\right)_3 = 0$ and, because $V_1(\boldsymbol{x})$ and $V_2(\boldsymbol{x})$ are not proportional, we need $\left(\boldsymbol{v}_{1,1}^{\top} \boldsymbol{\Gamma}^{\mathcal{N}}\right)_2 = \sqrt{2}\left(\alpha_s + \alpha_q\right) = 0$, which implies that $\alpha_s = -\alpha_q$. This condition is rather restrictive and it is not typically consistent with the parameter values used in the literature, as the majority of the research papers on pricing under GARCH component models impose both ARCH coefficients to be nonnegative. Finally, we notice that in the HN case, Part B of Condition 1 is satisfied by our diffusion limit only if we take $\alpha = 0$, which corresponds to a deterministic volatility case.

A.2.3. *Proof of Proposition 3.* The main characteristic of the pricing kernel of Assumption 2 is that it preserves the affine property of Assumption 1 after the change of measure is applied. Indeed, it is straightforward to show that for any real w and $\boldsymbol{v} = [\, v_1 \quad v_2 \,]^{\top}$, the joint cgf of $\Delta Y_{(k+1)\tau}^{(n)}$, $\Delta s_{(k+1)\tau}^{(n)}$, and $\Delta q_{(k+1)\tau}^{(n)}$ conditional on $\mathcal{F}_{k\tau}^{(n)}$ has the following affine representation under the risk-neutral measure $\mathbb{Q}^{(n)}$:

$$\mathcal{C}^{\mathbb{Q}^{(n)}}_{\Delta Y_{(k+1)\tau}^{(n)}, \Delta s_{(k+1)\tau}^{(n)}, \Delta q_{(k+1)\tau}^{(n)}}\left(w, \boldsymbol{v} \mid \mathcal{F}_{k\tau}^{(n)}\right) = \tilde{\mathcal{A}}^{\mathcal{D}}(w, \boldsymbol{v}; \tau) + \tilde{\mathcal{B}}_s^{\mathcal{D}}(w, \boldsymbol{v}; \tau)\, s_{k\tau}^{(n)} + \tilde{\mathcal{B}}_q^{\mathcal{D}}(w, \boldsymbol{v}; \tau)\, q_{k\tau}^{(n)}, \tag{A.14}$$

where the coefficients $\tilde{\mathcal{A}}^{\mathcal{D}}(w, \boldsymbol{v}; \tau)$ and $\tilde{\mathcal{B}}_u^{\mathcal{D}}(w, \boldsymbol{v}; \tau)$ satisfy the following relationships:

$$\tilde{\mathcal{A}}^{\mathcal{D}}(w, \boldsymbol{v}; \tau) = \mathcal{A}^{\mathcal{D}}(w + \theta(\tau), \boldsymbol{v} + \boldsymbol{\xi}(\tau); \tau) - \mathcal{A}^{\mathcal{D}}(\theta(\tau), \boldsymbol{\xi}(\tau); \tau), \tag{A.15}$$

$$\tilde{\mathcal{B}}_u^{\mathcal{D}}(w, \boldsymbol{v}; \tau) = \mathcal{B}_u^{\mathcal{D}}(w + \theta(\tau), \boldsymbol{v} + \boldsymbol{\xi}(\tau); \tau) - \mathcal{B}_u^{\mathcal{D}}(\theta(\tau), \boldsymbol{\xi}(\tau); \tau), \tag{A.16}$$

for $u \in \{s, q\}$. Therefore, the process for deriving the risk-neutral weak limits is based on the approach detailed in Appendix A.2.1 but adapted for this specific probability measure. We remark that it is not necessary to derive the risk-neutral dynamics to compute our diffusion limit under the $\mathbb{Q}$ measure.

The risk-neutral limit for the HN(C) model is derived as follows. First, using the approach of Augustyniak et al. (2023), we solve the martingale constraints in Equations (8) and (9) based on the coefficients of the $\mathcal{F}_{k\tau}^{(n)}$-conditional joint cgf of $\Delta Y_{(k+1)\tau}^{(n)}$, $\Delta s_{(k+1)\tau}^{(n)}$, and $\Delta q_{(k+1)\tau}^{(n)}$ under $\mathbb{P}^{(n)}$ computed in Equations (A.1)–(A.3). We obtain the following relationship between the risk preference parameters $\theta(\tau)$ and $\boldsymbol{\xi}(\tau)$:

$$\theta(\tau) = -\frac{1}{2} - \frac{\lambda(\tau)}{\tau} + 2\boldsymbol{\xi}(\tau)^{\top}\left(\frac{\lambda(\tau)\boldsymbol{\alpha}(\tau)}{\tau} + \frac{\boldsymbol{\alpha}(\tau) \odot \boldsymbol{\gamma}(\tau)}{\sqrt{\tau}}\right). \tag{A.17}$$

Downloaded from https://www.cambridge.org/core. UNIVERSIDAD AUTONOMA METROPOLITANA, on 14 Nov 2026 at 21:01:13, subject to the Cambridge Core terms of use, available at https://www.cambridge.org/core/terms. https://doi.org/10.1017/S0266466626100607

Under the limiting parameter constraints of Assumptions 3 and 4, the limit of the equity risk preference parameter exists and is given by

$$\theta = \lim_{\tau\to 0}\theta(\tau) = -\frac{1}{2} - \lambda + 2\boldsymbol{\xi}^{\top}(\boldsymbol{\alpha}\odot\boldsymbol{\gamma}). \tag{A.18}$$

Second, we introduce the first- and second-order partial derivatives for the risk-neutral cgf coefficients and express them in terms of the physical quantities using Equations (A.15) and (A.16). Thus, for any nonnegative integers i,j,k with $1 \le i+j+k \le 2$, and $u \in \{s,q\}$, we have

$$\tilde{\mathcal{A}}^{\mathcal{N}}_{i,j,k}(\tau) = \left.\frac{\partial^{i+j+k}\tilde{\mathcal{A}}^{\mathcal{N}}(w,\boldsymbol{v};\tau)}{\partial w^i \partial v_1^j \partial v_2^k}\right|_{w=0,\boldsymbol{v}=\mathbf{0}} = \left.\frac{\partial^{i+j+k}\mathcal{A}^{\mathcal{N}}(w,\boldsymbol{v};\tau)}{\partial w^i \partial v_1^j \partial v_2^k}\right|_{w=\theta(\tau),\boldsymbol{v}=\boldsymbol{\xi}(\boldsymbol{\tau})}, \tag{A.19}$$

$$\tilde{\mathcal{B}}^{\mathcal{N}}_{u,i,j,k}(\tau) = \left.\frac{\partial^{i+j+k}\tilde{\mathcal{B}}^{\mathcal{N}}_u(w,\boldsymbol{v};\tau)}{\partial w^i \partial v_1^j \partial v_2^k}\right|_{w=0,\boldsymbol{v}=\mathbf{0}} = \left.\frac{\partial^{i+j+k}\mathcal{B}^{\mathcal{N}}_u(w,\boldsymbol{v};\tau)}{\partial w^i \partial v_1^j \partial v_2^k}\right|_{w=\theta(\tau),\boldsymbol{v}=\boldsymbol{\xi}(\boldsymbol{\tau})}. \tag{A.20}$$

Using Equations (A.17) and (A.18), and the limiting parameter constraints of Assumptions 3 and 4, we compute the first-order limits. To lighten the notation, we set

$$R(\tau) = \sqrt{\tau}\,\theta(\tau) - 2\boldsymbol{\xi}(\tau)^{\top}(\boldsymbol{\alpha}(\tau)\odot\boldsymbol{\gamma}(\tau)), \tag{A.21}$$

and we note that $\lim_{\tau\to 0}\tau^{-\frac{1}{2}}R(\tau) = -\left(\lambda+\frac{1}{2}\right)$ and $\lim_{\tau\to 0}\left(1-2\boldsymbol{\alpha}(\tau)^{\top}\boldsymbol{\xi}(\tau)\right) = 1$, which explains the limiting values obtained below:

$$\begin{aligned}
\tilde{\mathcal{A}}^{\mathcal{N}}_{1,0,0} &= \lim_{\tau\to 0}\frac{\tilde{\mathcal{A}}^{\mathcal{N}}_{1,0,0}(\tau)}{\tau} = \lim_{\tau\to 0}\frac{r\tau}{\tau} = r,\\
\tilde{\mathcal{A}}^{\mathcal{N}}_{0,1,0} &= \lim_{\tau\to 0}\frac{\tilde{\mathcal{A}}^{\mathcal{N}}_{0,1,0}(\tau)}{\tau} = \lim_{\tau\to 0}\frac{-\alpha_s(\tau)+\dfrac{\alpha_s(\tau)}{1-2\boldsymbol{\alpha}(\tau)^{\top}\boldsymbol{\xi}(\tau)}}{\tau} = 2\alpha_s\boldsymbol{\alpha}^{\top}\boldsymbol{\xi},\\
\tilde{\mathcal{A}}^{\mathcal{N}}_{0,0,1} &= \lim_{\tau\to 0}\frac{\tilde{\mathcal{A}}^{\mathcal{N}}_{0,0,1}(\tau)}{\tau} = \lim_{\tau\to 0}\frac{\sigma^2(\tau)\left(1-\phi_q(\tau)\right)-\alpha_q(\tau)+\dfrac{\alpha_q(\tau)}{1-2\boldsymbol{\alpha}(\tau)^{\top}\boldsymbol{\xi}(\tau)}}{\tau}\\
&= \kappa_q\sigma^2 + 2\alpha_q\boldsymbol{\alpha}^{\top}\boldsymbol{\xi},\\
\tilde{\mathcal{B}}^{\mathcal{N}}_{u,1,0,0} &= \lim_{\tau\to 0}\frac{\tilde{\mathcal{B}}^{\mathcal{N}}_{u,1,0,0}(\tau)}{\tau} = \lim_{\tau\to 0}\frac{\lambda(\tau)+\dfrac{\sqrt{\tau}R(\tau)}{1-2\boldsymbol{\alpha}(\tau)^{\top}\boldsymbol{\xi}(\tau)}}{\tau} = -\frac{1}{2},\\
\tilde{\mathcal{B}}^{\mathcal{N}}_{s,0,1,0} &= \lim_{\tau\to 0}\frac{\tilde{\mathcal{B}}^{\mathcal{N}}_{s,0,1,0}(\tau)}{\tau}\\
&= \lim_{\tau\to 0}\frac{-(1-\phi_s(\tau))+\dfrac{\alpha_s(\tau)R^2(\tau)}{\left(1-2\boldsymbol{\alpha}(\tau)^{\top}\boldsymbol{\xi}(\tau)\right)^2}-\dfrac{2\alpha_s(\tau)\gamma_s(\tau)R(\tau)}{1-2\boldsymbol{\alpha}(\tau)^{\top}\boldsymbol{\xi}(\tau)}}{\tau}\\
&= -\kappa_s + 2\alpha_s\gamma_s\left(\lambda+\frac{1}{2}\right),
\end{aligned}$$

Downloaded from https://www.cambridge.org/core. UNIVERSIDAD AUTONOMA METROPOLITANA, on 14 Nov 2026 at 21:01:13, subject to the Cambridge Core terms of use, available at https://www.cambridge.org/core/terms. https://doi.org/10.1017/S0266466626100607

$$\begin{aligned}\tilde{\mathcal{B}}^{\mathcal{N}}_{s,0,0,1} &= \lim_{\tau\to 0}\frac{\tilde{\mathcal{B}}^{\mathcal{N}}_{s,0,0,1}(\tau)}{\tau} = \lim_{\tau\to 0}\frac{\dfrac{\alpha_q(\tau)R^2(\tau)}{\left(1-2\boldsymbol{\alpha}(\tau)^\top\boldsymbol{\xi}(\tau)\right)^2} - \dfrac{2\alpha_q(\tau)\gamma_q(\tau)R(\tau)}{1-2\boldsymbol{\alpha}(\tau)^\top\boldsymbol{\xi}(\tau)}}{\tau}\\ &= 2\alpha_q\gamma_q\left(\lambda+\frac{1}{2}\right),\\ \tilde{\mathcal{B}}^{\mathcal{N}}_{q,0,1,0} &= \lim_{\tau\to 0}\frac{\tilde{\mathcal{B}}^{\mathcal{N}}_{q,0,1,0}(\tau)}{\tau} = \lim_{\tau\to 0}\frac{\dfrac{\alpha_s(\tau)R^2(\tau)}{\left(1-2\boldsymbol{\alpha}(\tau)^\top\boldsymbol{\xi}(\tau)\right)^2} - \dfrac{2\alpha_s(\tau)\gamma_s(\tau)R(\tau)}{1-2\boldsymbol{\alpha}(\tau)^\top\boldsymbol{\xi}(\tau)}}{\tau}\\ &= 2\alpha_s\gamma_s\left(\lambda+\frac{1}{2}\right),\\ \tilde{\mathcal{B}}^{\mathcal{N}}_{q,0,0,1} &= \lim_{\tau\to 0}\frac{\tilde{\mathcal{B}}^{\mathcal{N}}_{q,0,0,1}(\tau)}{\tau}\\ &= \lim_{\tau\to 0}\frac{-\left(1-\phi_q(\tau)\right) + \dfrac{\alpha_q(\tau)R^2(\tau)}{\left(1-2\boldsymbol{\alpha}(\tau)^\top\boldsymbol{\xi}(\tau)\right)^2} - \dfrac{2\alpha_q(\tau)\gamma_q(\tau)R(\tau)}{1-2\boldsymbol{\alpha}(\tau)^\top\boldsymbol{\xi}(\tau)}}{\tau}\\ &= -\kappa_q + 2\alpha_q\gamma_q\left(\lambda+\frac{1}{2}\right).\end{aligned}$$

Replacing these quantities into Equation (A.10) allows us to obtain the risk-neutral drift coefficient from Equation (26). For any $u \in \{s,q\}$, we now compute the second-order limits using Equations (A.17) and (A.18) together with the convergence rates of Assumptions 3B and 4:

$$\begin{aligned}\tilde{\mathcal{A}}^{\mathcal{N}}_{2,0,0} &= \lim_{\tau\to 0}\frac{\tilde{\mathcal{A}}^{\mathcal{N}}_{2,0,0}(\tau)}{\tau} = \lim_{\tau\to 0}\frac{0}{\tau} = 0,\\ \tilde{\mathcal{A}}^{\mathcal{N}}_{1,1,0} &= \lim_{\tau\to 0}\frac{\tilde{\mathcal{A}}^{\mathcal{N}}_{1,1,0}(\tau)}{\tau} = \lim_{\tau\to 0}\frac{0}{\tau} = 0,\\ \tilde{\mathcal{A}}^{\mathcal{N}}_{1,0,1} &= \lim_{\tau\to 0}\frac{\tilde{\mathcal{A}}^{\mathcal{N}}_{1,0,1}(\tau)}{\tau} = \lim_{\tau\to 0}\frac{0}{\tau} = 0,\\ \tilde{\mathcal{A}}^{\mathcal{N}}_{0,2,0} &= \lim_{\tau\to 0}\frac{\tilde{\mathcal{A}}^{\mathcal{N}}_{0,2,0}(\tau)}{\tau} = \lim_{\tau\to 0}\frac{\dfrac{2\alpha_s^2(\tau)}{\left(1-2\boldsymbol{\alpha}(\tau)^\top\boldsymbol{\xi}(\tau)\right)^2}}{\tau} = 2\alpha_s^2,\\ \tilde{\mathcal{A}}^{\mathcal{N}}_{0,1,1} &= \lim_{\tau\to 0}\frac{\tilde{\mathcal{A}}^{\mathcal{N}}_{0,1,1}(\tau)}{\tau} = \lim_{\tau\to 0}\frac{\dfrac{2\alpha_s(\tau)\,\alpha_q(\tau)}{\left(1-2\boldsymbol{\alpha}(\tau)^\top\boldsymbol{\xi}(\tau)\right)^2}}{\tau} = 2\alpha_s\alpha_q,\\ \tilde{\mathcal{A}}^{\mathcal{N}}_{0,0,2} &= \lim_{\tau\to 0}\frac{\tilde{\mathcal{A}}^{\mathcal{N}}_{0,0,2}(\tau)}{\tau} = \lim_{\tau\to 0}\frac{\dfrac{2\alpha_q^2(\tau)}{\left(1-2\boldsymbol{\alpha}(\tau)^\top\boldsymbol{\xi}(\tau)\right)^2}}{\tau} = 2\alpha_q^2,\\ \tilde{\mathcal{B}}^{\mathcal{N}}_{u,2,0,0} &= \lim_{\tau\to 0}\frac{\tilde{\mathcal{B}}^{\mathcal{N}}_{u,2,0,0}(\tau)}{\tau} = \lim_{\tau\to 0}\frac{\dfrac{\tau}{1-2\boldsymbol{\alpha}(\tau)^\top\boldsymbol{\xi}(\tau)}}{\tau} = 1,\end{aligned}$$

Downloaded from https://www.cambridge.org/core. UNIVERSIDAD AUTONOMA METROPOLITANA, on 14 Nov 2026 at 21:01:13, subject to the Cambridge Core terms of use, available at https://www.cambridge.org/core/terms. https://doi.org/10.1017/S0266466626100607

$$\begin{aligned}
\tilde{\mathcal{B}}^{\mathcal{N}}_{u,1,1,0} &= \lim_{\tau\to 0} \frac{\tilde{\mathcal{B}}^{\mathcal{N}}_{u,1,1,0}(\tau)}{\tau} \\
&= \lim_{\tau\to 0} \frac{\dfrac{2\sqrt{\tau}\alpha_s(\tau)\left(\sqrt{\tau}\theta(\tau)-\gamma_s(\tau)+2\alpha_q(\tau)\xi_q(\tau)\left(\gamma_s(\tau)-\gamma_q(\tau)\right)\right)}{\left(1-2\boldsymbol{\alpha}(\tau)^\top\boldsymbol{\xi}(\tau)\right)^2}}{\tau} \\
&= -2\alpha_s\gamma_s, \\
\tilde{\mathcal{B}}^{\mathcal{N}}_{u,1,0,1} &= \lim_{\tau\to 0} \frac{\tilde{\mathcal{B}}^{\mathcal{N}}_{u,1,0,1}(\tau)}{\tau} \\
&= \lim_{\tau\to 0} \frac{\dfrac{2\sqrt{\tau}\alpha_q(\tau)\left(\sqrt{\tau}\theta(\tau)-\gamma_q(\tau)+2\alpha_s(\tau)\xi_s(\tau)\left(\gamma_q(\tau)-\gamma_s(\tau)\right)\right)}{\left(1-2\boldsymbol{\alpha}(\tau)^\top\boldsymbol{\xi}(\tau)\right)^2}}{\tau} \\
&= -2\alpha_q\gamma_q, \\
\tilde{\mathcal{B}}^{\mathcal{N}}_{u,0,2,0} &= \lim_{\tau\to 0} \frac{\tilde{\mathcal{B}}^{\mathcal{N}}_{u,0,2,0}(\tau)}{\tau} \\
&= \lim_{\tau\to 0} \frac{\dfrac{4\alpha_s^2(\tau)\left(\sqrt{\tau}\theta(\tau)-\gamma_s(\tau)+2\alpha_q(\tau)\xi_q(\tau)\left(\gamma_s(\tau)-\gamma_q(\tau)\right)\right)^2}{\left(1-2\boldsymbol{\alpha}(\tau)^\top\boldsymbol{\xi}(\tau)\right)^3}}{\tau} = 4\alpha_s^2\gamma_s^2, \\
\tilde{\mathcal{B}}^{\mathcal{N}}_{u,0,1,1} &= \lim_{\tau\to 0} \frac{\tilde{\mathcal{B}}^{\mathcal{N}}_{u,0,1,1}(\tau)}{\tau} \\
&= \lim_{\tau\to 0} \frac{\dfrac{\left(\begin{array}{l}4\alpha_s(\tau)\alpha_q(\tau)\left(\sqrt{\tau}\theta(\tau)-\gamma_s(\tau)+2\alpha_q(\tau)\xi_q(\tau)\left(\gamma_s(\tau)-\gamma_q(\tau)\right)\right) \\ \times\left(\sqrt{\tau}\theta(\tau)-\gamma_q(\tau)+2\alpha_s(\tau)\xi_s(\tau)\left(\gamma_q(\tau)-\gamma_s(\tau)\right)\right)\end{array}\right)}{\left(1-2\boldsymbol{\alpha}(\tau)^\top\boldsymbol{\xi}(\tau)\right)^3}}{\tau} \\
&= 4\alpha_s\alpha_q\gamma_s\gamma_q, \\
\tilde{\mathcal{B}}^{\mathcal{N}}_{u,0,0,2} &= \lim_{\tau\to 0} \frac{\tilde{\mathcal{B}}^{\mathcal{N}}_{u,0,0,2}(\tau)}{\tau} \\
&= \lim_{\tau\to 0} \frac{\dfrac{4\alpha_q^2(\tau)\left(\sqrt{\tau}\theta(\tau)-\gamma_q(\tau)+2\alpha_s(\tau)\xi_s(\tau)\left(\gamma_q(\tau)-\gamma_s(\tau)\right)\right)^2}{\left(1-2\boldsymbol{\alpha}(\tau)^\top\boldsymbol{\xi}(\tau)\right)^3}}{\tau} \\
&= 4\alpha_q^2\gamma_q^2.
\end{aligned}$$

Plugging these values into the matrix of asymptotic second-order cross-cumulants of Equation (A.11) leads to the same covariance matrix as under the physical measure, so that $\tilde{\boldsymbol{\Sigma}}^{\mathcal{N}}(\boldsymbol{X}_t) = \boldsymbol{\Sigma}^{\mathcal{N}}(\boldsymbol{X}_t)$. Condition (iii) of Theorem SM.1 (see Section SM.A of the Supplementary Material) and the multidimensional Feller constraints of Duffie and Kan (1996) are verified in the same way as in Appendix A.2.2.

Downloaded from https://www.cambridge.org/core. UNIVERSIDAD AUTONOMA METROPOLITANA, on 14 Nov 2026 at 21:01:13, subject to the Cambridge Core terms of use, available at https://www.cambridge.org/core/terms. https://doi.org/10.1017/S0266466626100607

SUPPLEMENTARY MATERIAL

Augustyniak, M., Badescu, A., Bégin, J.-F., & Jayaraman, S. K. (July 2026): Supplement to "On the relation between discrete- and continuous-time affine option pricing models," Econometric Theory Supplementary Material. To view, please visit: https://doi.org/10.1017/S0266466626100607.

FUNDING STATEMENT

Financial support from the Natural Sciences and Engineering Research Council of Canada (NSERC) is gratefully acknowledged by M.A., A.B., and J.-F.B. J.-F.B. also wishes to thank the financial support of Simon Fraser University.

COMPETING INTEREST STATEMENT

The authors declare that no competing interests exist.

REFERENCES

Aït-Sahalia, Y., Karaman, M., & Mancini, L. (2020). The term structure of equity and variance risk premia. *Journal of Econometrics*, 219(2), 204–230.

Alexander, C., & Lazar, E. (2021). The continuous limit of weak GARCH. *Econometric Reviews*, 40(2), 197–216.

Alitab, D., Bormetti, G., Corsi, F., & Majewski, A. A. (2020). A jump and smile ride: Jump and variance risk premia in option pricing. *Journal of Financial Econometrics*, 18(1), 121–157.

Andersen, T. G. (1994). Stochastic autoregressive volatility: A framework for volatility modeling. *Mathematical Finance*, 4(1), 75–102.

Andersen, T. G., Benzoni, L., & Lund, J. (2002). An empirical investigation of continuous-time equity return models. *Journal of Finance*, 57(3), 1239–1284.

Andersen, T. G., Fusari, N., & Todorov, V. (2015). The risk premia embedded in index options. *Journal of Financial Economics*, 117(3), 558–584.

Arvanitis, S. (2004). The diffusion limit of a TVP-GQARCH-M(1,1) model. *Econometric Theory*, 20(1), 161–175.

Augustyniak, M., Badescu, A., & Bégin, J.-F. (2023). A discrete-time hedging framework with multiple factors and fat tails: On what matters. *Journal of Econometrics*, 232(2), 416–444.

Babaoğlu, K., Christoffersen, P., Heston, S., & Jacobs, K. (2018). Option valuation with volatility components, fat tails, and nonmonotonic pricing kernels. *Review of Asset Pricing Studies*, 8(2), 183–231.

Badescu, A., Cui, Z., & Ortega, J.-P. (2017). Non-affine GARCH option pricing models, variance-dependent kernels, and diffusion limits. *Journal of Financial Econometrics*, 15(4), 602–648.

Badescu, A., Cui, Z., & Ortega, J.-P. (2019). Closed-form variance swap prices under general affine GARCH models and their continuous-time limits. *Annals of Operations Research*, 282, 27–57.

Badescu, A., Elliott, R. J., & Ortega, J.-P. (2015). Non-gaussian GARCH option pricing models and their diffusion limits. *European Journal of Operational Research*, 247(3), 820–830.

Bakshi, G., Cao, C., & Chen, Z. (1997). Empirical performance of alternative option pricing models. *Journal of Finance*, 52(5), 2003–2049.

Bandi, F., & Renò, R. (2016). Price and volatility co-jumps. *Journal of Financial Economics*, 119(1), 107–146.

Downloaded from https://www.cambridge.org/core. UNIVERSIDAD AUTONOMA METROPOLITANA, on 14 Nov 2026 at 21:01:13, subject to the Cambridge Core terms of use, available at https://www.cambridge.org/core/terms. https://doi.org/10.1017/S0266466626100607

Bardgett, C., Gourier, E., & Leippold, M. (2019). Inferring volatility dynamics and risk premia from the S&P 500 and VIX markets. *Journal of Financial Economics*, 131(3), 593–618.

Bates, D. S. (2000). Post-'87 crash fears in the S&P 500 futures option market. *Journal of Econometrics*, 94(1–2), 181–238.

Bates, D. S. (2022). Empirical option pricing models. *Annual Review of Financial Economics*, 14, 369–389.

Bégin, J.-F., Dorion, C., & Gauthier, G. (2020). Idiosyncratic jump risk matters: Evidence from equity returns and options. *Review of Financial Studies*, 33(1), 155–211.

Bollerslev, T. (1986). Generalized autoregressive conditional heteroskedasticity. *Journal of Econometrics*, 31(3), 307–327.

Bollerslev, T., & Todorov, V. (2023). The jump leverage risk premium. *Journal of Financial Economics*, 150(3), 103723.

Bormetti, G., Casarin, R., Corsi, F., & Livieri, G. (2020). A stochastic volatility model with realized measures for option pricing. *Journal of Business & Economic Statistics*, 38(4), 856–871.

Broadie, M., Chernov, M., & Johannes, M. (2007). Model specification and risk premia: Evidence from futures options. *Journal of Finance*, 62(3), 1453–1490.

Buccheri, G., Corsi, F., Flandoli, F., & Livieri, G. (2021). The continuous-time limit of score-driven volatility models. *Journal of Econometrics*, 221(2), 655–675.

Černỳ, A. (2004). Introduction to fast Fourier transform in finance. *Journal of Derivatives*, 12(1), 73–88.

Cheng, P., & Scaillet, O. (2007). Linear-quadratic jump-diffusion modeling. *Mathematical Finance*, 17(4), 575–598.

Cheng, X., Renault, E., & Sangrey, P. (2025). Identifying the volatility risk price through the leverage effect. *Journal of Econometrics*, 248, 105943.

Chernov, M., Gallant, A. R., Ghysels, E., & Tauchen, G. (2003). Alternative models for stock price dynamics. *Journal of Econometrics*, 116(1–2), 225–257.

Chorro, C., & Fanirisoa Zazaravaka, R. H. (2022). Discriminating between GARCH models for option pricing by their ability to compute accurate VIX measures. *Journal of Financial Econometrics*, 20(5), 902–941.

Christoffersen, P., Feunou, B., Jacobs, K., & Meddahi, N. (2014). The economic value of realized volatility: Using high-frequency returns for option valuation. *Journal of Financial and Quantitative Analysis*, 49(3), 663–697.

Christoffersen, P., Heston, S., & Jacobs, K. (2006). Option valuation with conditional skewness. *Journal of Econometrics*, 131(1–2), 253–284.

Christoffersen, P., Heston, S., & Jacobs, K. (2009). The shape and term structure of the index option smirk: Why multifactor stochastic volatility models work so well. *Management Science*, 55(12), 1914–1932.

Christoffersen, P., Heston, S., & Jacobs, K. (2013). Capturing option anomalies with a variance-dependent pricing kernel. *Review of Financial Studies*, 26(8), 1963–2006.

Christoffersen, P., Jacobs, K., Ornthanalai, C., & Wang, Y. (2008). Option valuation with long-run and short-run volatility components. *Journal of Financial Economics*, 90(3), 272–297.

Corradi, V. (2000). Reconsidering the continuous time limit of the GARCH(1,1) process. *Journal of Econometrics*, 96(1), 145–153.

Corsi, F., Fusari, N., & La Vecchia, D. (2013). Realizing smiles: Options pricing with realized volatility. *Journal of Financial Economics*, 107(2), 284–304.

Ding, Y. D. (2020). Weak diffusion limit of real-time GARCH models: The role of current return information. Working Paper, University of Cambridge.

Ding, Y. D. (2023). A simple joint model for returns, volatility and volatility of volatility. *Journal of Econometrics*, 232(2), 521–543.

Drost, F. C., & Nijman, T. E. (1993). Temporal aggregation of GARCH processes. *Econometrica*, 61(4), 909–927.

Duan, J.-C. (1995). The GARCH option pricing model. *Mathematical Finance*, 5(1), 13–32.

Duan, J.-C. (1996). A unified theory of option pricing under stochastic volatility. Working Paper.

Downloaded from https://www.cambridge.org/core. UNIVERSIDAD AUTONOMA METROPOLITANA, on 14 Nov 2026 at 21:01:13, subject to the Cambridge Core terms of use, available at https://www.cambridge.org/core/terms. https://doi.org/10.1017/S0266466626100607

Duan, J.-C. (1997). Augmented GARCH(p,q) process and its diffusion limit. *Journal of Econometrics*, 79(1), 97–127.

Duan, J.-C., & Pliska, S. R. (2004). Option valuation with co-integrated asset prices. *Journal of Economic Dynamics and Control*, 28(4), 727–754.

Duan, J.-C., Ritchken, P., & Sun, Z. (2006). Approximating GARCH-jump models, jump-diffusion processes, and option pricing. *Mathematical Finance*, 16(1), 21–52.

Duan, J.-C., Wang, Y., & Zou, J. (2009). Convergence speed of GARCH option price to diffusion option price. *International Journal of Theoretical and Applied Finance*, 12(3), 359–391.

Duffie, D., & Kan, R. (1996). A yield-factor model of interest rates. *Mathematical Finance*, 6(4), 379–406.

Engle, R. F., & Bollerslev, T. (1986). Modelling the persistence of conditional variances. *Econometric Reviews*, 5(1), 1–50.

Engle, R. F., & Lee, G. G. J. (1999). A long-run and short-run component model of stock return volatility. In R. F. Engle & H. White (Eds.), *Cointegration, causality and forecasting: Festschrift in honour of Clive W. J. Granger* (pp. 475–497). Oxford University Press.

Engle, R. F., & Ng, V. K. (1993). Measuring and testing the impact of news on volatility. *Journal of Finance*, 48(5), 1749–1778.

Eraker, B. (2004). Do stock prices and volatility jump? Reconciling evidence from spot and option prices. *Journal of Finance*, 59(3), 1367–1404.

Ethier, S. N., & Kurtz, T. G. (1986). *Markov processes: Characterization and convergence*. John Wiley & Sons.

Feunou, B., & Tédongap, R. (2012). A stochastic volatility model with conditional skewness. *Journal of Business & Economic Statistics*, 30(4), 576–591.

Filipović, D., & Mayerhofer, E. (2009). Affine diffusion processes: Theory and applications. In H. Albrecher, W. J. Runggaldier, & W. Schachermayer (Eds.), *Advanced financial modelling* (pp. 125–164). De Gruyter.

Fleming, J., & Kirby, C. (2003). A closer look at the relation between GARCH and stochastic autoregressive volatility. *Journal of Financial Econometrics*, 1(3), 365–419.

Fornari, F., & Mele, A. (1997). Weak convergence and distributional assumptions for a general class of nonlinear ARCH models. *Econometric Reviews*, 16(2), 205–227.

Fornari, F., & Mele, A. (2006). Approximating volatility diffusions with CEV-ARCH models. *Journal of Economic Dynamics and Control*, 30(6), 931–966.

Hafner, C. M., Laurent, S., & Violante, F. (2017). Weak diffusion limits of dynamic conditional correlation models. *Econometric Theory*, 33(3), 691–716.

Han, H., Khrapov, S., & Renault, E. (2020). The leverage effect puzzle revisited: Identification in discrete time. *Journal of Econometrics*, 217(2), 230–258.

Harvey, A., Ruiz, E., & Shephard, N. (1994). Multivariate stochastic variance models. *The Review of Economic Studies*, 61(2), 247–264.

Heston, S. L. (1993). A closed-form solution for options with stochastic volatility with applications to bond and currency options. *Review of Financial Studies*, 6(2), 327–343.

Heston, S. L., Jacobs, K., & Kim, H. J. (2024a). A new closed-form discrete-time option pricing model with stochastic volatility. Working Paper.

Heston, S. L., Jacobs, K., & Kim, H. J. (2024b). Volatility risk and monotonic pricing kernels. Working Paper.

Heston, S. L., & Nandi, S. (2000). A closed-form GARCH option valuation model. *Review of Financial Studies*, 13(3), 585–625.

Hull, J., & White, A. (1987). The pricing of options on assets with stochastic volatilities. *Journal of Finance*, 42(2), 281–300.

Ishida, I., & Engle, R. F. (2002). Modeling variance of variance: The square root, the affine, and the CEV GARCH models. Working Paper, New York University.

Jacod, J., & Shiryaev, A. N. (2003). *Limit theorems for stochastic processes* (2nd ed., Vol. 288, *Grundlehren der mathematischen Wissenschaften*). Springer.

Downloaded from https://www.cambridge.org/core. UNIVERSIDAD AUTONOMA METROPOLITANA, on 14 Nov 2026 at 21:01:13, subject to the Cambridge Core terms of use, available at https://www.cambridge.org/core/terms. https://doi.org/10.1017/S0266466626100607

Jones, C. S. (2003). The dynamics of stochastic volatility: Evidence from underlying and options markets. *Journal of Econometrics*, 116(1–2), 181–224.

Kallsen, J., & Vesenmayer, B. (2009). COGARCH as a continuous-time limit of GARCH(1,1). *Stochastic Processes and their Applications*, 119(1), 74–98.

Kim, J., & Meddahi, N. (2017). Revisiting continuous time limits of volatility processes. Working Paper.

Lesne, J. P., Prigent, J. L., & Scaillet, O. (2000). Convergence of discrete time option pricing models under stochastic interest rates. *Finance and Stochastics*, 4(1), 81–93.

Majewski, A. A., Bormetti, G., & Corsi, F. (2015). Smile from the past: A general option pricing framework with multiple volatility and leverage components. *Journal of Econometrics*, 187(2), 521–531.

Meddahi, N., & Renault, E. (2004). Temporal aggregation of volatility models. *Journal of Econometrics*, 119(2), 355–379.

Nelson, D. B. (1990). ARCH models as diffusion approximations. *Journal of Econometrics*, 45(1–2), 7–38.

Nelson, D. B. (1991). Conditional heteroskedasticity in asset returns: A new approach. *Econometrica*, 59(2), 347–370.

Nelson, D. B. (1992). Filtering and forecasting with misspecified ARCH models I: Getting the right variance with the wrong model. *Journal of Econometrics*, 52(1), 61–90.

Nelson, D. B., & Foster, D. P. (1994). Asymptotic filtering theory for univariate ARCH models. *Econometrica*, 62(1), 1–41.

Nelson, D. B., & Foster, D. P. (1995). Filtering and forecasting with misspecified ARCH models II: Making the right forecast with the wrong model. *Journal of Econometrics*, 67(2), 303–335.

Oh, D. H., & Park, Y.-H. (2023). GARCH option pricing with volatility derivatives. *Journal of Banking & Finance*, 146, 106718.

Ornthanalai, C. (2014). Lévy jump risk: Evidence from options and returns. *Journal of Financial Economics*, 112(1), 69–90.

Pitt, M., Malik, S., & Doucet, A. (2014). Simulated likelihood inference for stochastic volatility models using continuous particle filtering. *Annals of the Institute of Statistical Mathematics*, 66(3), 527–552.

Prigent, J.-L. (1999). Incomplete markets: Convergence of options values under the minimal martingale measure. *Advances in Applied Probability*, 31(4), 1058–1077.

Prigent, J.-L. (2003). *Weak convergence of financial markets* (Springer Finance). Springer.

Prigent, J.-L., & Scaillet, O. (2002). Weak convergence of hedging strategies of contingent claims. Working Paper.

Stentoft, L. (2011). American option pricing with discrete and continuous time models: An empirical comparison. *Journal of Empirical Finance*, 18(5), 880–902.

Stroock, D. W., & Varadhan, S. R. S. (1979). *Multidimensional diffusion processes*. Springer-Verlag.

Taylor, S. J. (1986). *Modelling financial time series*. Wiley.

Taylor, S. J. (1994). Modeling stochastic volatility: A review and comparative study. *Mathematical Finance*, 4(2), 183–204.

Wang, Y. (2002). Asymptotic nonequivalence of GARCH models and diffusions. *Annals of Statistics*, 30(3), 754–783.

Downloaded from https://www.cambridge.org/core. UNIVERSIDAD AUTONOMA METROPOLITANA, on 14 Nov 2026 at 21:01:13, subject to the Cambridge Core terms of use, available at https://www.cambridge.org/core/terms. https://doi.org/10.1017/S0266466626100607